Feasibility of an Engine Architecture using Bypass Cooled Cooling Air

for Current and Future High Bypass Turbofans

Lars A. H. Velthausz

TU Delft

Feasibility of an Engine Architecture using Bypass Cooled Cooling Air

for Current and Future High Bypass Turbofans

by

Lars A. H. Velthausz

to obtain the degree of Master of Science
at the Delft University of Technology,
to be defended publicly on 25^{th} of August, 2022 at 10:00 AM.

Student number:	4442253			
Project duration:	20^{th} of October, 2021 – 25^{th} of August, 2022			
Thesis committee:	Prof. dr. ir. P. Colonna,	FPP	TU Delft	thesis supervisor
	Dir. ir. J. A. Melkert,	FPP	TU Delft	
	Dr. ir. C. M. de Servi,	FPP	TU Delft	
	Dr. ir. F. Yin	ANCE	TU Delft	

An electronic version of this thesis is available at http://repository.tudelft.nl/.
Cover page image courtesy Bloom Engineering [1]

TU Delft

Acknowledgements

In writing this thesis, I've received support from several people that I'd like to acknowledge.

Piero and Carlo have provided excellent guidance and support throughout this process. Not only have they given useful technical insights but their kindness, flexibility and involved attitude regarding this project's process have been tremendously helpful. Furthermore, I would like to thank Arvind and Feijia for providing the basis and topic of the thesis in addition the baseline Leap-1A engine model.

Finally, I'd like to thank my friends, family, and in particular my partner, for their continued moral support. They have helped me stay focused and motivated through this marathon of project, as well as help me get my thoughts straight.

Lars A. H. Velthausz
Delft, August 2022

Abstract

This study analyses the feasibility of an engine architecture using bypass cooled cooling air as a method for reducing specific fuel consumption of current and future high bypass turbofan engines. As cooled cooling air reduces required turbine cooling massflow, a major source of loss in modern aeroengines, it is believed that the concept can improve engine efficiency. No extensive or explicit study on the merits of this concept has been performed, however.

Using the 0-D engine analysis software GSP, engine performance parameters at Take-Off and Cruise, such as, specific fuel consumption and (specific) thrust were evaluated against altering feed cooling air temperature by 0 to -300K and heat exchanger induced pressure losses of 0 to 8% in the bypass. This was done for two test cases; the Leap-1A engine (TOC OPR 50, CRZ BPR 11.1, TO FN 121kN) representing current conventional technology and GTF2050, a geared turbofan engine (TOC OPR 75, CRZ BPR 17.1, TO FN 174kN) with entry into service of 2050. For the Leap-1A engine the specific fuel consumption increased up to 1.9% at cruise and for GTF2050, the increase was up to 4.1%. It is shown that the change in fuel consumption is linear with the decrease in cooling fraction, as for both engines the specific fuel consumption increases by +0.34% per percent cooling air reduction. With a reduction in cooling fraction, the exhaust pressure of the core increases, resulting in a higher thrust (up to 2.3%). It is shown that the optimal take-off bypass ratio for minimum fuel consumption shifts up, for the GTF2050 engine from 16.4 to 17.5.

Furthermore, scenario tests and an exergy analysis were performed to find that the impact of different mechanisms; the pressure loss in heat exchanger has minor impact on performance; change in turbine efficiency has small impact; the effect of changed turbine massflow and heat rejection into the bypass are the dominant phenomena.

It is concluded that as a method for reducing fuel consumption, cooled cooling air with the bypass as a heat sink is not feasible for conventional architectures even with extreme design parameters such as high OPR and BPR. Heat rejection to the bypass cannot be effectively utilised and no improvement in core efficiency from reduced cooling air can compensate. In the edge case where there is no heat transfer in cruise, there is an observed specific fuel consumption benefit of up to 4%. The achievable benefit will be lower, however, when accounting for installation penalties.

It is recommended to focus turbine cooling studies on the impact and feasibility of active cooling massflow control without heat rejection, investigate alternative heat sinks for cooled cooling air (e.g. cryogenic fuel), and only consider bypass cooled cooling air as last resort when up-flowing cooling schemes is not permissible or ineffective.

Contents

List of Figures

List of Tables

Nomenclature

Abbreviation	Description
AOHEX	Air to Oil Heat Exchangers
BP(-OT)	Bypass (Off-Take)
BPR	Bypass Ratio
CC	Combustion Chamber
CCA	Cooled Cooling Air
CFD	Computational Fluid Dynamics
CO_2	Carbon Dioxide
CRZ	Cruise
EIS	Entry Into Service
FB	Fuel Burn
FOHEX	Fuel to Oil Heat Exhangers
(G)TF	(Geared) Turbofan
HEX	Heat Exchanger
HHV	Higher Heating Value
HP	High Pressure
HPC	High Pressure Compressor
HPT	High Pressure Turbine
IC	Intercooler or Intercooled
IPC	Intermediate Pressure Compressor (booster)
IRA	Intercooled & Recuperative Aero-engine
ISA	International Standard Atmosphere
ITB	Interstage Turbine Burner
JICF	Jet in CrossFlow
LHV	Lower Heating Value
LP	Low Pressure
LPC	Low Pressure Compressor
LPT	Low Pressure Turbine
(M)CL	(Maximum or Top of) Climb
(M)TO	(Maximum) Take-off
NGV	Nozzle Guide Vane (industry alternative for stator)
NO_x	Nitrogen Oxide(s)
NTU	Number of Transfer Units
OPR	Overall Pressure Ratio
OR	Open Rotor
PO	Power Offtake
SAS	Secondary Air System
SFC	(Thrust) Specific Fuel Consumption
SFN	Specific Thrust
SIT	Scenario Impact Test
SOT	Stator Outlet Temperature (T41)
SSL	Standard Sea-Level (condition)
TIT	Turbine Inlet Temperature (T4)

Abbreviation	Description
ACARE	Advisory Council for Aviation Research and Innovation in Europe
CAEP	Committee on Aviation Environmental Protection
GSP	Gas turbine Simulation Program
ICAO	International Civil Aviation Organization
NLR	Nationaal Lucht- en Ruimtevaartlaboratorium
SRIA	Strategic Research and Innovation Agenda

Symbol	Unit	Description
h	J/kg	Specific Enthalpy
A	m^2	Area
A_{exh}	m^2	(Nozzle) Exhaust Area
$\dot{m}$	kg/s	Massflow
$\dot{m}_c$	kg/s	Cooling Massflow
$\dot{m}_{core}$	kg/s	Core Massflow ($\dot{m}_{24}$)
$\dot{m}_{in}$	kg/s	Inlet Massflow ($\dot{m}_1$)
d_{fan}	m	Fan Diameter
c_p	J/kgK	Specific heat constant
ε	-	(Heat Exchanger) Effectiveness
ϵ_c	-	Cooling Effectiveness
$\dot{Q}$	W	Heat Flux
$\dot{q}$	W/m^2	Specific Heat Flux
U	W/m^2K	Effective Heat Transfer Coefficient
W	W	(Shaft) Work
R	J/kgK	Specific Gas Constant
t	m	Wall thickness
μ	Pa· s	Dynamic viscosity
P	Pa	Pressure
P_∞	Pa	Reference or Ambient Pressure
P_{exh}	Pa	Exhaust Pressure
ΔP_{HEX}	-	Heat Exchanger (Total Relative) Pressure Loss
Π	-	Pressure Ratio
ρ	kg/m^3	Density
T	K	Static/Total Temperature
T_c	K	Cooling Feed Temperature
T_g	K	Reference Gas Temperature (typically T4, T405 or T41)
T_b	K	Maximum Allowable (Blade) Metal Temperature
T_∞	K	Reference or Ambient Temperature
V	m/s	Velocity
V_{exh}	m/s	Exhaust Velocity
V_∞	m/s	Ambient Airspeed
η_{prop}	-	Propulsive Efficiency
η_{th}	-	Thermal Efficiency
η_{poly}	-	Polytropic Efficiency
η_{is}	-	Isentropic Efficiency
η_{comb}	-	Combustion Efficiency
s	J/kg·K	Specific Entropy
ζ	J/kg	Specific Exergy
$\wp_s$	J/K	Entropy Production
Ex	J	Exergy
$\dot{Ex}$	W	Exergy Rate
I	J	Exergy Destruction
$\dot{I}$	W	Exergy Destruction Rate
FN	N	(Net) Thrust
FG	N	(Gross) Thrust

1 Introduction

As the effects of climate change are becoming increasingly problematic, it is imperative that the aerospace industry–being a substantial contributor–becomes more sustainable. Governmental bodies have set ambitious goals to reduce emissions: ACARE has set a goal by 2050 to reduce carbon emissions per traveller per km by 75%, and NO_x emissions by 90% outright [2]: a goal which is to be achieved whilst the aerospace industry is growing steadily at around 3-5% per year [3].

Despite public desire for fully electric propulsion, aircraft designs will rely on liquid fuel-based aero engines as the primary source of power [4]. As an all-electric commercial-scale aeroplane requires significant improvements in the storage density of batteries, and other component performance for commercial applications [5], [6], it is therefore important to investigate and develop concepts that can improve the efficiency of aero-engines.

Over time, improvement in engine efficiency has been driven by many factors including improvements in component efficiency [7]. For civil aviation, the use of sole-jet engines has given way for turbofan engines with high bypass ratios. High bypass ratios offer greater propulsive efficiency: unfortunately, this is diminishing in returns as the weight and size of the engines scales up [8]. As well as improvements in propulsive efficiency, a universal design trend in aero engines to increase thermodynamic efficiency is higher overall pressure ratio (OPR) and increasing turbine inlet temperature (TIT) [7], [9], [10], an approach which puts more strain on the turbine cooling schemes. The remainder of this chapter will discuss the problem of this increased strain, and propose research objectives that aim to test a specific method of addressing this issue.

1.1. Problem Statement

In current aero engine designs, the TIT already exceeds the melting temperature of the material used downstream of the combustion chamber, requiring cooling by the turbine components. The amount of cooling air massflow $\dot{m}_c$ needed, as depicted in equation 1.1, scales with the ratio of the difference between the turbine inlet temperature T_g, the maximum allowable metal temperature T_b, and the difference between T_b and the feed cooling temperature T_c [11]–[13]. In the equation, $\dot{m}_{\text{core}}$ represent the core massflow. Additionally, the performance of a specific cooling scheme, a cooling effectiveness ϵ_c, is defined.

$$\frac{\dot{m}_c}{\dot{m}_{\text{core}}} \propto \frac{T_{\text{g}} - T_{\text{b}}}{T_{\text{b}} - T_c}, \frac{1}{\epsilon_c} \tag{1.1}$$

As shown in Figure 1.1, with the trend of increasing turbine inlet temperature, an even higher cooling performance is required. Additionally, this is the case whilst rising overall pressure is increasing the temperature of the cooling air. Subsequently, an increasingly large percentage of air is bled off for turbine cooling. Significant improvements have already been made in the effectiveness of the turbine

cooling schemes [7], [14]. Methods for the reduction in feed temperature are still in their infancy, however.

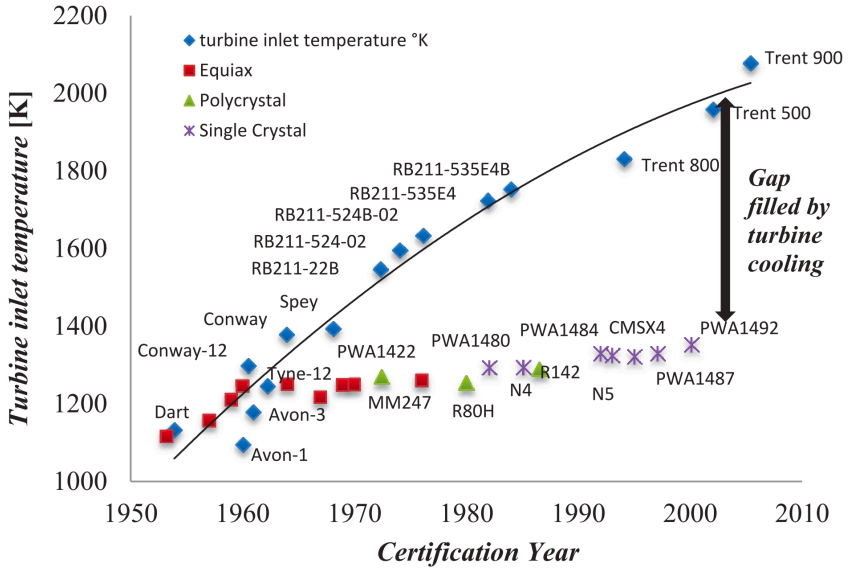

Figure 1.1: Turbine Inlet Temperature and Maximum Material Temperature development over time (Figure [15] data [14])

The primary issue with taking increasingly large massflow fractions from the core for cooling purposes is that the act of cooling is inherently inefficient (causes for this will be explored in more detail in section 2.1.2). To understand the order of magnitude of inefficiency, however, we can consider the 'exchange rates' between the cooling fraction, the specific fuel consumption (SFC) and the specific thrust (SFN). Kurzke [11] found for a sample pure jet engine that a 1% increase in cooling fraction would result in a thrust decrease of 0.33% when keeping the combustor outlet temperature (T4) constant, and 0.66% when keeping the stator outlet temperature (SOT) constant. Walsh [16] did a similar study for SOT constant for 1400 and 1600 K and found the same result for thrust. Notably, for the lower SOT case, fuel consumption actually decreased with increasing cooling fraction (namely -0.33% SFC for 1% cooling fraction)[1]. For the case with SOT=1600K the exchange rates changed to +0.44% SFC -1.53% SFN in line with the findings from Kurzke. Furthermore the impact of cooling flow when applied to a turbofan engine with a moderate bypass ratio of 4.5 was found to be larger than that for the true jet-engine. Namely, per percent cooling flow, the specific fuel consumption increased by +0.20 to +0.96% and the specific thrust changed by -1.29 to -2.02%.

In summary, the impact of cooling is overall significantly negative especially at higher bypass ratio and stator outlet temperature.

1.2. Research Question and Objectives

The 'Cooled Cooling Air' (CCA) concept promises to address this issue of cooling costs. By placing a heat exchanger in the bypass flow, and passing the cooling flow through it, the cooling feed temperature can be reduced–therefore improving the cooling potential per unit of massflow. In turn, the cooling fraction can be decreased, reducing the overall penalty from cooling. Although the concept has already been considered in literature, a dedicated investigation into the feasibility of the concept has yet to be conducted. The following research question has therefore been formulated:

Is the use of a heat exchanger in the bypass flow for the cooling of (HPT) cooling air a feasible strategy to improve future engine performance?

[1] for constant thrust however, the SFC would decay again, resulting in a net SFC increase

Given that the concept will likely have limits on its feasibility, it is interesting to understand the drivers behind this. Conversely, beyond the direct impact on cooling performance, the concept may also be an enabler for increasing the feasibility limits of the engine overall, potentially yielding even larger benefits. With this in mind, the following research objectives have been defined:

1. To evaluate and determine the feasibility of CCA as a strategy to improve turbine cooling performance, and therefore overall engine efficiency;
2. Identify important drivers, in overall engine design parameters, that affect the feasibility of the concept and compare with engine design trends;
3. Understand under which conditions is the CCA concept feasible to improve engine efficiency with fixed cycle temperature limits;and,
4. Associate the changes in cooling performance driven by CCA design parameters, with the loss mechanism and identify the mechanisms most affected.

2

Literature

2.1. Cooled Cooling Air

The Cooled Cooling Air concept aims to address the increasing turbine cooling duty. By means of a heat exchanger that draws air from the bypass, the cooling air is cooled down. This in turn leads to a reduction in cooling mass flow. A schematic of the concept as placed in the engine is presented in Figure 2.1.

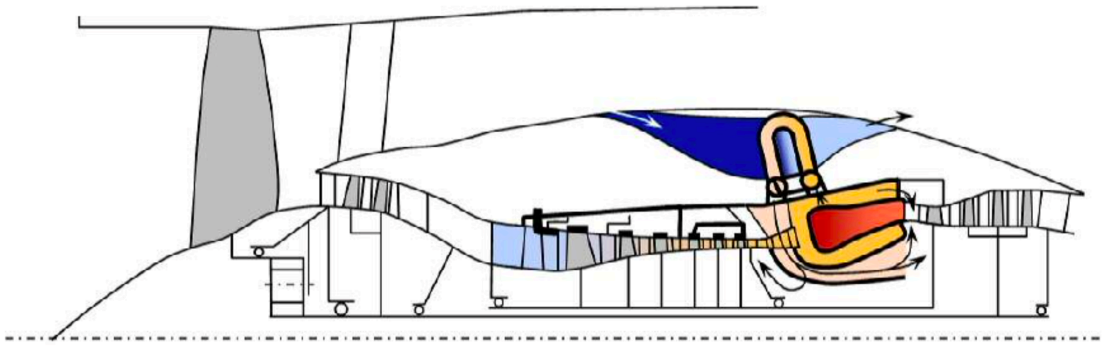

Figure 2.1: The Cooled Cooling Air concept as fitted on an engine [17]

In order to understand the CCA concept and the impact that it has the concept history will be explored in addition to the relevant mechanisms at play. In section 2.1.1 the literature dedicated to or mentioning the CCA concept is presented. In section 2.1.2 the loss mechanics due to turbine cooling in general are discussed. Followed by methods for the quantification of the required cooling massflow in section 1.1. Finally, relevant mechanisms and considerations to CCA specific are discussed in section 2.1.4.

2.1.1. Cooled Cooling

Cooled Cooling air as a strategy has been applied for over 2 decades in industrial gas turbines [16]. In these systems the cooling air is passed through a gas to air heat exchanger with the sink being the fuel (natural gas). Increasing the fuel temperature makes sense as it improves the combustion efficiency and the energy transferred from the cooling air is retained in the system.

The Initial investigation into cooled cooling air systems specifically for aero engines was performed by Beuring and Chang [12]. Both bypass air and fuel were considered as a heat sink, with both showing an impressive positive impact on fuel consumption. The investigation considered a temperature change to the cooling air of 111 and 222 K (200 and 400 ^{o} F). The systems were simulated on a scaled

engine with OPR 50 and varying BPR (0.51 for BP and 0.44 for fuel based system) against a conventional baseline engine with OPR of 32 and BPR 0.42. At cruise conditions, an improvement in SFC of -4.6% and -3.3% for the bypass and fuel based systems, respectively. The specific thrust for the engines however also decreased, with the bypass based system most affected with a 3.1% reduction. From the performed analysis, however, it is unclear what the specific contribution of the CCA system is, as the changes in both OPR and BPR will have impacted the results. It was remarked that for fuel, to prevent gumming and choking deposits, temperature limits on the fuel could jeopardise the feasibility of fuel as a heat sink.

Given the low storage temperature, cryogenic fuels do still seem to be a more promising heat sink for CCA [18]. The use of cryogenic fuel as the sink was proposed in a 2014 study modelling cooling air, the impact of cooled cooling air was quantified without modelling the effect of the increased fuel temperature, however. Here, a slight increase in SFC (+0.4%) and SFN (+0.6%) was found [19] for the use of cooled cooling air only. In this study, the cooling temperature was reduced by 300K and the required cooling flow dropped by 47% as a result.

More recently, a CCA system was part of the design concept ”Active Core” within NEWAC [20] (a large EU funded engine research projects; see section 2.2.2). As the name suggests, the cooled cooling air concept evaluates the potential benefit of actively controlling flows in the engine in order to uncouple the design point from the worst case scenario. For cooling air this is particularly interesting as during cruise the amount of cooling duty is significantly lower than at take-off. In the investigation the cooling fraction was still considered to be fixed across all phases of flight, however the flow from the bypass through the HEX is controlled. A benefit to SFC of ±0.9% for a 100K drop in the cooling air temperature was presented [20]. This result may perhaps not be generally applicable; “the technologies do not consistently benefit all phases of flight” [21]. If a similar or even larger benefit to SFC can be achieved by controlling the cooling flow directly was not investigated.

Another engine project implementing CCA, namely ULTIMATE, used the same active control strategy [22]. The marginal benefit of the CCA system was not evaluated independently. In other words, the concept was applied across all the scenarios, with the same CCA heat exchanger parameters. As the off-take ducts in the BP are a major source of loss, extensive design studies for them have been performed [23]–[25].

2.1.2. Turbine Cooling Loss Mechanisms

In order to appropriately assess the CCA concept, the relevant loss mechanisms related to cooling (and CCA as a whole) must be considered. Additionally, exploring these loss mechanisms will provide insight into both the required modelling fidelity for a meaningful result, and provide guidance into any limitations and caveats in the modelling if the required fidelity cannot be achieved in a more complete model. Farokhi [26] identifies four effects of turbine cooling, as listed

- Coolant massflow does not contribute to power conversion;
- Pressure loss inside the cooling passes;
- Mixing losses and increased profile drag that arise from coolant injection; and,
- Entropy rises as a result of heat transfer between the coolant and the gas.

Arguably, coolant massflow and pressure loss can be grouped together as loss of potential work. Similarly, coolant injection and heat transfer can be collected together as factors affecting turbine efficiency decrease. Such a grouping is done by Kurzke and Halliwell [11]. Taken in these combinations, it appears that loss of potential work yields the greatest impact on overall engine performance [27], [28]. The effects are visualised on a T-S diagram as given in Figure 2.2. Cooling fraction is reduced by 2% for both the stator (NGV) and rotor (blade) (4% in total) and isentropic efficiency is improved by 2%. Furthermore, the power output and SOT are kept constant. The NGV and blade cooling air are added discretely in front and behind the blade, respectively.

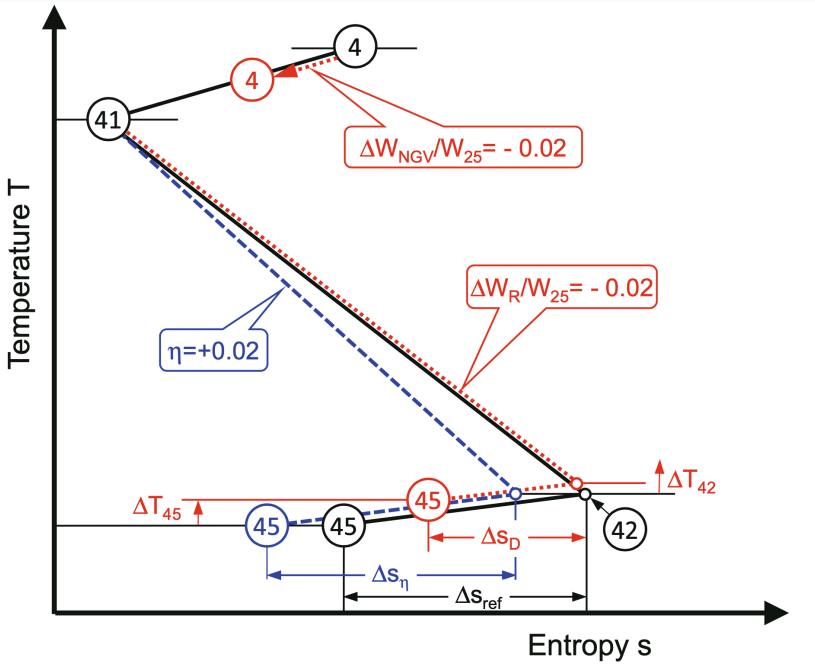

Figure 2.2: Effects of change in polytropic efficiency (blue) and cooling air massflow (red) with constant SOT and power output [29]

In this scenario, one can observe that a lower NGV cooling reduces the combustor outlet temperature required for a given stator outlet temperature. Note, that at the same time, a reduction in cooling massflow does lead to increased massflow through the combustion chamber. Dampening the reduction in fuel burn one might expect for a T4 decrease. Furthermore, the increased massflow through the combustion chamber, and hence the turbine, gives rise to an increased power output of the turbine and therefore the temperature drop over the whole turbine is reduced. Conversely, the potential maximum work output is increased.

Thermodynamic considerations alone are not sufficient to understand the impact of cooling on polytropic efficiency. The interaction between the nominal gas flow and injection of air, known as “jet in crossflow” (JICF), and the subsequent formation of films results in a highly complex flow field [30]. This interaction is extensively researched, with several literature reviews available on the topic (the reader is referred to [31]–[34]). In the JICF problem there are four types of vortical structures; a jet shear layer (prompted by Kelvin-Helmontz instability); a horseshoe vortex caused by the blocking of the gas flow boundary layer; wake vortices formed in the wake of the jet; and a counter-rotating vortex pair induced in the jet from the shear with the main gas flow [35], [36]. A schematic of JICF with the different vortical structures is given in Figure 2.3.

When it comes to predicting the losses attributable to cooling injection, especially without a specified turbine geometry, there is a degree of uncertainty. Regarding the preliminary methods for loss prediction, the assumption is that there is a linear relationship between the efficiency drop of the turbine and the cooling massflow. This relationship is summarised in Table 2.1. Alongside the modelling uncertainty, injection loss in the design of the cooling scheme is naturally fundamental to this ratio. Hence, there are variable results found in literature.

The work of Denton [37] focuses on classifying and understanding all relevant loss mechanisms in the turbine, and finds an expected 1% efficiency drop per percent cooling fraction. It should therefore additionally be considered relevant. Other sources make an estimate of the ratio on the basis of an idealised case where two streams meet at an angle. A background on this standard case can be found in books on internal flows [38].

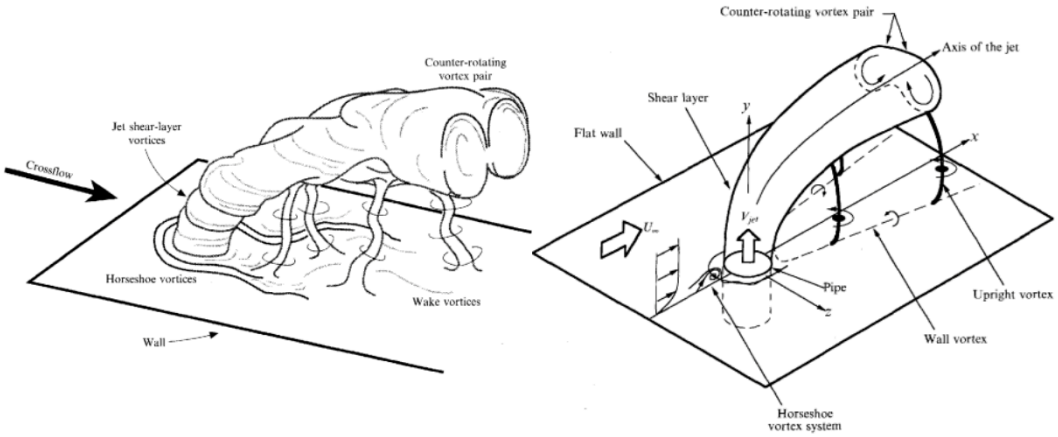

Figure 2.3: Vortical structures in a jet in crossflow [35], [36]

Kerrebock [39] in a book on the general design of aero engines provides a ratio of 0.5% isentropic efficiency drop per percent cooling fraction. Horlock [40] presents a comparison of accounting methods for turbine efficiency and indicates a ratio of 1.4%, though it is to be noted that given the objective of that research was a comparison of accounting methods, the ratio presented may not be relevant for modern design purposes. Walsh and Fletcher [16] provide ratios specific to the location of the coolant injection; the highest loss is caused by suction-side injection, with pressure-side injection being the lowest contributor. Furthermore, a distinction is made between stators and rotors, with rotors having a ratio that differs from stators by a factor of two. This is supported by Gaunter's methodology [27]. The algorithm for loss prediction can account for different cooling injection types. Of these types, the penalty for the scheme with predominantly leading edge film injection is reported below in 2.1. The reported ratios, however, are the lowest reported sourced from experimental and numerical research from before 1970 [41].

$-\Delta\eta_{is}$ per % $m_c/\dot{m}_{core}$		Source
1%		[37]
0.5%		[39]
1.4%		[40]
Stator	Rotor	
0.25-0.75%	0.5-1.5%	[16]
0.15-0.18%	0.3-0.36%	[27], [41]

Table 2.1: Turbine Efficiency drop per percentage cooling fraction

The key takeaways from the review of the loss mechanisms for turbine cooling are

- The reduction in turbine specific power output and entropy production from mixing are the dominant loss mechanism from cooling and hence for appropriate loss modelling the accurate prediction of the required cooling massflow is key;
- When quantifying the drop in turbine efficiency due to cooling injection, a linear ratio between the two can be used, where a value of ±0.5:1 for Stators seems appropriate; and,
- The turbine efficiency drop from cooling injection in rotors is twice as high as in stators.

2.1.3. Quantification of the Cooling Requirement

The required cooling massflow needs to be determined in order to quantify the impact of the CCA concept. A simple approach is to assume the massflow fraction with and limit the compressor exit temperature. Fundamentally, a relationship between the cooling feed temperature and the cooling

massflow needs to be defined. Assuming an initial design cooling massflow and feed temperature are available, the cooling requirement can be scaled. Rolt et al. [22] provide the following equation for the estimation of turbine cooling:

$$\dot{m}_c = \dot{m}_{\mathrm{c,ref}} \frac{(T_{\mathrm{g,ref}} - T_c)(\dot{m}_4/\dot{m}_{4,\mathrm{ref}})^{0.65}}{(T_{\mathrm{g,ref}} - T_{\mathrm{c,ref}})} \tag{2.1}$$

In this equation, the subscript ”ref” stands for the reference case that the cooling requirement is scaled from. An alternative yet similar approach, one that doesn't require a reference point but rather the maximum allowable material temperature and the fluid temperatures, as presented in equation 2.2. The constants can be tuned to match the design cooling scheme.

$$\frac{\dot{m}_c}{\dot{m}_{\mathrm{core}}} = b\left(\frac{T_{\mathrm{g}} - T_{\mathrm{b}}}{T_c - T_c}\right)^s \tag{2.2}$$

Typically, the cooling requirement has been modelled as linearly dependent with the temperature difference (ie. $s = 1$). Kurzke considers the entire turbine stage as one machine with $b = 0.04$. Walch and Flectcher [16] present a chart with a relationship defined for NGV and rotors separately. The cooling requirement is plotted against SOT and hence it is not clear what the value of constant b used is, yet it can still be observed that the relationship is linear with respect to the temperature($s = 1$), and additionally that the constant b is higher for rotors than stators. This is in line with the recommended values of Jonsson [42] with $b = 0.05$ for stators and $b = 0.06$ for rotors. In this work it is also suggested that the exponent s can be varied slightly around unity to match with the cooling system.

Tiemstra [19] presents a semi-empirical approach for evaluating cooling performance, and hence the cooling requirement. This approach evaluates the combined impact of cooling features, providing a prediction specific to cooling scheme design. This is also a drawback of the approach, as it requires a cooling scheme to be defined or assumed. A comparison, shown in Figure 2.4, suggests that the conventional scaling approach performs poorly at higher feed pressure.

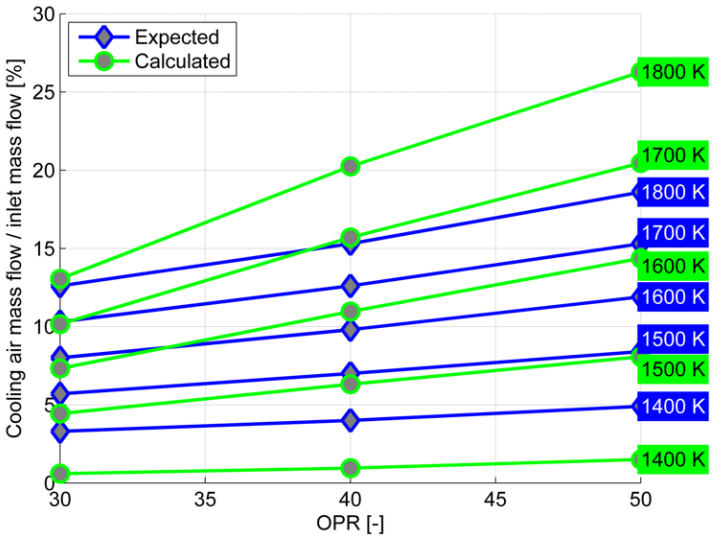

Figure 2.4: Comparison cooling requirement with maximum metal temperature of 1200 K as required by conventional scaling ($b = 0.04; s = 1$) [43] and cooling model [19]

In a later investigation [44], the model was compared to again to conventional scaling, but now with the values recommended by Johnson [42]. Again, the conclusion was drawn that the omission of a pressure component from the conventional method means that it underestimates the cooling requirement at high overall pressure ratios and overestimates at lower OPR. In the specific case tested in the investigation, there is a match in the methods regarding predicted cooling requirement for a take-off

overall pressure of 60 for $s = 0.97$. For high OPR, the exponent s should hence be reduced slightly from 1; and for low-to-moderate OPR, it should be increased slightly to improve the match across the domain.

2.1.4. Relevant Loss & Gain Mechanisms and General Considerations

There are several additional loss and gain mechanisms that are specific to the CCA concept; Pressure loss through the heat exchanger, energy rejection from core and entropy production from heat transfer, thrust recovery in the bypass and weight addition [22]. Beyond these loss/gain mechanisms there are some aspects of the CCA design that may influence engine design or vice versa, these are qualitatively discussed in this section. These individual mechanisms compound through the engine, and therefore the overall efficiency impact is a function of the engine design in total. This is detailed in section 2.2.

Additional Pressure Loss

Due to the need for an additional heat exchanger and associated ducts, pressure loss occurs in both the cooling flow and the BP off-take air.

For the cooling flow, it is important that the pressure loss be minimal; such that the cooling flow can endure the pressure losses through the complex cooling passages in the turbomachinary components and have a sufficiently high “pressure margin” to enter the gas path [45], [46]. This pressure margin is typically low given the advances of cooling schemes as well as reductions in pressure losses upstream of the cooling holes (CC & turbine inlet). For pressure loss sustained by the bypass off-take, the thrust that can be generated by this flow decreases.
Regarding the scale of these pressure losses, the heat exchangers for cooled cooling included in the NEWAC & ULTIMATE projects were assumed to have a pressure loss for the bleed air less than 1% and ±5% for the BP off-take flow [17], [22], [47]. Investigations into design of off-take ducts found an additional 3-7% loss for the BP off-take flow [23]–[25].

Thrust Recovery

As the bypass flow temperature increases, the energy rejected by the cooling flow can be partially ’recovered’ in the form of increased thrust [22]. An exergy assessment of an intercooled engine showed that the loss of thrust caused by the pressure loss in the heat exchanger was similar to the thrust ’recovered’ from the expansion at a higher temperature [48].

Engine Weight Change

Changes to the engine weight have a direct impact on the performance of the aircraft as a whole (see section 2.2.1). Heat exchanger systems add weight to the engine. However, given that the cooled cooling air system increases the specific power output of the core, the engine can be downsized. Bruening and Chang [12] calculated an increase of 4.3% in engine thrust to weight ratio.

Qualitative Considerations

- Induced thermal stresses. These occur as a lower cooling temperature creates an increased temperature difference between the inner and outer wall of the components. This may therefore limit the minimum cooling temperature.
- Increased air requirements for lean combustion may become restrictive for the maximum cooling fraction [17].
- The relationships between cooling effectiveness and massflow may not hold for excessive temperatures [19].
- Alternative NGV material, like ceramics, could reduce the need for cooling significantly [49], [50]
- Complexity of cooling feed systems: NGV can be both root- and tip-fed, whereas blades can only be root fed [14]. This means that feeding the cooling air from the HEX into the blades is non-trivial, as the air needs to travel from the heat exchanger located in the bypass past the main gas path into the centre of the engine (see figure 2.1).

2.2. Overall Engine Considerations and Trends

Chasing higher performance engines have changed radically over time; the bypass ratio, turbine inlet temperature and the overall pressure ratio have all increased significantly. The historical trend of this is depicted in Figure 2.5.

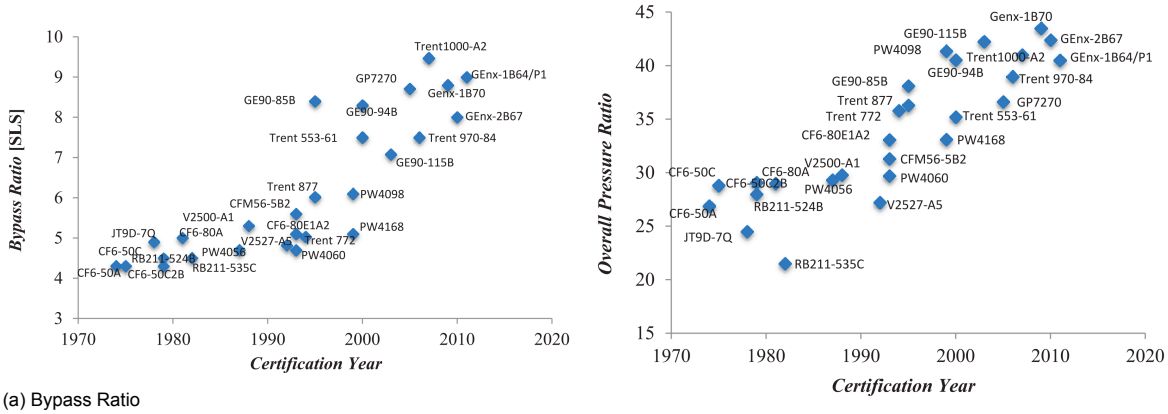

(a) Bypass Ratio

(b) Overall Pressure ratio

Figure 2.5: Certified engine design parameter trend [15]

The feasibility of the CCA concept is dependent on overall engine design parameters. It is therefore interesting to consider current and future engine designs. This also permits prediction about whether the concept will become more feasible in the future.

2.2.1. Engine Design Drivers

As a starting point for engine design, the driving constraints and objectives are evaluated. Besides inherent engineering aspects, there exist also external drivers, either defined by governmental regulation or as the result of interfaces with the aircraft; for example the safety requirements of a blade-off event [14] or power supply to the aircraft's environmental control system [51].

In Figure 2.6, a mind-map is presented with the most relevant drivers for engine design. Given the scope of the research and the targeted fidelity of the results, not all aspects driving detailed engine design are detailed in the scope of this study. This is highlighted in the figure via colour-coding.

Furthermore, a distinction between the natural drivers is made qualitatively in Figure 2.6. Some are clear physical constraints that must be respected, whilst other driving metrics can only be assessed following an (initial) engine design. The latter can hence be considered from a design perspective to be target objectives for optimisation. The remainder of this section is structured along these drivers.

Performance

Engine performance is naturally a key design driver, with two main dimensions: thrust and efficiency. Net thrust (FN) is the result of a net velocity (and pressure) difference between the inlet and outlet. Typically, the core exhaust is choked, and hence there is a net pressure differential at the outlet that also produces thrust. This relationship is given by

$$\mathrm{FN} = \sum \dot{m}_{\mathrm{exh}}(V_{\mathrm{exh}} - V_{\infty}) + A_{\mathrm{exh}}(P_{\mathrm{exh}} - P_{\infty}). \tag{2.3}$$

Here, the subscript "exh" refers to the exit state and ∞ to the free stream conditions. From a design perspective, the required thrust is a fixed to suit target airframes. Typically, multiple thrust requirements, in combination with mission profiles ("thrust ratings"), are defined along the development [14]. It is often useful, as well as the absolute thrust, to evaluate the thrust per unit of intake air also known as the specific thrust (SFN), given by the relationship

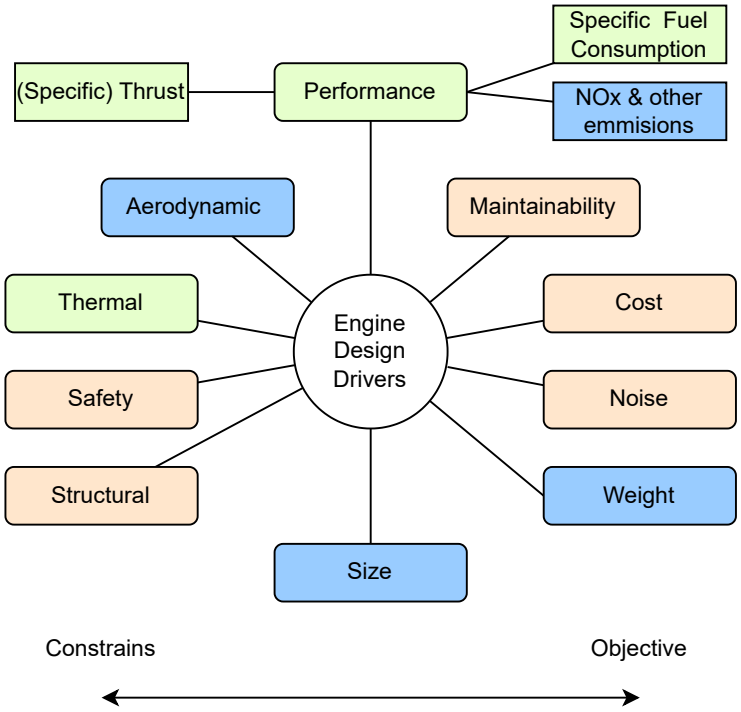

Figure 2.6: Mind-map of the relevant drivers of engine design on a qualitative constraint – objective axis. Green: drivers that form the core focus of the analysis, Blue: a subset of the drivers considered, Red: not covered.

$$\mathrm{SFN} \doteq \frac{\mathrm{FN}}{\dot{m}_{\mathrm{in}}}. \tag{2.4}$$

Notably, with increasing bypass ratio and decreasing fan pressure ratio, the total massflow of engines increases significantly for the same thrust levels and hence SFN decreases. For commercial aviation, the specific thrust is useful for comparing architectures that would have similar inlets, and can provide insights into take-off and climb performance [14].

The definition of overall engine efficiency is the ratio of useful work output over the work input. The useful power output is the thrust multiplied by the aircraft speed (free stream velocity). The power input comes from chemical energy stored in the fuel; namely fuel massflow, $\dot{m}_{\mathrm{f}}$, multiplied by the lower heating value, LHV.

$$\eta_{\mathrm{tot}} \doteq \frac{\mathrm{FN} \cdot V_{\infty}}{\dot{m}_f \mathrm{LHV}} = \eta_{\mathrm{prop}} \eta_{\mathrm{th}} \tag{2.5}$$

Alternatively, the performance parameter SFC (Specific Fuel Consumption) is also often used. SFC is the ratio of fuel massflow to thrust

$$\mathrm{SFC} \doteq \frac{\dot{m}_{\mathrm{f}}}{\mathrm{FN}} = \frac{V_{\infty}}{\eta_{\mathrm{tot}} \mathrm{LHV}}. \tag{2.6}$$

The overall efficiency can be broken down into two components: thermal and propulsive efficiency (see 2.5). The thermal efficiency defines how effectively the (ideal) thermal power released from fuel is converted to kinetic energy of engine exhaust flows. Conversely, propulsive power describes how effectively this kinetic power is used to generate thrust for the aircraft:

$$\text{Thermal Power Input} \xrightarrow{\eta_{\mathrm{th}}} \text{Kinetic Power} \xrightarrow{\eta_{\mathrm{prop}}} \text{Thrust Power}$$

The thermal efficiency is determined by all forms of loss inside the engine and in an ideal cycle is limited to the Carnot efficiency. Using this, the maximum thermal efficiency is

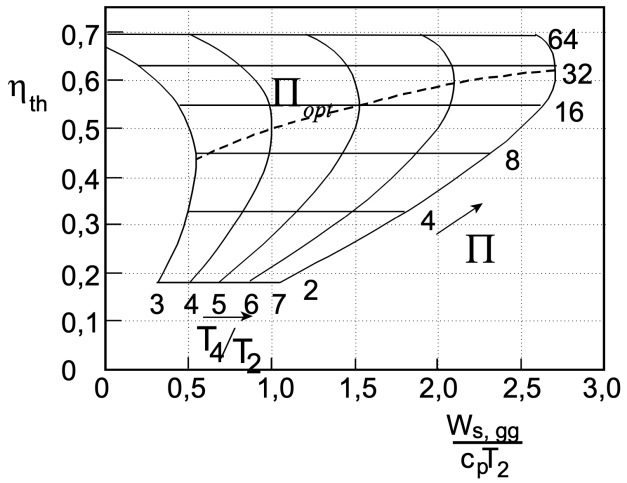

Figure 2.7: Ideal thermal efficiency and kinetic power output for various pressure (Π) and temperature ratios; where the optimal pressure ratio yields, by definition, maximum kinetic power [52]

$$\eta_{\text{carnot}} \doteq 1 - \frac{T_{\text{low}}}{T_{\text{high}}} \Rightarrow \eta_{\text{th}}^{\text{max}} = 1 - \frac{1}{\text{OPR}^{\frac{\gamma-1}{\gamma}}}. \tag{2.7}$$

The ideal kinetic power, $W_{\text{s,gg}}$, in the flow is defined by the ideal turbine power output minus the ideal compressor required power. The specific form of this ideal kinetic power is

$$\frac{W_{\text{s,gg}}}{c_p T_2} = \frac{T_4}{T_2}\Big(1 - \frac{1}{\text{OPR}^{\frac{\gamma-1}{\gamma}}}\Big) - \Big(\text{OPR}^{\frac{\gamma-1}{\gamma}} - 1\Big). \tag{2.8}$$

From this equation, one can find that for a given temperature ratio, there exists an overall pressure ratio which maximises the power output. This pressure ratio is called the optimal pressure ratio. The ideal thermal efficiency and the ideal specific kinetic power are plotted for various temperature and pressure ratios in Figure 2.7.

It can be observed that for increasing thermal efficiency at maximum power output, the temperature ratio and the (optimal) pressure ratio increase. This fundamental thermodynamic result on core performance is the driver behind the increase in TIT and OPR seen in modern engines.

Considering the propulsive efficiency in an idealised case (no nacelle friction, velocity misalignment), as given below, yields

$$\eta_{\text{prop}} = \frac{\sum \dot{m} V_\infty (V_{\text{exh}} - V_\infty)}{\sum \frac{1}{2}\dot{m}\Big(V_{\text{exh}}^2 - V_\infty^2\Big)}. \tag{2.9}$$

Note that $\lim_{V_{\text{exh}} \to V_\infty}(\eta_{\text{prop}}) = 1$: which is to say, the smaller the exit velocity, and thus smaller residual kinetic energy in the wake, the higher the efficiency. Naturally, decreasing the velocity difference also reduces the thrust per unit massflow. To ensure sufficient thrust power, yet maximise efficiency, modern engines have increased massflow significantly at lower velocities. This translates to the observed rise in BPR and decline of FPR.

Next, engine emissions are considered. When it comes to CO_2 emissions they are directly related to the fuel burn. But for Nitrous Oxide (NO_x) emissions, another key factor in aircraft environmental impact [2], [53], the details of the combustion process itself is also key.

The NO_x formation mechanisms, thermal and prompt, increase significantly with temperatures and pressures above a certain point [54]. Any increase in TIT and OPR without improvements in combustion technology hence lead to increased NO_x emissions. There is therefore an implicit trade-off to be

made between NO_x and CO_2 when determining the appropriate OPR. This trade-off has been codified in the emission targets by the Committee on Aviation Environmental Protection (CAEP), as is shown in Figure 2.8:

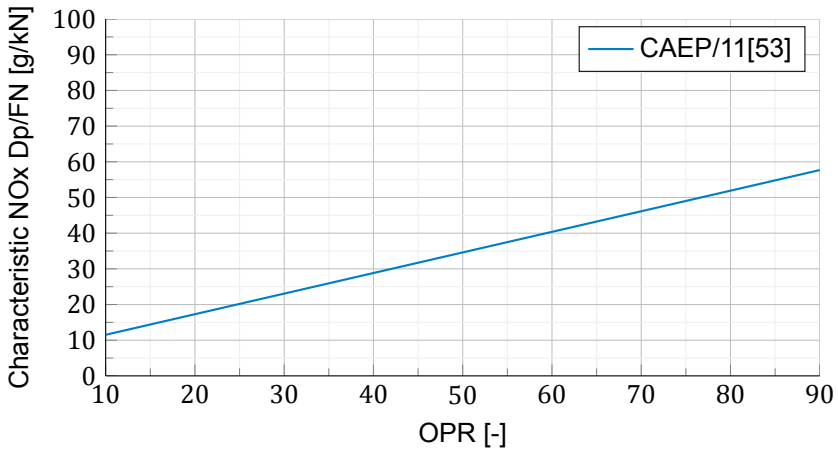

Figure 2.8: NO_x target as function of overall pressure ratio

Thermal Management

Thermal management is essential to engine design, and becoming an increasing challenge for aircraft and engine design [51]. Turbine cooling is the most consequential of thermal management challenges. The requirements on turbine cooling and its impact are discussed in previous sections 2.1.2 and 2.1.3. Van Heerden et al. [51] present an extensive overview of current and potential future thermal management in engines and aircraft. From this, two topics will be highlighted in the rest of this section: T3 temperature limits and oil engine cooling.

With the increase of OPR, the temperature at the HPC outlet has been ever-increasing to the point that the temperature of the compressor components are nearing their limits. Given the high degree of complexity when it comes to designing compressor blades, and the choice of their materials, this issue is not easily overcome. Many design studies, even for engines into 2050, thus constrain T3 as is noted in Table 2.2.

An important component of thermal management in the engine is cooling by means of lubricating oil. Shafts and gears generate a substantial amount of heat due to friction; the energy is absorbed by the lubricant. The lubricant in turn needs to be cooled, this is done by means of so-called Fuel to Oil Heat Exhangers (FOHEX) in addition to Air to Oil Heat Exchangers (AOHEX) [55]–[58]. The fuel is stored at low temperatures and acts as a good sink. Additionally, increasing the temperature of the fuel also increases combustion efficiency [58]. The fuel temperature however cannot become too high as gumming or even coking deposits would form. Hence, the fuel alone is not always sufficient to cool the lubricant and is then supplemented by AOHEX [55]. Note that the fuel can therefore not be used as a sink for the CCA concept, unlike as suggested by Gu and Min [59].

Aerodynamics

Aerodynamic considerations show up in almost all levels of engine design. In particular when it comes to turbomachinery, the right number of stages, the use of variable stator vanes or bleed to prevent engine stall, etc. [11]. The scope of this section will be limited to tip losses in blades and specifically the constraints that arise from it. First, losses related to compressibility effects that limit tip speed are discussed. Second, losses related to tip leakage that limit the last compressor blade's height are considered.

In order to limit losses from transonic effects the flow speed near the tip of turbomachinery components should be limited [11]. In practical terms, this limits the speed of the fan tip, which is the rotational speed by the fan diameter. For higher BPR and engine massflow the fan diameter increases meaning the rotational speed has to decrease. In conventional 2-spool architectures, this also means the rotational speed of the low pressure turbine, also known as the booster; and the low pressure turbine are also reduced. For both, this negatively impacts the component efficiency. Additionally, the LPC stage pressure ratio that can be reasonably achieved reduces: meaning that the number of stages would need to increase to maintain the same LPC pressure ratio. Introducing a gear between the LPC and fan is a way to decouple the rotational speeds for the components; allowing them to operate at the most efficient operating conditions. A graphical demonstration of the relationship between BPR and the turbomachinery components is given in Figure 2.9.

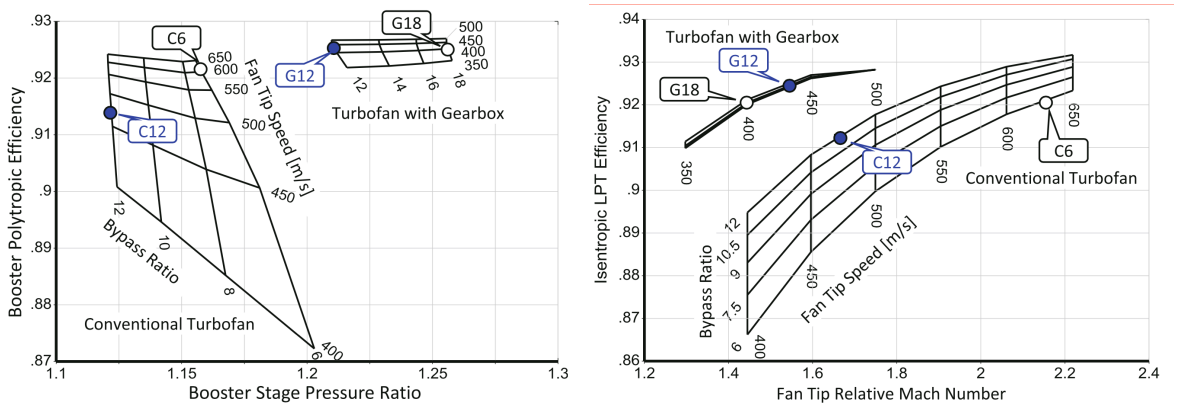

(a) Low Pressure Compressor/ "Booster" efficiency and pressure ratio (b) Low Pressure Turbine efficiency

Figure 2.9: Impact of BPR for given fan tip speed on low pressure turbo-machinery component parameters for conventional and geared turbofans [11]

An alternative solution to a gear is to opt for a 3-Spool architecture. The LPT turbine rotational speed is still linked to the fan; but the compressor between the fan and HPC is uncoupled. Note that no future engine concept uses this architecture (see section 2.2.2).

Tip leakage is another relevant turbomachinery loss mechanism. Air flows from the pressure side of the blade over the edge to the suction side, potentially creating separation bubbles and vortices. In Figure 2.10a this phenomena is visualised.

The impact of this effect is dependent on the ratio of the blade height and the gap between the tip and the wall; in which a small tip gap is favourable [37]. The blade height is determined by axial flow area and (for example) the mean radius of the rotor. The former is dictated by the total (core) massflow and pressure; and the latter is a non-trivial choice based on structural and aerodynamic considerations. For high OPR, the axial flow area is such that the last blade row on the HPC is of the order of tens of millimetres [22]. At this scale, the tip leakage losses start growing unacceptably large. Significant advancements aimed at reducing the impact, such as the use of shrouded blades and active clearance control systems, are detailed in literature [61]. Despite these advances, tip leakage can still have a large impact for very low blade heights. One method to model the impact is to apply a correction to the efficiency as function of the blade height, as is shown in Figure 2.10b. Often, the blade height is directly or implicitly (via OPR) constrained, as can be observed in Table 2.2.

Size

The overall size of an engine has both practical and performance implications. Engines are designed with a range of airframes in mind. In order to ensure there is enough clearance between the engine and the ground, the fan diameter cannot be too large.

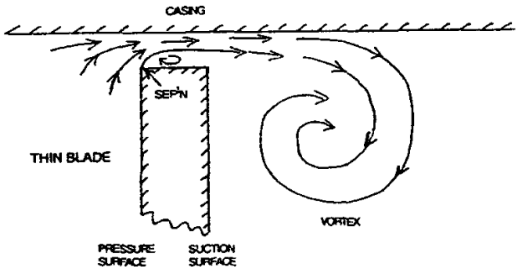

(a) Schematic of flow over the tip over an unshrouded blade [37]

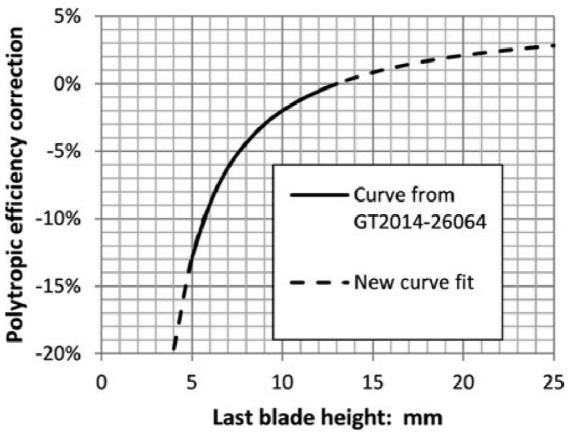

(b) HPC Efficiency Correction for excessive tip leakage as a function of the last blade height [22], [60]

Figure 2.10: Blade tip leakage

In terms of the performance impact, the size of the engine dictates the size of the nacelle. Air flowing past the nacelle experiences drag, reducing overall thrust. Additionally, the nacelle weight increases with the diameter. The drag and the weight grow with the BPR whereas the fundamental propulsive efficiency has decreasing benefit from increasing BPR. This implies there is an optimum BPR for overall "installed engine" performance [11]. For this feasibility study a specific airframe is not defined, but in comparison to the reference baseline engines, the fan diameter may not grow.

Weight

Managing weight in aircraft design in general involves careful management of tradeoffs, as there is a risk of positive feedback loops making it difficult to find suitable equilibria. Namely, for every unit of mass the aircraft, needs to generate lift. This, in turn, causes drag, which is to be overcome by the engine by burning fuel. An incremental increase in the aircraft weight means that for all these steps additional extra weight is added. This is demonstrated in Figure 2.11.

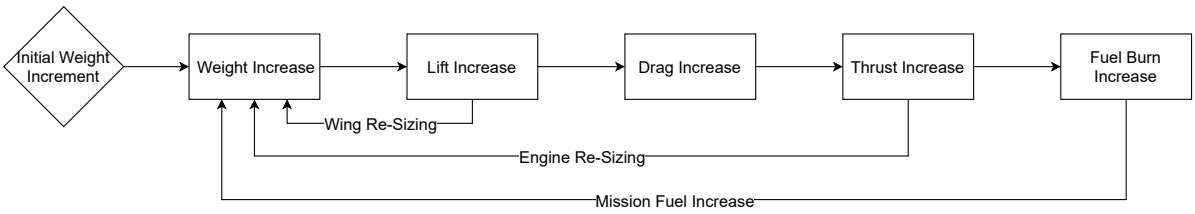

Figure 2.11: Schematic of The Aircraft Weight Feedback Loop

This feedback loop naturally holds for changes in engine weight too. In order to quantify the impact of the weight changes of an engine without an aicraft model one can consider semi-emperical relationships like the one given in equation 2.10 [62].

$$\Delta\text{FB} = 151\Delta\overline{\text{SFC}} + 0.206(\Delta W) + 1.6\left(\frac{d_{\text{fan}}}{d_{\text{fan,ref}}} - 1\right) \tag{2.10}$$

This specific equation was developed for a mission of length 13000 km or 7000NM. The ΔFB is the additional fuel burnt over the whole mission, $\Delta\overline{\text{SFC}}$ is the weighted average of the change in SFC for MTO (1%), MCL (6%) and CRZ (93%).

Engine Design Constraints

The various drivers explored above, as well as other factors, inform the appropriate constraints to apply in conceptual design studies. In Table 2.2, a non-exhaustive overview is given of various design

constraints as found in recent projects. The aim of this table is to inform the constraints applied to this thesis.

Comp.	Parameter	Consrain	Engine Type	Note	Ref.
HPC	Last blade height	>12 mm >12.7 mm >15 mm	IRA		[63] [64] [65]
	Max. outlet temp. (T3)	880K @CRZ	yr. 2050 GTF & OR	”for cooling and structural integrity reasons”	[66]
		1063K @MTO 992K @MCL 880K @CRZ	yr. 2050 GTF& IC TF	Limit from ’2050 Baseline engine’ operating point	[22]
		900K @MTO 1000K	IC TF yr 2025 GTF & ITB TF	 ”to ensure satisfactory engine life”	[67] [68]
	OPR	75	yr. 2025 GTF & ITB TF		[68]
CC	Max. outlet temp (T4)	1950K @MCL 1950K@MTO 1890K@MCL	IRA yr. 2050 GTF& IC TF		[63] [22]
		1850K @MTO 2200K @MTO	IC TF yr. 2025 GTF & ITB TF		[67] [68]
HPT	Max. metal temp. (T_b)	1350K 1337K @MTO	generic GTF & OR IRA		 [63]

Table 2.2: Summary of Specific Engine Constrains from Literature

2.2.2. Recent Research on Innovative Configurations

To examine the feasibility of the CCA going forward in time, it is interesting to investigate what a future engine will look like. Although developments are being made on (hybrid) electric propulsion, this is considered out of scope. This section discusses specific engine design concepts, most of which were part of large EU funded projects. The purpose of this is to identify engine trends and identify a good future engine baseline for the thesis project. Additionally, attention is paid to specific concepts and architecture that may yield synergies with the CCA concept.

As a starting point; Sieber [69] provides a review of large engine projects (that commenced prior to 2015). An overview including more recent projects is provided in Table 2.3. Of the engine projects, the following four have developed whole engine platforms; NEWAC, LEMCOTEC, ENOVAL & ULTIMATE.

In NEWAC four engine concepts were developed for entry into service (EIS) of 2050; with Intercooled and Recuperative Core (OPR ±25); “Active Core” (OPR 35-40); “Flow controlled core” (OPR 35-40); Intercooled core (40-50). The first two concepts are 2-shaft geared turbofans, the flow controlled concept a geared counter rotating fan engine and the last concept used a 3-spool direct drive turbofan. In the active core concept, the cooled cooling air is implemented as is discussed in section 2.1.1. The NEWAC project also operated as validator for new lean combustion methods [17].

LEMCOTEC and ENOVAL were highly integrated projects. The main objective of LEMCOTEC is the development and validation of engine-core technologies for future engines whereas ENOVAL accesses whole engine concepts with some of these core technologies. Three engines with EIS 2025 were developed as part (with hardware realised at module level). The full engine concepts are all

geared turbofan engines with BPR 16.2 at various sizes (TO FN: 86kN, 252kN, 340kN) with corresponding OPR (55, 73, 59).

The ULTIMATE project is comparatively a significantly smaller project (3.1 M€) [70]. In total 7 different engine concepts with EIS 2050 were developed. 5 of which are geared turbofans, and 2 are geared counter rotating open rotor concepts. In the concepts various novel combined cycles as well as combustion technologies, such as pulsed detonation combustion, were tested [71].

Next to these engine projects, Mastropierro et al. [66] modelled and optimised a midsize (FN: 183kN) geared turbofan and open rotor engine designs for EIS 2050, using “Propulsion Object Oriented Simulation Software”. the optimised GTF design has a BPR of 16.8 and OPR 75. This research is particularly noteworthy for the extensive engine data provided.

Three common core architectures can be found in the reviewed literature. Namely Conventional, Intercooled and Intercooled Recuperated. Figure 2.12 shows the thermal efficiency of the architectures, as well as a representative T-S plot. Of the architectures, IRA is the most thermally efficient, but is limited in OPR. This ultimately limits the ability to increase BPR and therefore propulsive efficiency. IRA is most suited for small engines, for which the ideal pressure ratio is lower due to the last blade height penalty and general parasitic losses [11], [88]. Given the low comparative OPR the T3 is modest and hence turbine cooling is less of a concern. In the Intercooled architecture, T3 is similar to a conventional cycle, in spite of the higher OPR. This means both architectures have high turbine cooling requirement. Given that for the intercooler the BP air is already used as a heat sink, it may be more difficult to install a heat exchanger for CCA too.

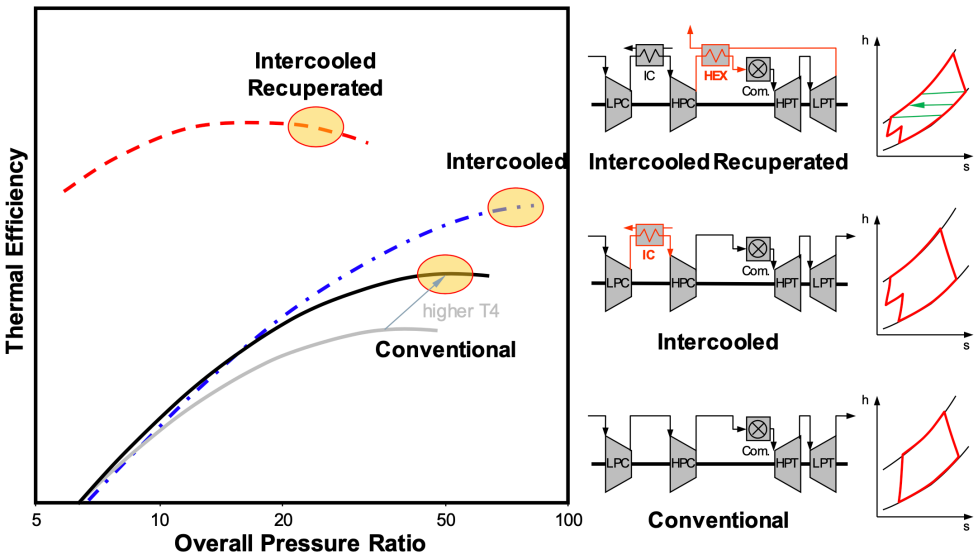

Figure 2.12: Qualitative representation thermal efficiency of different architectures as function of OPR [69]

High level conclusions that can be drawn from the considered literature are summarised below;

- Bypass Ratios are expected to grow to 16-20 for future engines (EIS 2025-2050).
- The expected OPR is strongly architecture dependent; with Intercooled and recuperated OPR<30; (geared) conventional turbofan OPR 50-75 and for Intercooled 50-90.
- HPC tip leakage and material temperature limits form the current constrain on T3/OPR (not turbine cooling).
- All future concepts utilise lean combustion methods.

- Geared Turbofan engines with 2 spools seems to become the new norm, with no direct drive 2 spool and few 3 spool concepts being proposed by researchers or manufacturers.

Project			Focus		Ref
Abbrv.	Title	Year	Tech.	Comments	
UEET	Ultra Efficient Engine Technology	1999-2005	Core, LP, Noise, Subsystem & integration	Turbofan, BPR 10-20, OPR 35; Geared Turbofan; Intercooled Turbofan	[72]
EEFAE	Efficient and Environmentally Friendly Aero Engine	2001-2005	Core & LP	Turbofan, BPR 7, OPR 35; Geared Turbofan; Intercooled Recuperated	[73]
SILENCER	Significantly Lower Community Exposure to Aircraft Noise	2001-2007	Noise	Turbofan, aircraft, nacelle, new design and retrofit	[74], [75]
VITAL	Environmentally Friendly Aero Engine	2005-2011	LP	Turbofan, Geared Turbofan, Contra- rotating Turbofan, BPR 10-14	[76], [77]
NEWAC	New Aero Engine Core Concepts	2007-2011	Core	Turbofan, Geared Turbofan, OPR 40-50; Intercooled & Intercooled Recuperated	[17], [20], [78]
DREAM	Validation of Radical Engine Architecture Systems	2008-2012	OR & Alt. Fuel	Open Rotor, (Turbofan)	[79]
OPENAIR	Optimisation for Low Environmental Noise Impact Aircraft	2009-2013	Noise	Turbofan, Geared Turbofan, aircraft	[80], [81]
LEMCOTEC	Low Emissions Core-Engine Technologies	2012-2017	Core	Turbofan, Geared Turbofan, Open Rotor, OPR up to 70	[82], [83]
E-BREAK	Engine Breakthrough Components and Subsystems	2013-2017	Subsystem	Turbofan, Geared Turbofan, Open Rotor, Turboshaft	[84], [85]
ENOVAL	Engine Module Validators	2014-2018	LP	Turbofan, Geared Turbofan, BPR up to 20	[86], [87]
ULTIMATE	Ultra low emissions technology innovations for mid-century aircraft turbine engines	2015-2018	Core, LP & Waste heat recovery	Intercooled Geared Turbofan with Pulsed detonation combustion/ supercritical-CO_2 cycle/..., (Counter Rotating) Open Rotor	[70], [71]

Table 2.3: Overview of large recent European engine programs and UEET (Part replicated from [69])

3

Methodology

3.1. Engine Analysis

In this section, the engine analysis method will be discussed. Important definitions and the fundamentals of 0-D cycle analysis are presented. There are excellent resources on engine design available (the reader is referred to [11], [14], [16]). A few items that are of particular relevance to the thesis are highlighted in the section: modelling of a cooled engine and operating conditions.

For the engine analysis, the 0-D engine analysis software tool developed by NLR and TU Delft is used. Extensive information on the development and characteristics of the software can be found in literature [89]. For the purposes of this thesis, some important characteristics of the software will be highlighted throughout this chapter.

3.1.1. General Engine Analysis

As a starting point for the general engine analysis, the engine is idealised into a set of discrete conditions. These conditions are so-called stations and provided with a unique identifier. This is done in accordance with the standard guidelines [90]. A schematic of the engine with stations numbering used across this report is provided in figure 3.1. Note that there are elements included which may not be present in specific cases, like the gear and heat exchanger. These elements are still modelled but functionally dormant (ie. Gear ratio=1:1, $\eta_{gear} = 1$).

The core thermodynamic principles make up the fundamental rule-set for the engine analysis. As only the steady states at the stations are defined, the conservation of mass

$$\sum \dot{m} = 0 \tag{3.1}$$

and the conservation of energy

$$W + \dot{Q} + \sum \dot{m}_i h_i = 0 \tag{3.2}$$

without accumulation terms, are sufficient. The thermodynamic gas model used by GSP completely defines the thermodynamic state of a substance through the pressure, temperature, and composition of the substance

$$h_i, s_i = \mathrm{f}(T_i, P_i, \text{composition}) \tag{3.3}$$

The entropy production within the system is defined as the sum total of the entropy from heat transfer and the net contribution of entropy transfer from mass flows.

$$\frac{\dot{Q}}{T_{\text{ref}}} + \sum \dot{m}_i s_i = \wp_s \tag{3.4}$$

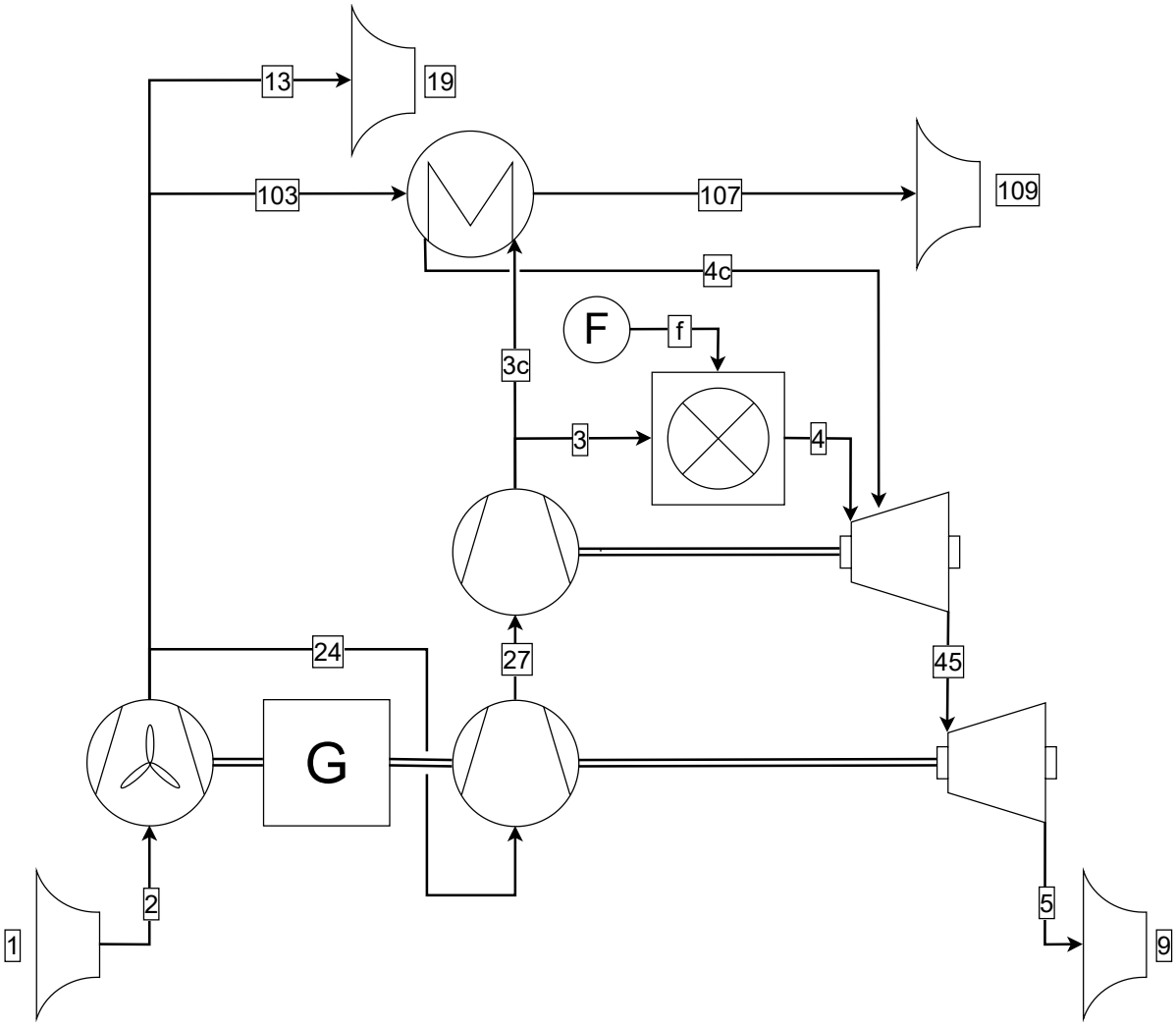

Figure 3.1: Process flow diagram of a 2 shaft geared turbofan with a CCA HEX in the bypass (see figure A.1 for an annotated version)

Turbomachinery

The turbomachinery components are modelled as single-stage machines. Firstly, the compressors are modelled as single-stage machines with the corresponding equations for Euler work

$$W = \dot{m}(h_{\text{in}} - h_{\text{out}}) \tag{3.5}$$

and isentropic efficiency:

$$\eta_{\text{is}} = \frac{\Delta W_{\text{ideal}}}{\Delta W} = \frac{h_{\text{in}} - h_{\text{out,ideal}}}{h_{\text{in}} - h_{\text{out}}} \tag{3.6}$$

The polytropic efficiency is a construct which defines the isentropic expansion or compression as a sequence of infinitely small ideal expansion and compression processes, each with the same constant isentropic efficiency. The formula for the polytropic efficiency under such a definition is given by Equation 3.7:

$$\eta_{\text{poly}} = \frac{\sum \delta W_{\text{ideal}}}{\sum \delta W} = \frac{dh_{\text{ideal}}}{dh} \tag{3.7}$$

With the ratio of temperature for polytropic gasses

$$\frac{T_{\text{out,ideal}}}{T_{\text{in}}} = \left(\frac{P_{\text{out}}}{P_{\text{in}}}\right)^{(\gamma-1)/\gamma} \tag{3.8}$$

the isentropic and polytropic efficiencies can be related symbolically

$$\frac{T_{\text{out}}}{T_{\text{in}}} = \left(\frac{P_{\text{out}}}{P_{\text{in}}}\right)^{(\gamma-1)/\eta_{\text{poly}}\gamma} = \frac{1}{\eta_{\text{is}}}\left(1 + \frac{P_{\text{out}}}{P_{\text{in}}}\right)^{(\gamma-1)/\gamma} - 1 \tag{3.9}$$

For turbines, the numerator and denominator are flipped when compared to compressor in the definition of isentropic efficiency

$$\eta_{\text{is}} = \frac{\Delta W}{\Delta W_{\text{ideal}}} = \frac{h_{\text{in}} - h_{\text{out}}}{h_{\text{in}} - h_{\text{out,ideal}}}, \tag{3.10}$$

and polytropic efficiency

$$\eta_{\text{poly}} = \frac{\sum \delta W}{\sum \delta W_{\text{ideal}}} = \frac{dh}{dh_{\text{ideal}}}. \tag{3.11}$$

Similarly, as was done for the compressor efficiencies, for turbines, the following relationship applies under the same underlying assumptions.

$$\frac{P_{\text{out}}}{P_{\text{in}}} = \left(\frac{T_{\text{out}}}{T_{\text{in}}}\right)^{\gamma/((\gamma-1)\eta_{\text{poly}})} = \left(\frac{1}{\eta_{\text{is}}}\left(\frac{T_{\text{out}}}{T_{\text{in}}} - 1\right) + 1\right)^{\gamma/(\gamma-1)} \tag{3.12}$$

In order to simulate the off-design performance of the different turbomachinery components, so-called “performance maps” are used. Performance maps are defined using the pressure ratio and corrected mass flow

$$\dot{m}_{\text{cor}} = \dot{m}\frac{P_{\text{ref}}}{P_{\text{in}}}\sqrt{\frac{T_{\text{in}}}{T_{\text{ref}}}\frac{R}{R_{\text{ref}}}\frac{\gamma_{\text{ref}}}{\gamma}}, \tag{3.13}$$

and the corrected rotor speed

$$N_{\text{cor}} = N\sqrt{\frac{T_{\text{ref}}}{T_{\text{in}}}\frac{R_{\text{ref}}}{R}\frac{\gamma_{\text{ref}}}{\gamma}} \tag{3.14}$$

The compressor map, used for the low and high pressure compressors in this thesis, is given as a sample in 3.2. The map is scaled in accordance with the specified design point state to tailor the performance map to the specific application. Though it can be argued there are inaccuracies introduced by using such a general performance map for the off-design performance, such an approach is common for preliminary engine design [11], [14], [16].

In order to be able to apply the last blade correction to the HPC in case, if relevant, the last blade height is to be determined. In order to do this, information about the compressor gas path is needed. The hub-to-tip ratio is assumed to be 0.925 and the Mach number at the compressor outlet is 0.254 based on suggested value in literature [17]. Using the definition for the blade height

$$h_b = R_{\text{tip}} - R_{\text{hub}} \tag{3.15}$$

and the flow area

$$A_3 = \pi(R_{\text{tip}}^2 - R_{\text{hub}^2}) \tag{3.16}$$

the last blade height can be related to the flow area and the hub-to-tip ratio

$$h_b\left(1 + \frac{R_{\text{tip}}/R_{\text{hub}}}{(1 - R_{\text{tip}}/R_{\text{hub}})^2}\right) = \frac{A_3}{\pi}. \tag{3.17}$$

Furthermore, the flow area can be determined using the massflow, assumed mach number and the thermodynamic state at the HPC outlet

$$A_3 = \frac{\dot{m}_3}{\rho_3 V_3} = \frac{\dot{m}_3}{P_3/(RT_3)\cdot M_3\sqrt{\gamma RT_3}} = \frac{\dot{m}_3\sqrt{RT_3}}{P_3 M_3\sqrt{\gamma}}. \tag{3.18}$$

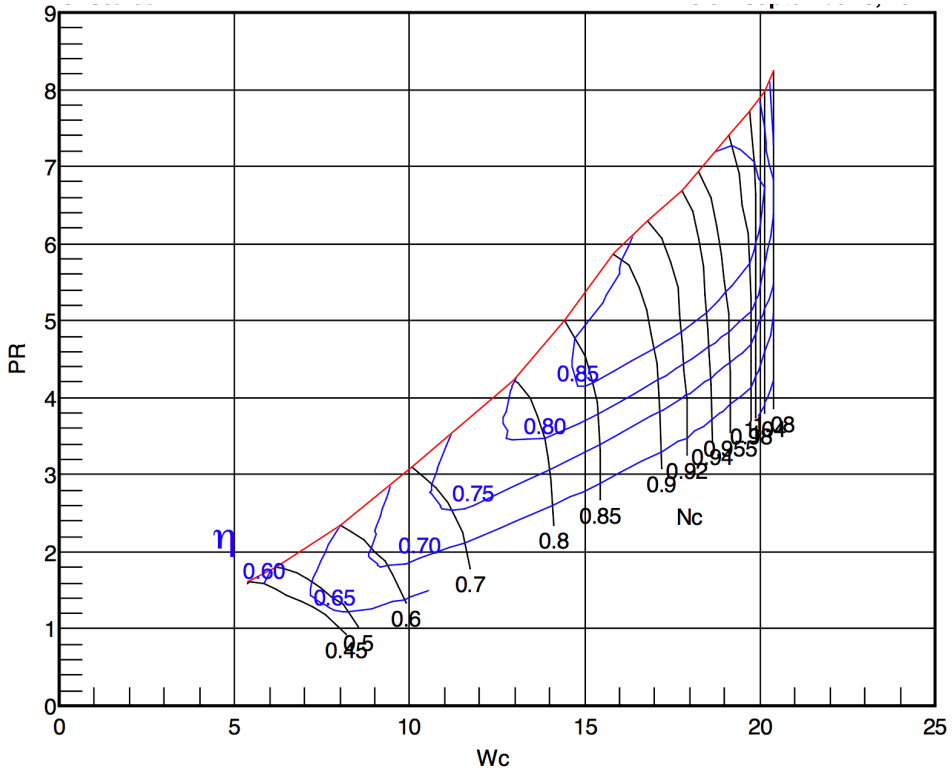

Figure 3.2: Sample compressor map used for determining off design performance [89], where Wc is the corrected massflow, Nc is the corrected rotor speed and PR is the pressure ratio. The red line (along the top) indicates the surge line.

Combustion Chamber

The energy released from an ideal chemical reaction per unit of fuel in the combustion chamber is defined by the lower heating value (LHV). The lower heating value of the fuel, Jet A/A-1, is 43.2MJ/kg [91]. The difference between the ideal and real energy release, caused by the formation of combustion radicals, is defined by the combustion efficiency, η_{comb}. The enthalpy at the exit of the combustion (station 4) can be determined using the energy balance

$$\dot{m}_4 h_4 - \dot{m}_3 h_3 = \dot{m}_f \text{LHV}\, \eta_{\text{comb}} \tag{3.19}$$

The massflow at the exit of the combustor is the sum of the entry air massflow, $\dot{m}_3$, and the fuel massflow, $\dot{m}_f$. In this thesis, the outlet temperature (thus implicitly h_4) of the combustor is fixed and the fuel massflow is to be solved using the aforementioned equation. Note that the gas mixture is different post-combustion, and as a result, the specific heat is increased.

Heat Exchanger

Despite being core to the cooled cooling air concept, the heat exchanger performance is prescribed. This was to be an initial step of the approach in order to established requirements on a detailed heat exchanger design. However, as the cooled cooling concept is shown by the results to be infeasible, there is no need to define a more detailed model.

The heat exchanger performance is prescribed implicitly by setting a coolant feed temperature change, ΔT_c,

$$T_{4c} = T_3 + \Delta T_c \quad \text{where } \Delta T_c \leq 0 \tag{3.20}$$

With the new coolant temperature, the enthalpies at the hot side of the heat exchanger are defined and the cold side outlet condition (h_{107}) and the heat duty can be determined:

$$\dot{Q} = \dot{m}_c (h_{3c} - h_{4c}) = \dot{m}_{103} (h_{107} - h_{103}) \tag{3.21}$$

A common heat exchanger performance metric and/or design input is the effectiveness ε, given by

$$\varepsilon = \frac{Q}{Q_{max}} = \frac{\dot{Q}}{[\dot{m}c_p]_{min}|T^a_{\text{in}} - T^b_{\text{in}}|}. \tag{3.22}$$

For numerical reasons, the coolant feed temperature change as is taken as the input parameter, however. As the parameter directly determines the cooling fraction, the simulation stability is greatly improved when compared to a prescribed effectiveness.

Exhaust Nozzle
The main gas flow(s) accelerate(s) through the exhaust nozzles before leaving the engine. Thrust is produced in the process as shown in Equation 2.3. The velocity at which the flows leave is dependent on the total pressure of the flow and the ambient pressure. The critical pressure ratio, a ratio of upstream and downstream pressure marking the transition from choked to unchoked flow, is defined as

$$PR_{crit} = \left(1 - \frac{\gamma - 1}{\eta_{\text{is}}(\gamma + 1)}\right)^{(\gamma-1)/\gamma} \tag{3.23}$$

As for convergent nozzles, the flow is limited to mach number of 1, the velocity can be determined for both choked ($PR < PR_{crit}$) and unchoked flow ($PR > PR_{crit}$):

$$V_{exh} = \begin{cases} \sqrt{\gamma R T s_9} & P_9/P_\infty > PR_{crit} \\ \sqrt{2(h_9 - hs_9)} & \text{otherwise} \end{cases} \tag{3.24}$$

The static enthalpy at the outlet is determined from the ideal expansion shown in Equation 3.8.

3.1.2. Cooled Engine Analysis

In a cooled engine, one needs to account for the impact that the introduction of this air has on the turbine performance. Turbine cooling air is added in a distributed fashion across the stages. The equations used in the engine analysis, however, are 0-D. A solution to this is to consider the cooling flow to be added discretely before and after the turbine [11]. The air added before the turbine, so-called ”non-chargeable”, will contribute to the power output of the turbine, whereas the air added after the turbine does not contribute to the power generation and is called ”chargeable”. Typically, all of the stator cooling air and only some of the rotor cooling air are considered non-chargeable in single-stage machines.

As most current and future high pressure turbines in literature use a two-stage high pressure turbine, the aforementioned approach is adapted under the assumption that the two-stage machine can be modelled as a virtual one-stage machine. The cooling flows are subsequently accounted as chargeable or non-chargeable based on the perceived impact they have. This method of accounting is shown in Figure 3.3.

In GSP, a distinction is made between the portion of cooling flow contributing to the extraction of power (“Press. Frac.”) and affecting just the total massflow rate (“Frac. Eff. T.flow”). The “Press. Frac.” parameter dictates what part of the flow is considered non-chargeable. In GSP, this flow expands with the turbine pressure ratio, but starting from the feed temperature to a fictitious outlet temperature. This means that for the same work that is extracted per unit, massflow is lower when compared to the main gas flow. Note that the mixing with the main flow as discussed below occurs after this expansion. The “Frac. Eff. T.flow” parameter is used to specify if the massflow of the cooling flow is to be considered part of the total turbine flow for the purposes of specifying the operating point on the turbomachinery performance maps only. It should be noted that this only affects off-design performance, as the maps are scaled at the design point. For the purposes of this investigation, the distinction between these two effects is not made and corrected massflow and the parameters “Press. Frac.” and “Frac. Eff. T.flow” are kept the same.

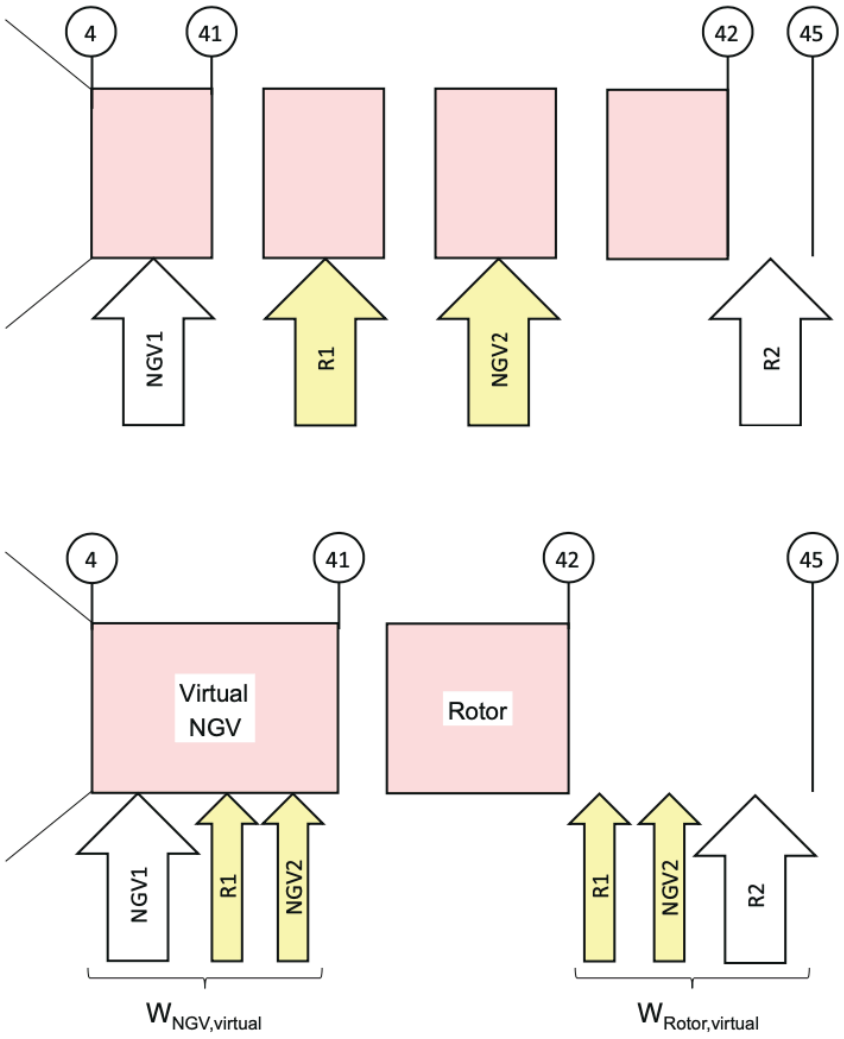

Figure 3.3: Method of accounting for multi-stage turbine cooling flow [11]

Another important consideration is how the cooling and bulk flows are mixed. Several methods for this are discussed in Greitzer et al. [38]. In GSP, the flow is instantaneously mixed using a mass-average. Any excess pressure is not considered, however the option to account for the increase in enthalpy for the cooling flow from flowing through a rotating channel can be included. Power is extracted from the shaft to increase the enthalpy of the cooling flow. If the net power output of the turbine is to remain constant, The average enthalpy of the flow at station 41 will be slightly larger and will be slightly lower at station 42. Crucially, the enthalpy at station 45 is unchanged, however, under the assumption that the turbine efficiency is unaffected. The overall engine performance is hence not affected, and therefore the choice was made not to model this specific effect.

In this study, the required cooling massflow is calculated according to the method given by Equation 2.2 (with $b = 0.05$ for stators and $b = 0.06$ for rotors, and $s = 0.97$) given its ease of use and good correspondence for the considered OPR domain when compared to higher order methods. The gas temperature, required in the method, is determined for the (virtual) stator and rotor separately. The gas temperature is approximated as the geometric average between the inlet and outlet stations for a fictitious uncooled turbine. Specifically, the temperature of the stations of this fictitious uncooled turbine is calculated using the actual pressure ratio, turbine efficiency, the combustor outlet temperature and an assumed degree of reaction of 0.5. The gas temperature for the stator is

$$T_{g,\text{stator}} = T_4\left(\frac{3}{4} + \frac{1}{4}(\Pi_{\text{HPT}})^{\eta_{\text{poly}}(\gamma-1)/\gamma}\right), \tag{3.25}$$

and for the rotor

$$T_{g,\text{rotor}} = T_4\left(\frac{1}{4} + \frac{3}{4}(\Pi_{\text{HPT}})^{\eta_{\text{poly}}(\gamma-1)/\gamma}\right). \tag{3.26}$$

3.1.3. Operating Conditions

Aero engines go through cycles with many different thrust settings and environments, and thus they go through different operating conditions. For preliminary design, typically three representative points are selected: Take-Off, Top of Climb, and Cruise [11], [68]. The first two conditions represent extremes the engine can be expected to operate nominally, whereas the latter is where the engine works for the majority of the time. At Take-Off conditions, the maximum operating temperatures are reached, as well as often the highest spool speeds. Therefore, the cooling circuit and the mechanical integrity of the shafts and disks are assessed at this condition. The Top of Climb condition is the most demanding condition from an aerodynamic point of view, and the maximum corrected massflow and overall pressure ratio occurs there. Finally, the Cruise condition, given the long duration, is by far that which most affects overall fuel consumption of the engine. The weights for the different flight phases to the average SFC in equation 2.10 exemplifies of this. Hence, at Cruise, the specific fuel consumption should be minimised.

Given that the focus of this thesis is the cooling system, the Take-Off conditions will be investigated and considered as the primary design point. Although multipoint design studies are common nowadays [11], this is not natively possible with the GSP software tool. As well as Take-Off, the Cruise condition will also be considered; as ultimately the objective of the investigated CCA solution (and therefore the metric for feasibility) is to reduce the specific fuel consumption at Cruise conditions.

Regarding the ambient conditions, the international standard atmosphere (ISA) is used with a +15K temperature off-set at Take-Off. The specifications of the environment at the considered operating conditions are presented in Table 3.1.

Parameter	Unit	Take-off	Cruise	Top of Climb*
Altitude	km	0	11.3	10.7
Ambient Static Temperature	K	303.15	216.65	228.60
Ambient Mach Number	-	0.2	0.78	0.82
Water Vapour Mass Fraction	-	0.01	0.01	0.01

Table 3.1: Atmospheric conditions for ISA air of the operating conditions (*Top of Climb only for verification)

3.2. Approach & Test Cases

3.2.1. Overall Performance Analysis

In order to address research objective 1, which covers the feasibility of CCA as a strategy to improve turbine cooling performance, the CCA concept has been applied directly to two engine test cases. Dedicated GSP models were implemented to assess the achievable SFC at Cruise and Take-Off as a function of the main HEX design parameters.

With increasing CCA heat exchanger effectiveness, the massflow (fraction) through the combustion chamber and the HPT increase. This results in an increased core-specific power output. This means that for the same engine parameters, the core exhaust pressure increases for higher coolant temperature change, and subsequently net engine thrust increases. However, excess(-ive) core exhaust pressure implies unused potential in the exhaust, unfairly penalising the CCA concept in terms of SFC. One method of using this excess energy is increasing the bypass ratio.

In an ideal scenario, one would re-optimise the engine. This includes all engine parameters: fan pressure ratio, bypass ratio, overall pressure ratio and potentially even T4. However, this is a difficult exercise: conversely increasing bypass ratio without accounting for induced changes in component efficiencies is a fair (and generous) method to use the excess energy.

Hence, the parameters that were changing in the engine design are the effectiveness of the heat exchanger (in this case, determined by ΔT_c), and the BPR. In the simulations completed for this study, the ΔT_c was varied from 0K to -300K. This domain was chosen to align to the temperature change common in the literature (see section 2.1.1), which is typically determined at around -200K. Furthermore, increasing temperature differences between the cooling temperature and gas temperature significantly beyond the domain chosen for these simulations would result in an increasing level of thermal stresses induced onto the turbomachinery components (see section 2.1.4).

The bypass ratio domain used in these simulations is informed by initial trials of granularly increasing the bypass ratio until the exhaust pressure is insufficient (ie. lower than ambient pressure). This results in a take-off bypass ratio domain for the Leap-1A engine covering the range 10.22 to 11.72, with the higher bypass ratio only achievable when employing the CCA heat exchanger. For the GTF2050 engine, following a similar approach, a take-off bypass ratio domain of 16.14 to 17.94 was determined for investigation.

With these parameters, an initial performance domain was established, presented in section 5.2.1. Every state in the engine is determined, and the SFC, thrust, and exhaust pressure in particular, are examined to determine the feasibility of the CCA model as applied to an existing engine design.

These specific fuel consumption results are then normalised to be expressed in percentage terms with respect to the baseline SFC. This permits comparison of trends between the two test cases, as well as between the two operating conditions under consideration, on a like-for-like basis.

Subsequently, when the result is then mapped for bypass ratio versus exhaust pressure at a given heat exchanger coolant temperature change, it is possible to establish a function to determine the bypass ratio such that the exhaust pressure is kept constant. This permits the easy addition of further variables to the study, in this case the pressure loss in the heat exchanger, which enables a more holistic assessment of the overall efficiency of the system–further addressing research objective 1.

3.2.2. Scenario Impact Tests

Scenario Impact Tests (SITs) were conducted to establish the feasibility of the CCA concept, and the applicability of the earlier results, in exceptional conditions. This additionally provides useful data that can establish more clearly the dominant factors driving the underlying results. These SITs covered:

1. Evaluating the impact at Take-Off of the cooling flow-to-HPT efficiency relationship

2. Evaluating the Cruise SFC for lower CCA HEX effectiveness than at the design condition (TO)

3. Evaluating the Sensitivity of specific fuel consumption on cooling requirement parameters

From literature, it is known that increasing cooling flow has a definite impact on turbine efficiency. The scale of this impact is highly dependent on turbomachinery design parameters and the cooling scheme employed. Even so, for a given turbomachinery geometry, it is difficult to predict the added losses from the cooling injection. Therefore, it is useful to examine the order of impact from changing the turbine efficiency. A significantly higher or lower result from tests run under alternative HPT efficiency assumptions can therefore be indicative of relevance (and dominance of any effect on overall efficiency) of this specific mechanism. SIT 1 tested this by comparing the nominal results (using the method discussed above) to the same simulation where the value of the HPT efficiency is fixed at the baseline instead of being variant in cooling massflow.

SIT 2 follows the guidance of literature regarding the marginal impact of the heat exchanger at Cruise. For every ΔT_c value set for Take-Off, multiple ΔT_c were tested (at increments of 0.2x covering the range from 1.2x to 0x) for the corresponding Cruise conditions.

The final scenario (SIT 3) aims to test the robustness of the underlying relationship between cooling temperature and required massflow assumed in the overall performance impact simulations. These simulations follow Equation 2.2, which covers the cooling massflow needed based on cooling temperature, material allowable temperature, and gas flow temperature; with a decrease in the cooling temperature also decreasing the required massflow. Values for the input parameters exponent s and the maximum allowable material temperature are varied from 0.9 to 1.05 and 1380 K to 1440 K respectively. The values for the constant b are not considered, as the impact on cooling requirement is simply linear. Note that the exponent s and the allowable material temperature are varied beyond the range found in literature. Thus, if the initial results hold even at these different input parameters, the underlying principles of the Performance Impact Analysis can be understood to be robust.

These SIT tests therefore address research objectives 2 and 3 regarding the parameters and conditions necessary for feasibility, and provide the foundations for further investigation of research objective 4, which is explored in detail in the Exergy Analysis detailed below.

3.2.3. Exergy Analysis

In order to better understand the phenomena driving the impact of the cooled cooling air concept on engine SFC, an exergy analysis is performed. Exergy is a measure of the total available work that can be extracted from an energy source (for the fundamentals of exergy analysis, the reader is referred to [92], [93]).

Exergy destruction during a process is therefore a quantification of irreversibly and equivalent to the loss of potential work. Considering the scale of the exergy destruction and rejection at each component provides insight into the relative impact of different loss sources. Furthermore, the change in the exergy destruction and rejection as a function of the CCA HEX design parameters reveals pros and cons of the CCA concept with respect to the different loss mechanisms. This result provides a definite answer about its feasibility and limits from a thermodynamic standpoint. In the following paragraphs, the definitions and equations used for the exergy analysis are presented.

The definition of exergy, ζ, at station i reads

$$\zeta_i = h_i^0 - h_\infty^0 - T_\infty(s_i - s_\infty) \tag{3.27}$$

Where the subscript ∞ refers to the condition in the reference environment, which, in gas turbine simulation, corresponds to the (typically SSL) ambient environment [93]. Note that exergy, as is the work potential, is wholly dependent on the choice of reference environment.

Combining the balance equations for energy and entropy of an open control volume, at steady state with no chemical reactions and discrete interactions, lead to the exergy balance reported in Equation 3.28:

$$\Big[\sum \dot{m}\zeta\Big]_{in} - \Big[\sum \dot{m}\zeta\Big]_{out} + \sum Q\Big(1 - \frac{T_\infty}{T}\Big) - W - I = 0 \tag{3.28}$$

Here, the subscripts in and out refer to flows in and out of the control volume. Q and T refer to the heat flux and associated heat transfer temperature (i.e. wall temperature). W refers to the work performed by the flow. Finally, I is the exergy destruction, which is proportional to the entropy generation $\wp_s$

$$I = T_\infty \wp_s \tag{3.29}$$

It is possible to distinguish between differing kinds of exergy following the introduction of fuel in the combustor. The fuel exergy is defined as chemical energy, and is composed of two parts: reactive and concentration exergy. The former relates to the energy associated with chemical reaction of the species not in the reference environment whereas the latter is the exergy related to the change in the concentration of the species [93]. A definition of the chemical exergy (per mole) $\bar{\zeta}_{ch}$ of an ideal gas mixture is given in equation 3.30

$$\bar{\zeta}_{ch} = \sum_k \chi_k \bar{\zeta}_{ch}^k + RT_\infty \sum_k \chi_k \ln \chi_k \quad \text{with} \quad \bar{\zeta}_{ch}^k = -RT_\infty \sum_k \ln \chi_k^\infty \tag{3.30}$$

Where $\bar{\zeta}_{ch}^k$ is the chemical exergy per mole of species k and χ_k and χ_k^∞ are the molar concentrations of species k in the current mixture and the reference mixture respectively. By definition, combustion air has a chemical exergy of 0. After the combustor, the net chemical exergy of the working fluid is then greater. Due to the addition of cooling air, and through the expansion process the specific chemical exergy of the working fluid is not constant, and will vary through the engine.

It is clear that the chemical exergy cannot be calculated assuming the concentration of fuel in the environment. As the fuel practically does not exist in the reference system, equation 3.30 is undefined. It would result that $\chi_k^\infty = 0$ and that $\ln(\chi_k^\infty) \to -\infty$. To resolve this issue, one can consider an ideal reaction of the hydrocarbons in the fuel to form carbon dioxide and water, species that do exist in the reference system (i.e. the environment).

$$\mathrm{C_xH_y} + \left(\mathrm{x} + \frac{1}{4}\mathrm{y}\right)\mathrm{O_2} \rightarrow \mathrm{xCO_2} + \frac{1}{2}\mathrm{yH_2O} \tag{3.31}$$

The chemical exergy of the fuel $\bar{\zeta}_f^{ch}$ can now be expressed as a function of the higher heating value (HHV) or enthalpy of formation and the chemical exergy and entropy of the species (derivation [94]).

$$\bar{\zeta}_f^{ch} = \overline{HHV} - T_\infty\left[\bar{s}_f + \left(x + \frac{1}{4}y\right)\bar{s}_{O_2} - x\bar{s}_{CO_2} - \frac{1}{2}y\bar{s}_{H_2O}\right] - \left(x + \frac{1}{4}y\right)\bar{\zeta}_{O_2}^{ch} + x\bar{\zeta}_{CO_2}^{ch} + \frac{1}{2}y\bar{\zeta}_{H_2O}^{ch} \tag{3.32}$$

For a large set of common gaseous fuels, the value of the chemical exergy has been determined and expressed as a ratio with respect to a lower heating value, $\Phi = \zeta_f^{ch}/LHV$ [95]. The fuel assumed in the analysis, Jet A/A-1, can be modelled as an equivalent molecule of form $C_{11}H_{21}$ with an LHV=43.2MJ/kg [91] and Φ=1.06 [94], [95].

For the high pressure turbine, there are multiple mechanisms at play that induce exergy destruction. Some that are specifically dependent on the cooling massflow, as discussed in Section 2.1.2. For the exergy analysis, a distinction will be made between mixing losses and losses from expansion. Mixing losses arise from the heat transfer between the cooling flow and the main gas flow and viscous losses. The pressure drop of the coolant flow from the heat exchanger outlet to the mixed out state are accounted here. The viscous losses from the injection of coolant specifically are not included here, rather they are calculated from the change of expansion loss based on the reduced turbine efficiency.

$$\dot{I}_{\text{mixing}} = T_\infty\left((\dot{m}_{41}s_{41} - \dot{m}_{c,\text{stator}}s_{4c} - \dot{m}_4 s_4) + (\dot{m}_{45}s_{45} - \dot{m}_{c,\text{rotor}}s_{4c} - \dot{m}_{41}s_{42})\right) \tag{3.33}$$

Regarding the expansion loss, exergy destruction is determined from the entropy production

$$\dot{I}_{\text{expansion}} = T_\infty \dot{m}_{41}\left(s_{42} - s_{41}\right) \tag{3.34}$$

or the exergy balance

$$\dot{I}_{\text{expansion}} = \dot{m}_{41}\left(\zeta_{41} - \zeta_{42}\right) - W_{\text{HPT}}. \tag{3.35}$$

In order to understand the changes caused by the reduction in cooling temperature, the effects are uncoupled (by running multiple simulations). First, the cooling massflow and temperature are reduced. Second, the turbine efficiency is increased. Third, the engine bypass ratio is increased (to utilise the exergy increase at the outlet). It should be noted that the exergy loss quantity is dependent on the pressure ratio of the turbine. Furthermore, the pressure ratio is dependent on the combustor and coolant massflow and inlet temperature. Therefore, when associating exergy losses to these specific effects, the order of the effects is relevant.

As exergy left in exhaust flows outside the control volume can not be accessed any more, one can speak of an exergy loss despite no exergy destruction.

$$\dot{Ex}_{\text{exh,lost}} = \dot{Ex}_{\text{exh,th}} + \dot{Ex}_{\text{exh,ch}} + \dot{Ex}_{\text{exh,lost,kin}} \tag{3.36}$$

All the thermal, calculated with static exhaust temperature, (and chemical exergy) left in the exhaust flow is considered lost. Given that the mere act of (kinetic) exergy leaving the control volume is the sole mechanism by which propulsive power is generated, not all the kinetic exergy leaving the system is lost. Conceptually the same as propulsive efficiency, the following is a definition of the lost or unused exergy in the flow.

$$\dot{Ex}_{\text{exh,lost,kin}} = [\dot{m}\zeta_{\text{kin}}]_{\text{exh}} - V_\infty \mathrm{FN}_{\text{exh}} = \dot{m}_{\text{exh}}\left(\left(\frac{V_{\text{exh}}^2}{2} - \frac{V_\infty^2}{2}\right) - \left(V_\infty(V_{\text{exh}} - V_\infty)\right)\right) - V_\infty A_{\text{exh}}(P - P_\infty) \tag{3.37}$$

$$\dot{Ex}_{\text{exh,lost,kin}} = \dot{m}_{\text{exh}}\left(\frac{V_{\text{exh}}^2}{2} - V_{\text{exh}}V_\infty + \frac{V_\infty^2}{2}\right) - V_\infty A_{\text{exh}}(P - P_\infty)$$

The core exhaust, with its high excess temperature, will therefore a high exergy loss both per unit massflow and in absolute terms. Conversely, given the low thermal exergy and modest kinetic exergy of the bypass flow, the specific exergy loss of the BP is low. Nonetheless, given the high massflow, the bypass' exhaust loss is a significant contributor to the overall exergy destruction.

3.2.4. Test Cases

In this thesis, two test cases are used as baseline for the investigations: the Leap-1A and a conceptual future engine “GTF2050”. In this section, the two engines will be introduced, including the rationale for choosing them. Following that, the design and operating conditions of the engines will be presented.

The CFM Leap-1A engine is a mid-sized engine with max thrust of up to 155 kN that was introduced into service in 2016. A so-called “workhorse” of the aeronautical industry, it has been applied to short- and mid-haul flights with over 2400 engines in service already [96]. A render of the engine is provided in Figure 3.4a.

The Leap-1A engine was chosen as a baseline as it represents the cutting edge of the current engine generation’s technology. The specific variant considered is the Leap-1A26 with a nominal take-off thrust of 121 kN, as a specific numerical model was available in house for this variant.

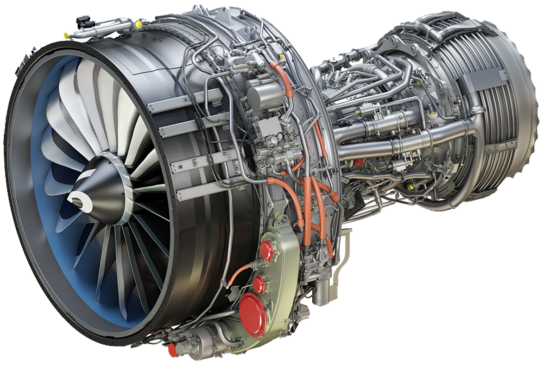

(a) CFM Leap engine **Leap-1A/-1BEngines**

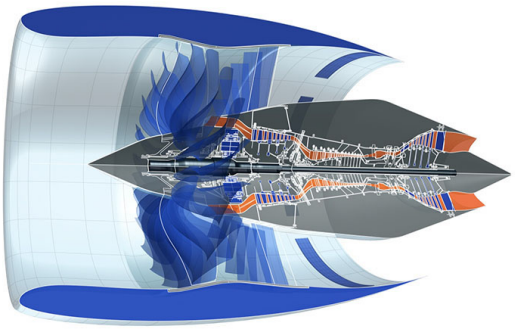

(b) Enoval high BPR ratio geared turbofan engine [97] similar to the GTF2050

Figure 3.4: Representative renders of the testcase engines

The “GTF2050” is a geared turbofan engine concept for entry into service around 2050. In Figure 3.4b a render is given of what such an engine might look like (note that the figure is from another engine project ENOVAL). The engine is an adaptation of the engine concept presented by Mastropiero et al. [66]. The concept is in line with general trends (BPR 16-20, OPR 50-70, two-spool geared architecture) as discussed in section 2.2.2. Compared to the Leap-1A engine, this concept engine represents a conventional mid-size future engine with a higher design take-off thrust of 183 kN. This specific reference was chosen as the paper presenting the engine contains an extensive set of operating parameters particularly useful for verifying the model implementation.

However, the GTF2050 modelled in this thesis differs from the engine presented by Mastropiero et al. [66] in the material selected for the high-pressure turbine, and therefore in the high pressure turbine temperature limit. In the reference, it is assumed that the NGV will be made out of a ceramic material that will not require any cooling. The total cooling fraction required in this theoretical engine is hence only 6%. Given the expectations of future engine technology as discussed in Chapter 2, this is a rather optimistic assumption. Regardless, the CCA concept requires that a significant (nominal) amount of cooling air is used to make any sense. Therefore the material used in the HPT of the adapted engine will have a maximum allowable material temperature of 1380K in line with the findings presented in Table 2.2. The implications, as discussed in Section 4.1.2, of this modelling assumption are that T4 is adapted from 2040 to 2080 and the cooling fraction from 6% to 27% at Take-Off.

For both of the reference engines, the overall engine parameters for the design Take-Off and Cruise condition are presented in Table 3.2.

The component efficiencies are defined at the TO condition as presented in Table 3.3. For the turbomachinery components, the cruise and off-design efficiency will be scaled using generic performance

Parameter	Unit	Leap-1A		GTF2050	
		TO	CRZ	TO	CRZ
Thrust (Net), FN	kN	120.6	20.05	174.2	30.23
Bypass ratio, BPR	-	10.42	11.1	16.14	17.10
Overall pressure ratio, OPR	-	34.0	36.98	60.1	62.1
Specific thrust, SFN	m/s	235.1	116.9	173.8	79.8
Specific fuel consumption, SFC	g/kNs	9.86	14.68	8.37	13.69
Fan Diameter	m	1.98		2.84	
Inlet massflow, $\dot{m}_1$	kg/s	512	171	1002	379
Fuel massflow, $\dot{m}_f$	kg/s	1.20	0.29	1.37	0.38
Cooling massflow, $\dot{m}_c$	kg/s	5.75	2.20	16.01	5.73
Cooling fraction, $\dot{m}_c/\dot{m}_{24}$	-	0.15		0.274	
HPC exit temperature, T3	K	960	730	1057	865
Combustor exit temperature, T4	K	1938	1550	2080	1680
HPT SOT, T41	K	1877	1488	1926	1580
Fan pressure ratio BP	-	1.593	1.54	1.39	1.386
Fan pressure ratio core	-	1.549	1.5	1.27	1.67
LPC pressure ratio	-	1.695	1.7	2.3	2.46
HPC pressure ratio	-	15.66	14.5	20.92	19.90
LP shaft rotational speed	rpm	3892	3663	7928	7330
HP shaft rotational speed	rpm	17490	16312	16336	13958

Table 3.2: Leap-1A and GTF2050 overall baseline engine parameters at Take-Off and Cruise

maps. Note that in contrast to the work of Mastropierro, in this simulation the turbomachinery nominal performance is specified in the model by defining the polytropic efficiency rather than isentropic efficiency. The impact of isentropic efficiency is dependent on the specific pressure ratio to which it is applied [98]. It is therefore not fair to assess the performance using the isentropic efficiency of a (yet-to-be-designed) component when the pressure ratio is not yet fixed, when the pressure ratio of the component is varied in the analysis.

Parameter	Unit	LEAP-1A	GTF2050
Fan η_{poly}	-	0.92	0.93
Fan core η_{poly}	-	0.92	0.93
booster/LPC η_{poly}	-	0.91	0.87
HPC η_{poly}	-	0.92	0.85
Combustor η_{comb}	-	0.9995	0.9995
Combustor PR	-	0.95	0.97
Mechanical η_{is}	-	0.995	1
Mechanical fixed loss	kW	0	50 per shaft
Fan Gear η_{is}	-	n.a.	0.995
Fan Gear ratio	-	n.a.	4.3:1
HPT uncooled η_{poly}	-	0.9255	0.8858
HPT nominal η_{poly}	-	0.908	0.825
LPT η_{poly}	-	0.89	0.90

Table 3.3: Leap-1A and GTF2050 design (TO) component efficiencies

3.3. Overview of Key Assumptions

Type	Assumption	Relevant Section(s)	Impact	Mitigation/ Justification
General Engine Modelling	Component Design Efficiencies/Pressure losses	2.2.1 3.2.4	Moderate (Neutral)	Bench-marked against literature. Will affect also affect baseline performance. marginal cost of cooling is dependent however, in part, on HPC and HPT performance.
	Core size can be scaled without affecting component efficiencies (except HPC)	3.1.1	High (Optimistic)	Limited scaling of massflow only.
	Component off-design Performance	3.1.1	Low (Neutral)	Dependency of CCA parameter on operating condition of turbo-machinery is limited (only HPT moderate impact, which is accounted for)
	CRZ and TO operating conditions sufficient to assess concept feasibility	3.1.3	Medium	
Cooling	Off-take at HPC exit	3.1.2	High (Optimistic)	First stage cooling flow from bulk of total cooling flow.
	Maximum allowable TBC temperature not considered	2.1.4	Medium (Neutral)	Requires more detailed design of the cooling scheme than is in scope for the investigation. Likely respected when upon appropriate T_b limit.
	Cooling Massflow fraction cruise is fixed at take-off value	6.2	High (Neutral)	Necessary assumption for fidelity model. Investigation into active cooling flow management given as recommendation.
	Required cooling fraction can be determined using feed and gas temperature	2.1.3 3.1.2 3.2.2 5.3.3	High (conservative)	Comparison with higher fidelity methods [19] show decent match for OPR ±60 [44]. Alternative coefficients simulated in SIT3
	All HPT cooling flows affected by CCA HEX	2.1.4	Medium (Optimistic)	First stage cooling flow from bulk of total cooling flow
	HPT stage efficiency is linearly dependent on cooling massflow	2.1.2 3.2.2 5.3.1	Low (Neutral)	Small contribution compared to lost work effect [27], [40] and confirmed in SIT1.
	Total pressure of cooling flow assumed at gas pressure for mixed thermodynamic state	2.1.4	High (Optimistic)	
HEX	A heat exchanger with a total relative pressure loss of less than 8% can be designed to meet the required effectiveness	3.1.1 3.2.1	Low (Neutral)	Required effectiveness is low (<0.4).
	The method of determining heat exchanger effectiveness at cruise by means of prescribing the Take-Off coolant temperature change is sufficient to assess concept feasibility	3.2.2 5.3.2	High (Optimistic)	Alternative cruise performances evaluated in SIT2.

Table 3.4: Overview of Key Assumptions; Impact is a qualitative assessment based on (uncertainty of) relevance to CCA performance assessment; where an “optimistic” impact is favourable for the CCA feasibility

4

Method Verification

4.1. Baseline Engine Implementation

4.1.1. Leap-1A

In order to validate the Leap-1A26 model, information made available as part of the certification process was used. Specifically, the fuel flow from the ICAO's emission databank [99] was compared to the predictions of the numerical model developed. At four conditions the fuel flow, as obtained from rig tests, is specified: Take-Off, Top of Climb, Approach and Idle. The model parameters are chosen such that take-off fuel consumption adheres to the reference data. The fuel massflow for the other conditions was changed for until the thrust setting was matched. The comparison with the simulation results is presented in Table 4.1. The ambient condition of the cases Take-Off and Top of Climb are as specified in Table 3.1. The atmospheric conditions assumed for the calculation of the engine performance at the Approach and Idle operating points are taken to be the same as at Take-Off, and the fuel flow is changed until the thrust matches the thrust setting reported in the emission databank. However, the airspeed of the Approach and Idle case are Mach 0 and 0.4 respectively.

Case	Thrust setting	Reference (ICAO)	Error
Take-Off	100%	0.855kg/s	input
Top of Climb	85%	0.705kg/s	1.9%
Approach	30%	0.242kg/s	8%
Idle	7%	0.088kg/s	12%

Table 4.1: Leap-1A26 Model Validation based on fuel flow as reported by the ICAO [99]

The GSP model is tuned with respect to the data of the engine corresponding to Take-Off conditions, that then is considered as the design point. At the Top of Climb condition the match is good considering generic turbo-machinery performance maps are employed for off-design calculations. At low thrust settings, there is a substantial mismatch, however. Given that the shaft speeds at these conditions is low compared to the design point, the accuracy of the turbomachinery maps is more relevant and hence an error in performance between the real engine and the model is likely. At this operating condition, bleed valves are used to prevent compressor stall. A difference in bleed flow changes the massflow in the engine and hence the operating condition of both the compressors and that of the turbines. An error in the bleed flow is therefore a likely cause for the relatively large error in fuel consumption.

Although a better match over the whole domain is desirable, the conditions of interest (TO & CRZ) are predicted well as at these conditions no bleed flow is used to prevent stall. Regarding the CRZ specifically, the ambient conditions are similar to those of TOC and, unlike the approach and idle operating points, the shaft speed is reasonably high.

4.1.2. GTF2050

In order to verify the GTF2050 engine model as well as the use of GSP in general, the reference engine for the GTF2050 from Mastropiero et al. [66] has been replicated. This is done for all the operating conditions in the paper; Take-Off, Cruise and Top of Climb. In the GSP model, the Take-Off condition is taken as the design condition. The results of this verification exercise are presented in Table 4.2.

Parameter	Unit	Reference			Deviation		
		TO	CRZ	TOC	TO	CRZ	TOC
Thrust(Net), FN	kN	183.46	32.56	49.99	<0.01%	-0.02%	-0.95%
Bypass ratio, BPR	-	16.14	16.84	16.08	Input	+0.13%	+0.36%
Overall pressure ratio, OPR	-	60.1	62.1	75.4	Input	<0.01%	**-3.73%**
Specific thrust, SFN	m/s	183.1	84.6	111.3	<0.1%	-0.04%	-1.80%
Specific fuel consumption, SFC	g/kNs	8.28	12.60	13.73	<0.1%	+0.04%	+1.34%
Inlet massflow, $\dot{m}_1$	kg/s	1002	385	449	Input	+0.02%	+0.87%
Cooling fraction, $\dot{m}_c/\dot{m}_{24}$	-	0.063	0.063	0.063	Input	Input	Input
HPC exit temperature, T3	K	1053	860	1011	<0.1%	<0.1%	+2.1%
HPT SOT, T41	K	1921	1540	1890	Input	Input	Input
Fan pressure ratio BP	-	1.39	1.39	1.51	Input	<0.5%	-0.5%
Fan pressure ratio core	-	1.27	1.29	1.37	Input	<0.5%	-0.5%
LPC pressure ratio	-	2.3	2.67	2.43	Input	<0.5%	+0.4%
HPC pressure ratio	-	20.92	19.90	22.65	Input	<0.2%	-3.6%
LP shaft rotational speed	rpm	7928	7330	8380	Input	**+3.65%**	**-2.68%**
HP shaft rotational speed	rpm	16336	13958	16439	Input	**+2.74%**	**-4.19%**

Table 4.2: Reference engine [66] engine parameters and replication error GTF2050 at Take-Off, Cruise and Top of Climb.

In general, a good match can be observed between the GSP model and the reference engine. Given that the design condition is TO and extensive information was available to calibrate the model, there is a near identical match for this operating condition. Regarding the prediction at Top of Climb, OPR and the RPM of the two stools are the quantities that deviate most from the reference engine. This suggests that the turbomachinery performance maps are likely not sufficiently similar to the maps used in Mastropierro et al. This result was somewhat expected, as the performance maps used are the default ones in the GSP suite and belong to turbomachinery with a lower pressure ratio than those of compressors and turbines of an EIS2050 engine. For the Cruise condition, which is together with the design point the operating condition where the CCA concept will be assessed, the match is still close.

Regarding the impact of the cooling flow on the overall engine performance, in the reference engine, the cooling fraction is set to 6.3% as opposed to the computed 24% using the prediction method for cooling flows adopted in this study. In order to compensate for the 'lost' turbine work the combustor temperature is increased by 40 K. Comparing the reference case and the baseline case used in the rest of the thesis; the overall thrust reduces from 32.56 kN to 30.23 kN and the SFC at the Cruise condition increases from 12.6g/kNs to 13.69g/kNs. Similarly, at the Take-Off condition the thrust reduces 183.4 kN to 173.83 kN, a 5% reduction. Notably, the Take-Off SFC only decreases by 2% from 8.28 g/kNs to 8.38 g/kNs. This comes down to more efficiently using the energy in the core, with the exhaust total pressure reducing from ± 1.7 bar (chocked) to ± 1.15 bar (unchocked). Note that this exhaust pressure may be considered too low for an actual engine, as with engine degradation the exhaust pressure will reduce lest the combustor temperature is increased.

4.2. Cooling Model Implementation

The testing of the cooling model implementation is documented in this section. By looking at the model response when a change in the coolant temperature is imposed, it is possible to confirm the model has been implemented correctly, as discussed in the following from both a quantitative and qualitative point of view.

In Figure 4.1 the cooling fraction as well as the HPT efficiency are plotted as function of the heat exchanger coolant temperature change.

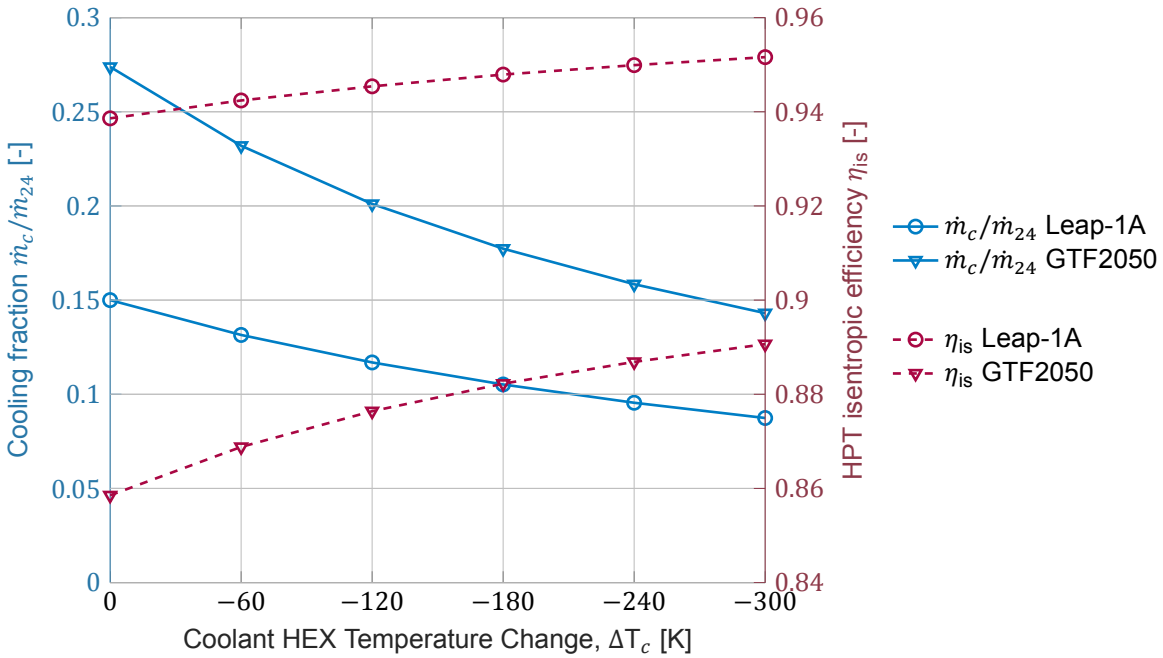

Figure 4.1: Verification of cooling model: coolant fraction and HPT isentropic efficiency as function of the HEX effectiveness.

As expected, the required coolant fraction decreases while increasing heat exchanger effectiveness. Notice that the impact of a finite temperature change across the heat exchanger has a decaying impact on the required cooling flow. The HPT efficiency is assumed to be linearly dependent on the cooling massflow, hence the observed trend is coherent ($d\dot{m}_c/d\eta_{is} = \text{constant}$).

The relationship used to predict the required cooling massflow, see 2.2, is proportional to the temperature difference between the gas flow bulk temperature and the maximum allowable material temperature. At the same time, it is inversely proportional to the difference between the blade temperature and the cooling air temperature. It follows that the required massflow is nearly linearly dependent with the ratio of these two temperature differences. In Figure 4.2 the cooling fraction and marginal temperature ratio are plotted. Note that the cooling air massflow rate curve pertaining to the Leap-1A engine has been calculated by considering a lower value of the constant ($b_{\text{matched}} = 0.85 b_{\text{nom}}$) from equation 2.2 in order to match the reference 15% cooling flow at nominal TO condition.

If the original value of b is used, the curve for Leap-1A and for GTF2050 collapse onto each other. Furthermore, the lines are nearly linear with a coefficient of ± 0.105. This value is approximately equal to the sum of the two model constants $b_{\text{stator}} = 0.05$ and $b_{\text{rotor}} = 0.06$. It can therefore be concluded that the cooling model is implemented correctly.

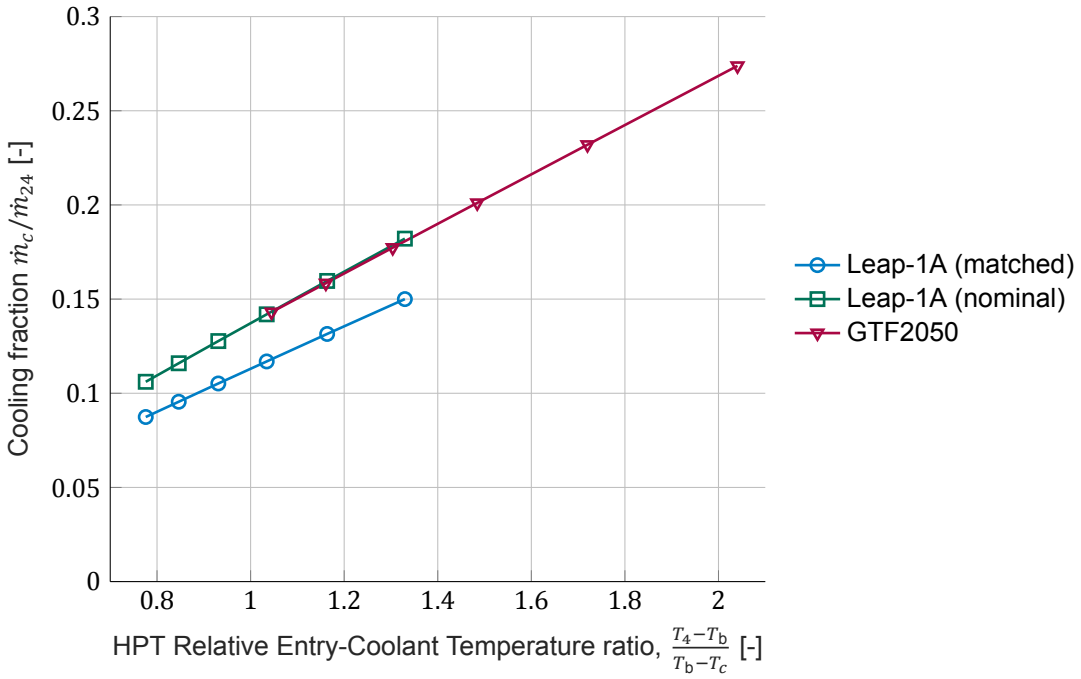

Figure 4.2: Verification of the cooling model: cooling fraction as function of HPT relative entry to coolant temperature (variable for equation 2.2).

.

4.3. Exergy Analysis Implementation

The code for the exergy analysis has been implemented in the Matlab environment. In order to verify that the exergy equations are applied correctly, the code has been used to reproduce the results of the exergy analysis for an intercooled turbofan engine that is documented in the literature [48], [100].

In these papers, several different engine configurations were considered as well as some unconventional intercooled configurations were presented. For the purposes of verification, the “IC geared” configuration was used, as it is the simplest configuration that still includes a heat exchanger. Furthermore, the Take-Off condition will be considered for the comparison, as the component performances are explicitly stated for this operating point. The engine parameters from the paper [100] are reported[1] in Table 4.3.

Parameter	Unit	Value
Thrust (net)	kN	291.91
SFC	g/kNs	8.20
BPR	-	17.1
OPR	-	79
Fan η_{poly}	-	0.935
IPC η_{poly}	-	0.922
HPC η_{poly}	-	0.925
HPT η_{poly}	-	0.907
LPT η_{poly}	-	0.9325
Fan BP PR	-	1.446
Fan Core PR	-	1.25[1]
IPC PR	-	4.95
HPC PR	-	12.77
T3 (HPC exit)	K	885
T45 (LPT entrance)	K	1417
Inlet massflow $\dot{m}_1$	kg/s	1214
Core entry massflow $\dot{m}_{24}$	kg/s	69
Cooling fraction $\dot{m}_c/\dot{m}_{24}$	-	0.14

Table 4.3: Engine Take-Off parameters for a geared intercooled engine from literature [100] to be used for verification of the exergy analysis implementation

The engine working fluid is modelled as an ideal gas, with c_{p}=1.006 kJ/kg in the case of air and c_{p}=1.21 kJ/kg in the case of the flue gas. Note that for the exergy analysis performed for the GTF2050, the ’real’ gas model of GSP is instead used. Beyond the ideal gas assumption, several other assumptions have been made to match the cycle to the specified performance, as discussed below.

In order to find the temperature difference across the intercooler, the inlet and outlet temperature were computed from the surrounding components. The intercooler inlet temperature was based on the fan and IPC pressure ratio, efficiency and an assumed inlet temperature of 288.15K. The intercooler outlet temperature was computed using the HPC pressure ratio, efficiency, and exit temperature. With the stated specific fuel consumption and the thrust, it is easily found that the fuel massflow is 2.39 kg/s. Based on this massflow rate and assuming that LHV=43.2MJ/kg, $\eta_{\text{comb}} = 0.9995$, as for the GTF2050, to determine the temperature at the combustor outlet, it results that the value is about $\pm$ 2110 K is found. This result exceeds the maximum allowable temperature (1900 K) indicated in paper [100]. On the contrary, if the LPT inlet temperature is taken equal to the original value reported in the paper, a value of 1844K was found for T4. This latter value was deemed more realistic and was used in further calculations.

For both the high pressure and the low pressure shafts, a mechanical loss of 50 kW is assumed, the same as applied to the GTF2050.

[1] Fan core PR computed from LPC & HPC PR, OPR and assumed constant pressure across the IC

As there is no information in this paper regarding the fraction of the BP flow used for the intercooler, this is assumed to be 10% of the total massflow rate at the Take-Off condition. This assumption is based on observing drawing of the engine gas path, the massflow rate of the air to be cooled. Regarding the gas path, the report refers to an “openness” setting of 60% at Take-Off. This is interpreted to mean that at Take-off, the effective flow area is 60% that of the geometric flow area on the drawing.

Furthermore, for an ambient airspeed of 50 m/s the model prediction of the net engine thrust matched the value reported in the reference perfectly. At this condition, the nozzle of the bypass flow and that of the bypass off-take flow are unchoked. Whereas the nozzle of the core flow is chocked.

The computed thermodynamic states as well as the mass flows for each of the engine stations are provided in Table 4.4.[2]

Station	Description	T [K]	P [bar]	$\dot{m}$ [kg/s]
1	Inlet	288.15	1	1214
21	Fan Core exit	309	1.25	69
23	IPC exit	506	6.19	69
25	IC exit	457	6.19	69
3	HPC exit	885	79	59.34+9.66[2]
4	CC exit	1844	75.05	61.73
45	HPT exit	1417	30.81	71.39
5	LPT exit	798	3.56	71.39
9	Core exhaust	685	1.92	71.39
13	Fan BP exit	323	1.446	1145
19	BP exhaust	323	1	1030.5
105	BP-OT IC exit	323	1.37	114.5
109	BP-OT exhaust	352	1	114.5

Table 4.4: Thermodynamic states at engine stations for replicated geared intercooler from literature [100].

A breakdown of the corresponding exergy losses according to the results in ref [100], both for the reference and as found via the implemented model, is given in Figure 4.3.

In general, the match with the reference model is good. The total exergy loss in the whole engine is 0.95% higher than the reference one.

the largest discrepancies are observed for the exhaust nozzles. This is also where the largest uncertainty in the calculations are, as the impact on the design assumptions (i.e. duct losses) are compounded over the engine. When combining the exergy losses from the BP and BP-OT exhausts, the net result is higher still than in the original study. Increasing IC pressure loss would shift some of the excess BP exergy loss to the IC. Furthermore, the exergy destruction for the high pressure components, including the combustor, is slightly over-estimated. The uncertainty about the combustor exit temperature is likely to be the cause. Regarding the high pressure compressor and turbine, the small discrepancy in loss could in part be the result of the mechanical efficiency that is applied onto the shaft (it is unknown what this loss is in the reference model).

[2]where 59.34+9.66 represents CC inlet and HPT cooling air respectively

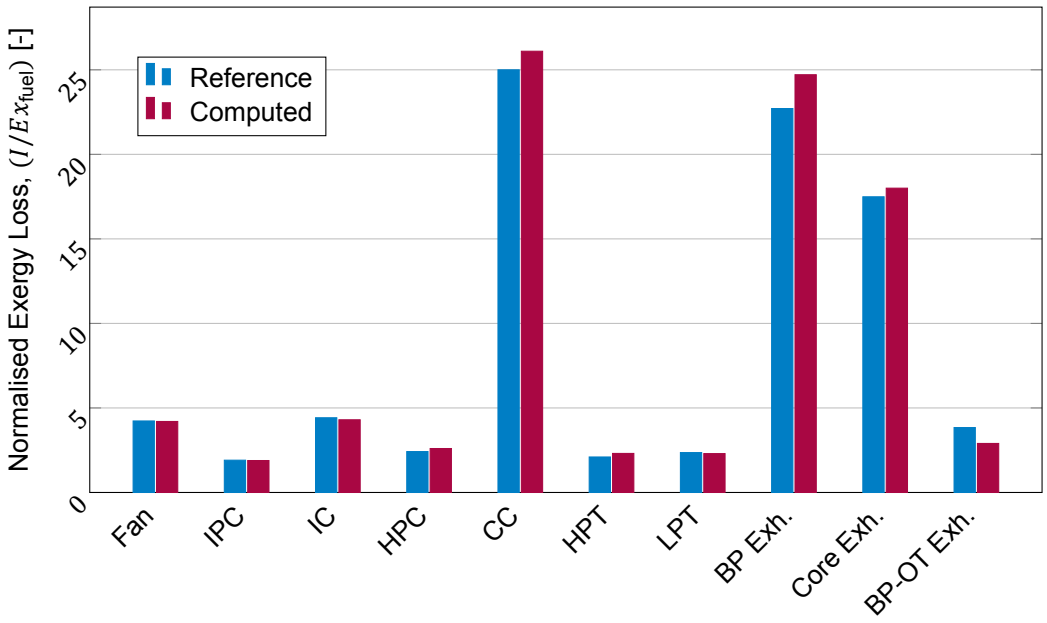

Figure 4.3: Irreversibility breakdown (exergy destruction and unused exergy in exhaust) according to the results in [100] and calculated with the model.

5

Results & Discussion

5.1. Summary of Results Presented

The adoption of a CCA configuration is assessed for both the LEAP and GTF2050 engine. To this purpose, the performance of the two engines is evaluated for different values of the main design variable of the heat exchanger ΔT_c and of the BPR. The results from these simulations are given in the carpet plots in Figures 5.1 (TO) and 5.2 (CRZ) for Leap-1A and Figures 5.3 (TO) and 5.4 (CRZ) for the GTF2050.

The first observations are that for both Take-Off and Cruise, as well as for both of the engines, the SFC significantly increases with the value of ΔT_c. For the Leap-1A engine, the SFC at take increases from the baseline 9.86 to 10.12 g/kNs for the $\Delta T_c = -300$. At Cruise the SFC increases from 15.2 to 15.5. Similarly, for the GTF2050 engine, the specific fuel consumption ranges from 8.38 to $\pm$8.68 g/kNs.

For both engines, the specific thrust increases at both conditions. The change is $\pm$2.4 m/s for the Leap-1A and $\pm$ 4.5 m/s for the GTF2050 at Take-Off and $\pm$2 m/s for both engines at Cruise. This change is driven by the increased core exhaust pressure, which is the result of an increased massflow through the combustion chamber and high pressure turbine.

These values are subsequently normalised with respect to the baseline fuel consumption and thrust, in order to compare the relative change. This percentage change plot is given in Figures 5.6 (TO) and 5.7 (CRZ). It is shown that for both conditions, the order of the SFC and the SFN change as a function of the coolant temperature change for the GTF2050 is double that of the Leap-1A. When looking at the impact of a percentage cooling flow change, it is found to be similar for both engines, as is demonstrated in Figure 5.8.

To quantify the performance impact of pressure loss across the heat exchanger, a nominal case (without any pressure loss) was compared to a case with 8% relative pressure loss. For the 8% pressure loss case, the SFC and SFN changed by approximately 0.2% at both TO and CRZ conditions.

In order to better understand the interactions between pressure loss and coolant temperature change, a detailed analysis was then conducted into the bypass off-take thrust. The results of this analysis showed that an increase in relative pressure loss, at all temperatures, results in lower net thrust. Additionally, the magnitude of this interaction is greater for higher coolant feed temperature changes.

These results show that locally, therefore, pressure loss has quite a significant impact on thrust. However, in terms of overall engine performance, the impact is quite small relative to the impact of the cooled cooling air more.

Three scenario impact tests, as described in section 3.2.2, were then conducted:

1. Evaluating the impact at Take-Off of the cooling flow to HPT efficiency relationship

2. Evaluating the Cruise SFC for lower CCA HEX effectiveness than at design condition (TO)
3. Evaluating the Sensitivity of specific fuel consumption on cooling requirement parameters

SIT 1 showed that without a change to the HPT efficiency, the overall SFC increased slightly further in comparison to the nominal overall performance impact as in the aforementioned simulations. The relevance of the effect increases as the exhaust pressure approaches the ambient pressure. The percentage range is from 20% at $1.1P_{\infty}$ to 9% for >$1.25P_{\infty}$. From this, we can conclude that this mechanism of changing turbine efficiency is both relevant and not dominant when considering the other mechanisms.

The SIT 2 results, which tested incremental changes in the effectiveness of the heat exchanger at Cruise, demonstrated that for a cruise effectiveness equal, there was still an SFC penalty from applying the CCA concept. For substantially reduced cruise effectivenesses, there is an SFC benefit (however, this does not include weight and pressure penalties). The observed performance improvement from the reduction in (uncooled) cooling air at Cruise is 0.18% SFC per percent of cooling air, which is in line, albeit on the low end, comparing to findings in literature [11], [16].

The results of SIT 3, which adjusted the parameters of the relationship predicting the required cooling fraction, found that the SFC trends did not (significantly) depend on the chosen input parameters. The maximum allowable material temperature does influence the required cooling fraction strongly, and therefore has a significant impact on the absolute value of the specific fuel consumption.

The final set of results presented in this chapter concern the Exergy Analysis conducted as part of this study. This involved a decomposition of all of the sources of exergy loss in the GTF2050 engine for four test cases, covering inputs where ΔT_c was at 0K and -300K, and where ΔP_{HEX} was at 0% and 8%. This provided a summary of the ΔT_c , ΔP_{HEX} and cross-product ΔT_c and ΔP_{HEX} dimensions. The results showed that for cases that have a higher ΔT_c , the exergy loss has a notable increase, with only minimal increases associated with a positive change in ΔP_{HEX}, at both low and high ΔT_c cases. These results are in line with the higher SFC corresponding to these dimensions.

To further understand these findings, the set of underlying components with the greatest observed movement was then analysed (see Figure 5.21). Breaking this down to two primary groups of components: the heat exchanger and the downstream nozzle; and the high-pressure turbine and downstream components, a detailed examination was then conducted on the different mechanisms that cause exergy loss, and how they are affected by the ΔT_c and ΔP_{HEX} dimensions identified earlier. From this exercise, the relative impact of the mechanisms are quantified (see section **??** for further detail and discussion).

5.2. Overall Performance Impact

5.2.1. Coolant Feed Temperature Change Impact at Various Bypass Ratios

The specific fuel consumption and specific thrust are plotted as function of the design parameters: bypass ratio and the coolant temperature change. Note that the bypass ratio at Cruise (not plotted) is larger than the design bypass ratio. First, the results for the Leap-1A engine are presented in Figures 5.1 and 5.2 for the Take-Off and Cruise conditions. Second, the performance of the GTF2050 is given in Figures 5.3 and 5.4 for the Take-Off and Cruise conditions.

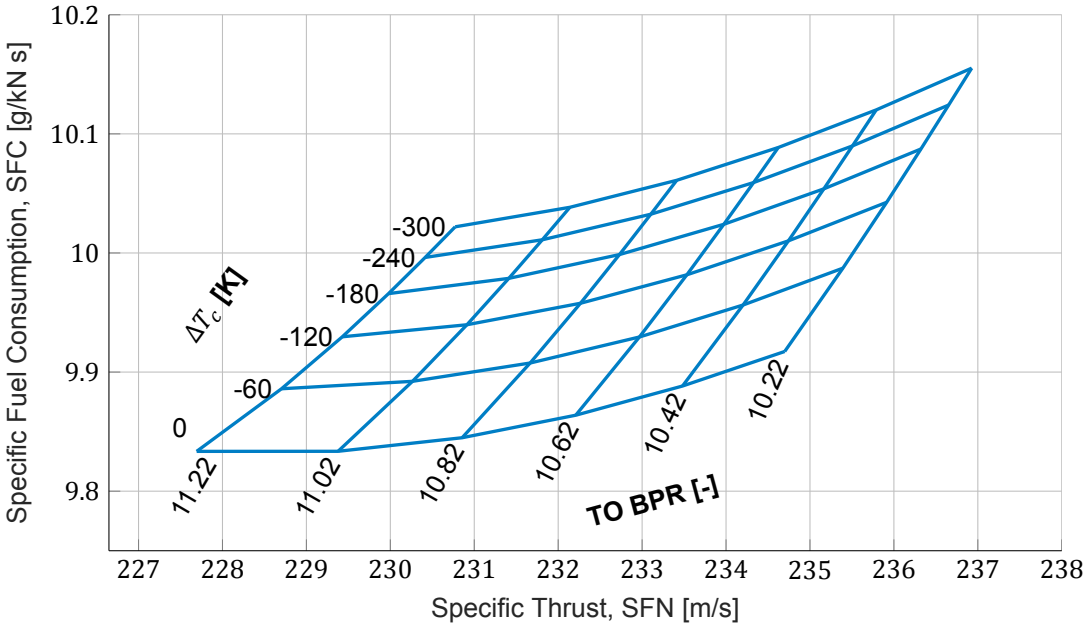

Figure 5.1: Leap-1A Specific fuel consumption and specific thrust as a function of bypass ratio and coolant temperature change at Take-Off

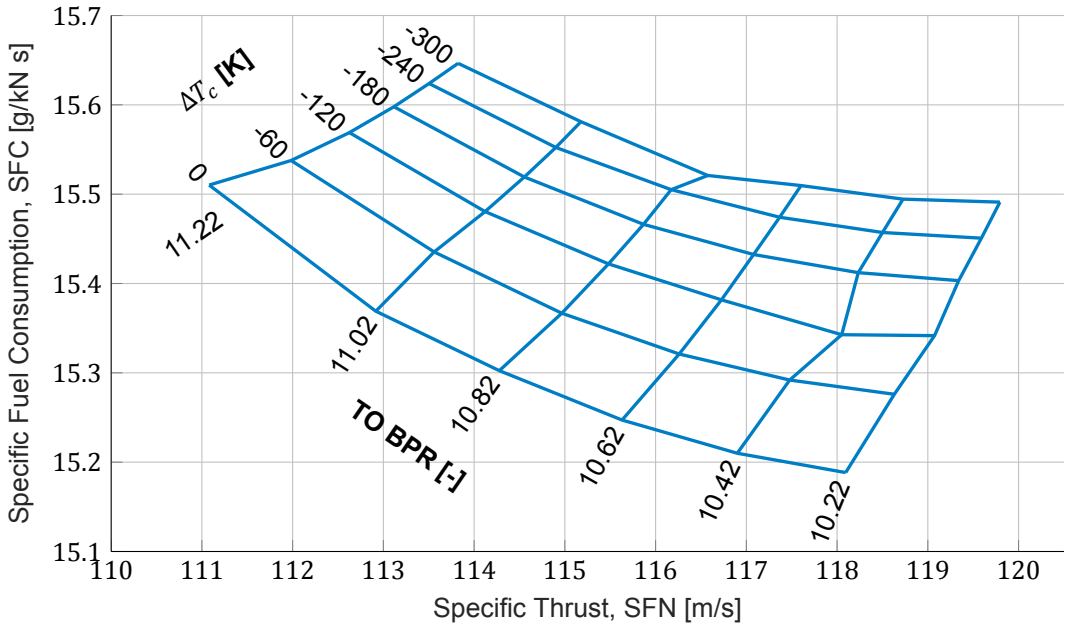

Figure 5.2: Leap-1A Specific fuel consumption and specific thrust as a function of bypass ratio and coolant temperature change at Cruise

As these figures show, for the Leap-1A engine, at both conditions the specific fuel consumption and specific thrust increase with coolant temperature change. This provides some preliminary evidence for the infeasibility of the cooled cooling air concept in reducing fuel consumption.

More coolant through the combustion chamber results in a higher fuel flow (from 1.18 to 1.24 kg/s at TO for $\Delta T_c = -300$K) to reach T4. Subsequently, higher massflow through turbines and lower cooling-related losses decreases the pressure ratio required to supply HPC.

For the design bypass ratio (10.42), the required HPT pressure ratio experiences a 4% decrease at both TO and CRZ conditions. This leads to a higher core exhaust pressure, as can be observed in Figure 5.13. In this case, gross thrust is increased by 1.07kN at takeoff and 0.29kN at Cruise. Additionally, the thrust of the bypass off-take increases slightly due to the expansion at higher temperatures: at takeoff, this change in gross thrust is from 6.93 to 7.47 kN; at Cruise the equivalent change is from 2.58 to 2.68 kN.

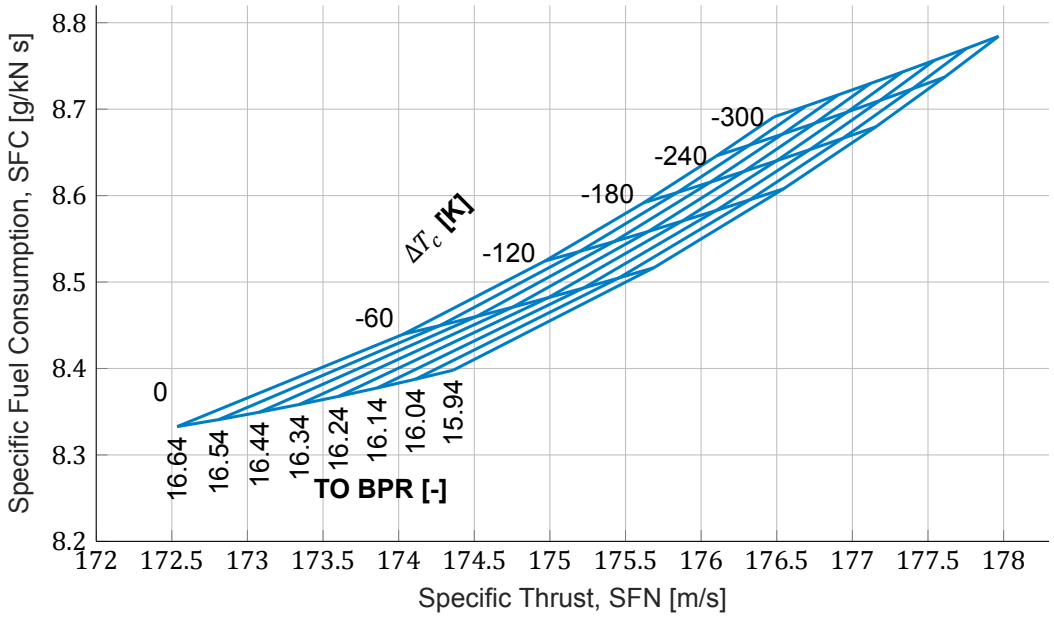

Figure 5.3: GTF2050 Specific fuel consumption and specific thrust as a function of bypass ratio and coolant temperature change at Take-Off

Particularly notable for the GTF2050 engine is that the bypass ratio yielding the minimum Cruise SFC increases with the use of cooled cooling air. This observation is also valid for both the Leap-1A engine, but less obvious as all the tested BPR's are above the optimum. For the GTF2050, at this Cruise-SFC minimising optimum BPR, the SFC still increases compared to an uncooled baseline engine.

Given that the baseline BPR at Cruise is nearly optimal, the optimal BPR can be approximated for the lower coolant temperatures by fixing the exhaust pressure. This is because for this constraint, the propulsive efficiency of the exhausts remains constant. Moreover, for this condition, the thrust is nearly constant (changing <0.2%). Note: although the specific thrust is slightly higher for the core exhaust than the bypass, this is balanced by the increased thrust in the bypass off-take due to the heat transfer. In Figure 5.5 the BPR for constant exhaust pressure is shown. Initially this optimum was determined using the exhaust pressure at Take-Off, however, this yields an exhaust pressure Cruise that is lower than the baseline. Hence, another curve is plotted for which the cruise exhaust pressure is kept constant.

In both the GTF2050 and Leap-1A engines, the same trends are observed: SFC and SFN increase with coolant temperature change. For the largest coolant temperature change case (-300K),

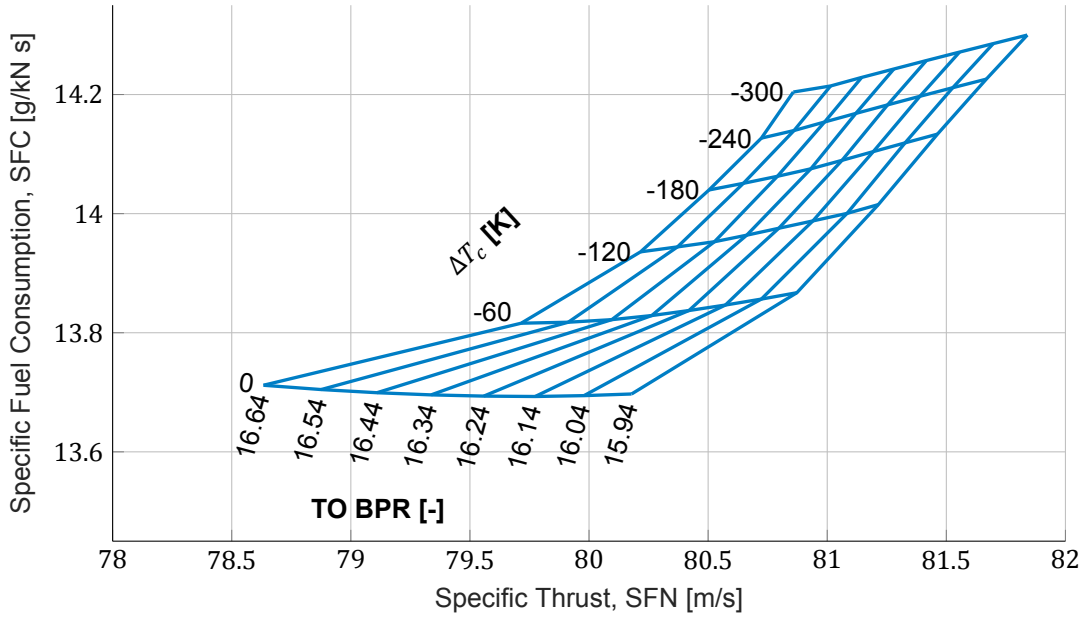

Figure 5.4: GTF2050 Specific fuel consumption and specific thrust as a function of bypass ratio and coolant temperature change at Cruise

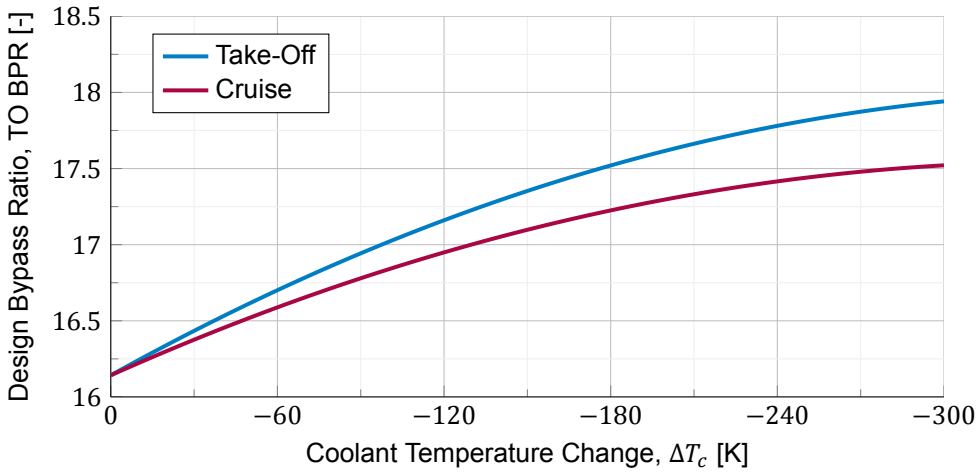

Figure 5.5: Design bypass ratio for achieving constant core exhaust pressure at Take-Off and Cruise for the GTF2050 engine with varying coolant temperature

the GTF2050 engine shows a larger absolute change in SFN compared to the Leap-1A, with SFN at +4.5m/s versus +2.4m/s at takeoff. In this case, both engines have a similar SFN of +2m/s at Cruise.

At both conditions, the GTF2050 engine has a higher SFC change (in both absolute and relative terms). Compared to the baseline, the GTF2050 engine the SFC increases by +4.5% at Take-Off to +4.2% at Cruise. For the Leap-1A engine, the changes are +2.3% to +1.9% respectively. To better compare the specific fuel consumption and the specific thrust, Figures 5.6 and 5.7 are plotted for Take-Off and Cruise respectively.

.

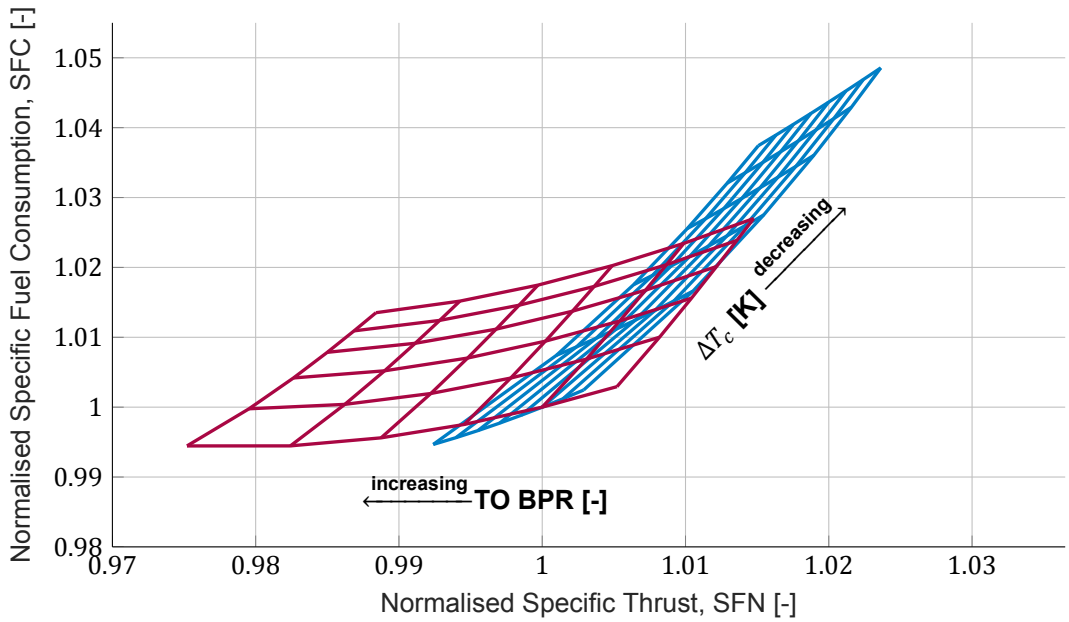

Figure 5.6: Normalised specific fuel consumption and specific thrust as a function of bypass ratio and coolant temperature change at Take-Off. In blue the GTF2050 and in red the Leap-1A

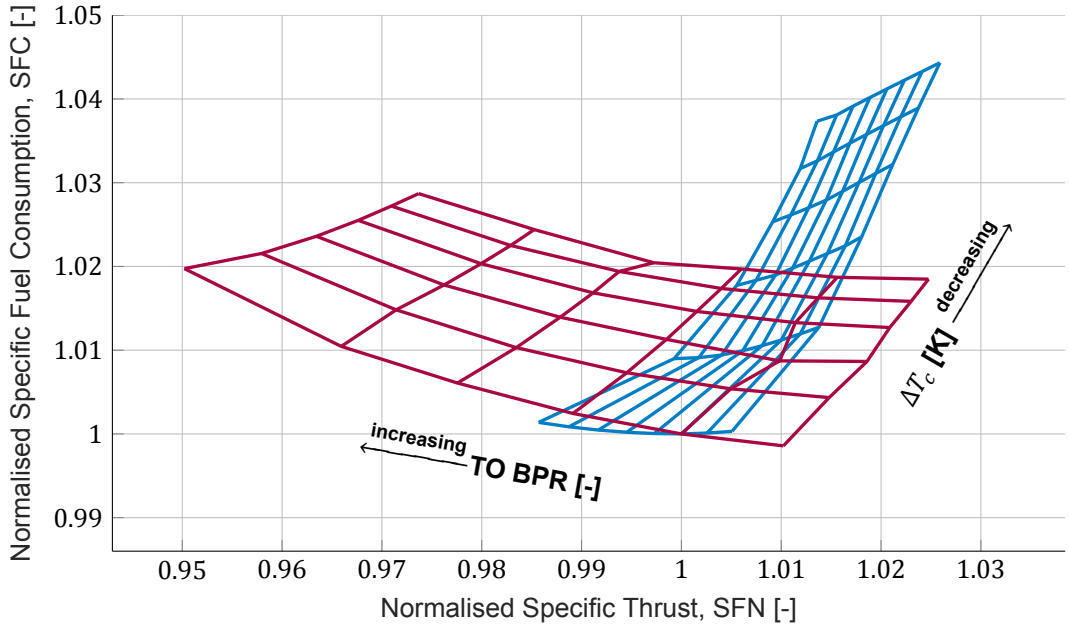

Figure 5.7: Normalised specific fuel consumption and specific thrust as a function of bypass ratio and coolant temperature change at Cruise. In blue the GTF2050 and in red the Leap-1A

The rate of change (given by the ratio $\frac{\text{SFC}}{\text{SFN}}$) seems to be about the same for GTF2050 and Leap-1A. The normalised change for a given BPR is double that in the case of the GTF2050 compared to the Leap-1A. For the same temperature coolant change, the impact on the required cooling fraction is larger for the GTF2050 engine than the Leap-1A as was also earlier shown in Figure 4.1. This is demonstrated when considering the cooling fraction versus the SFC change shown in Figure 5.8. This result implies that the dominant mechanisms must primarily scale with the cooling massflow as opposed to just the coolant temperature change.

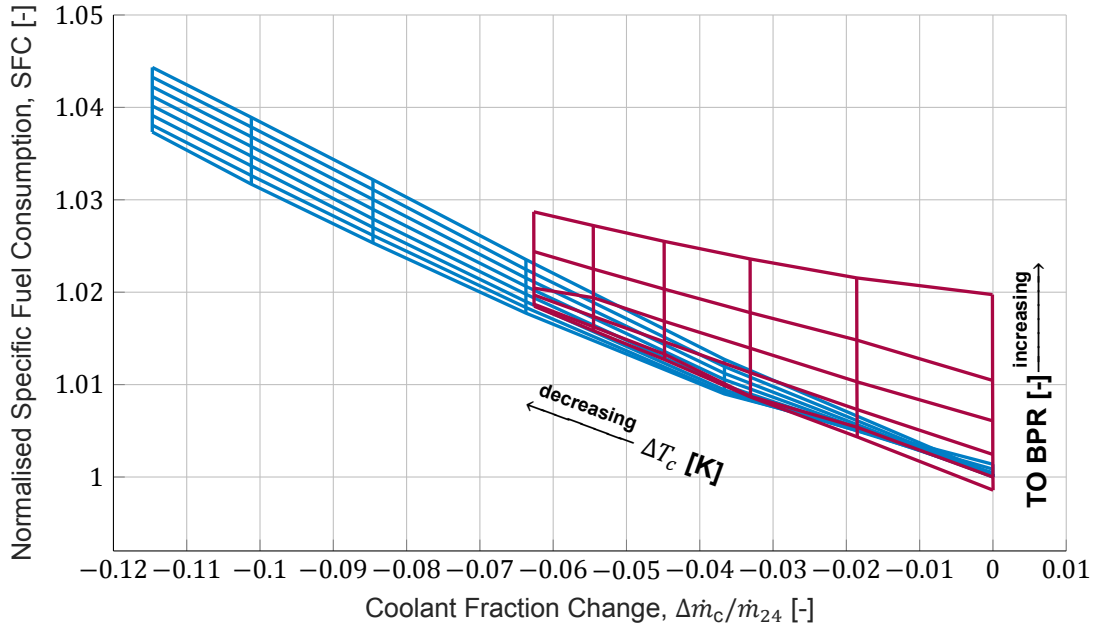

Figure 5.8: Normalised specific fuel consumption as a function of bypass ratio and coolant fraction change at Cruise. In blue the GTF2050 and in red the Leap-1A

5.2.2. Heat Exchanger Pressure Loss Impact

To examine the impact of pressure loss in the heat exchanger, relative total pressure loss values from 0 to 8% are prescribed and the impact on specific fuel consumption and thrust is tested across the whole domain. Results are shown based on the GTF2050 engine, but the observations also hold for the Leap-1A engine. The actual pressure loss is dependent on the design of the heat exchanger and will correlate with the design effectiveness. The trade-off between the design effectiveness and acceptable pressure loss can be made quantitatively with the result of this analysis: the direct impact on SFC and SFN of an 8% pressure loss is shown in Figures 5.9 and 5.10 for Take-Off and Cruise respectively.

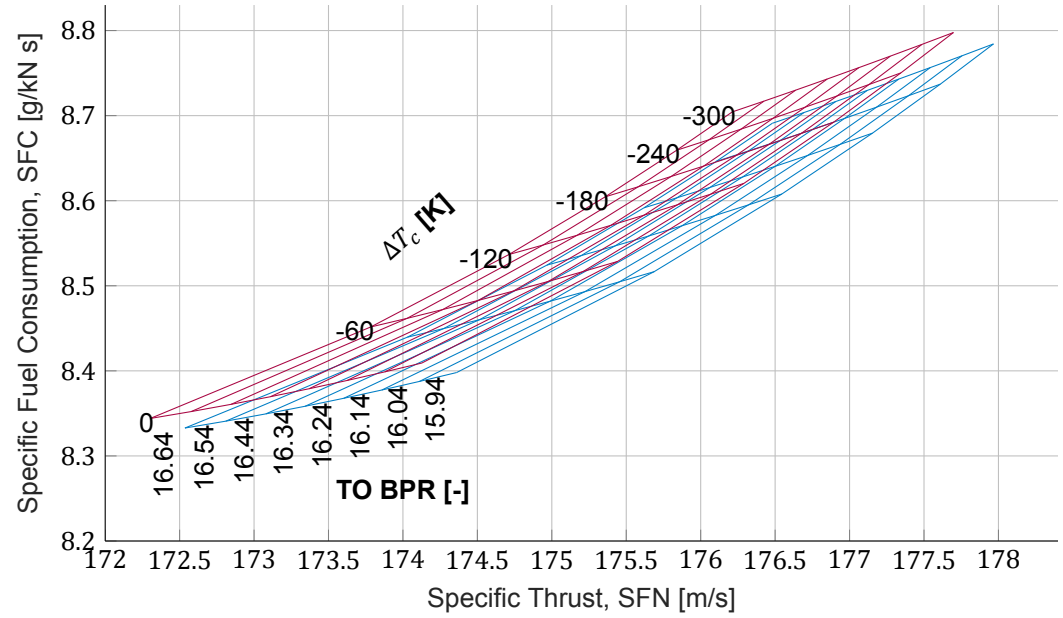

Figure 5.9: Impact of pressure loss across the cooled cooling air heat exchanger on specific fuel consumption and specific thrust for the GTF2050 at Take-Off. In Blue 0% and in red 8% total relative pressure loss.

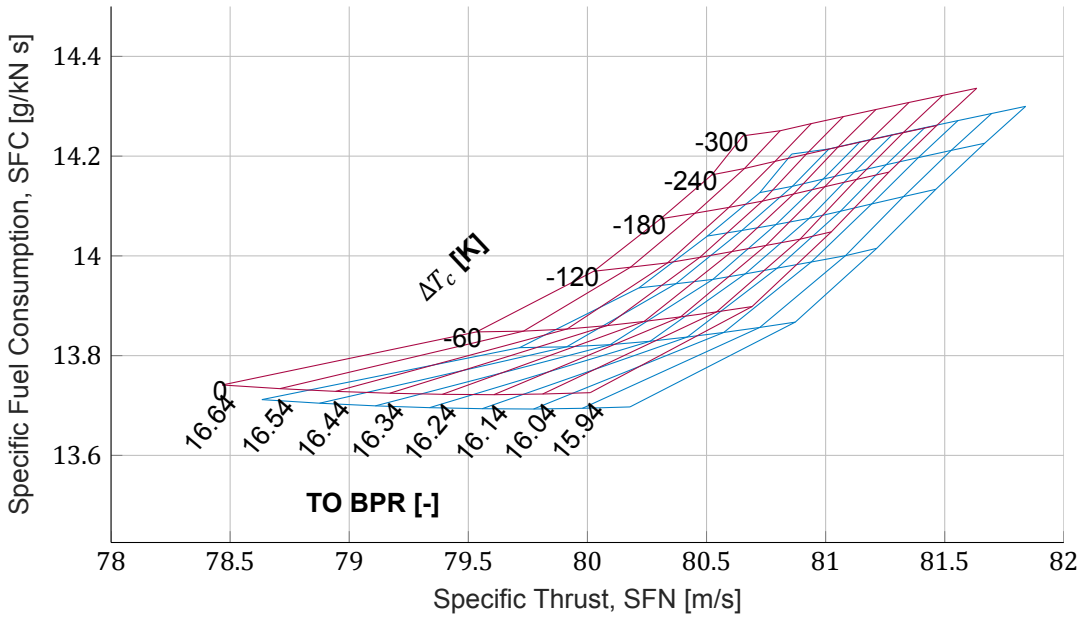

Figure 5.10: Impact of pressure loss across the cooled cooling air heat exchanger on specific fuel consumption and specific thrust for the GTF2050 at Cruise. In Blue 0% and in red 8% total relative pressure loss.

With a fixed off-take fraction of 1.5% (noting that the optimal fraction is likely smaller given the current maximum effectiveness of approximately 0.35). Additionally, under this model, as the BPR increases, the off-take massflow is also increased, while coolant flow decreases. The optimal off-take massflow is likely to be lower, especially for increasing BPR. Consequently, the observed performance penalties are conservative in nature.

As the applied pressure loss on the bypass off-take flow has no upstream influence, any observed changes to SFC and SFN are a direct function of changes to the bypass off-take thrust. With this, the SFC and SFN are inversely proportional, and hence the relative change is the same for both[1]. This shift appears to be a fixed amount across the domain of approximately +0.2% SFC and -0.2% SFN at both Take-Off and Cruise.

In order to quantify the relationship better, the bypass off-take thrust is considered more closely. For the different coolant temperature change settings, the impact of pressure loss on normalised (local) net thrust is calculated. The results for Take-Off are shown in Figure 5.11 and in Figure 5.12 for Cruise. As the inflow state for the bypass off-take is the same across the whole domain, the following analysis is independent of the bypass ratio.

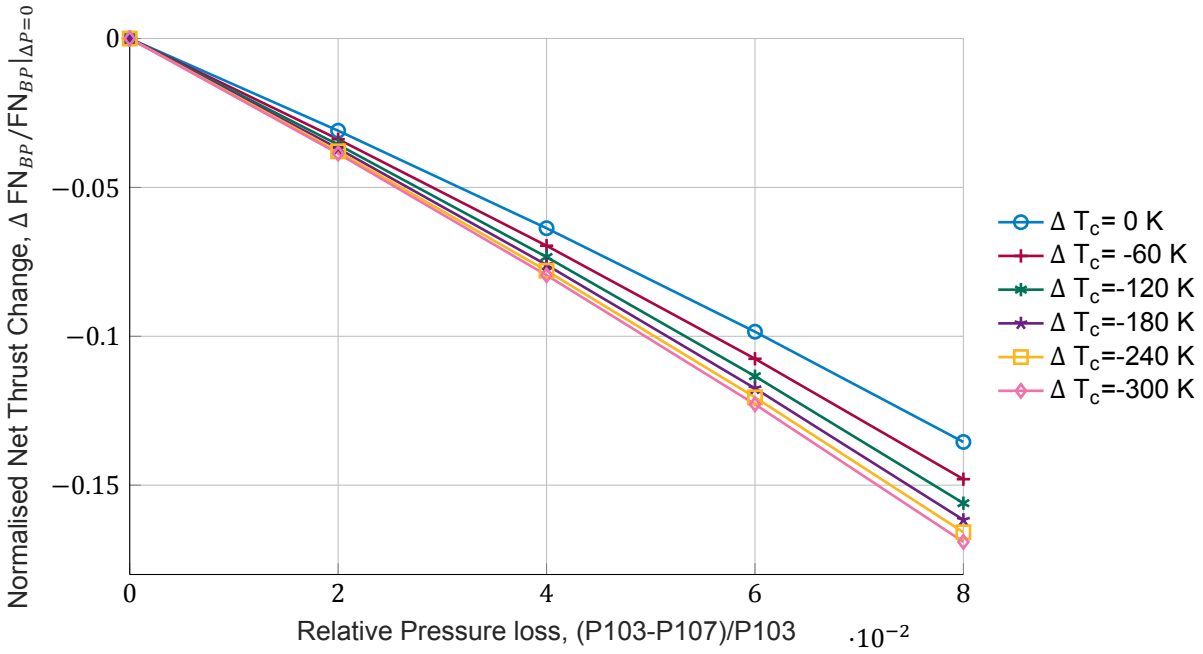

Figure 5.11: Normalised bypass off-take thrust impact of pressure loss across the cooled cooling air heat exchanger for the GTF2050 at Take-Off

In both conditions, the pressure loss is amplified in terms of thrust reduction. As pressure loss increases, the marginal thrust penalty grows. This can be attributed to the relationship between the exhaust exit pressure, temperature and the jet velocity.

$$V109 = \sqrt{2c_p T109}\sqrt{1-(P_\infty/P109)^{(\gamma-1)/\gamma}} \propto FG_{BP-OT} \quad \text{for an unchocked nozzle} \tag{5.1}$$

Considering only the pressure-dependent square root and filling this in at Take-Off, P103 is 1.448 bar and the ambient pressure is 1.013 bar.

[1]This equal relative change is valid only for small changes in overall thrust with constant inlet and fuel massflow: $\frac{SFN_1}{SFN_2} = \frac{FN_1}{FN_2}$ whereas, $\frac{SFC_1}{SFC_2} = \frac{FN_2}{FN_1}$

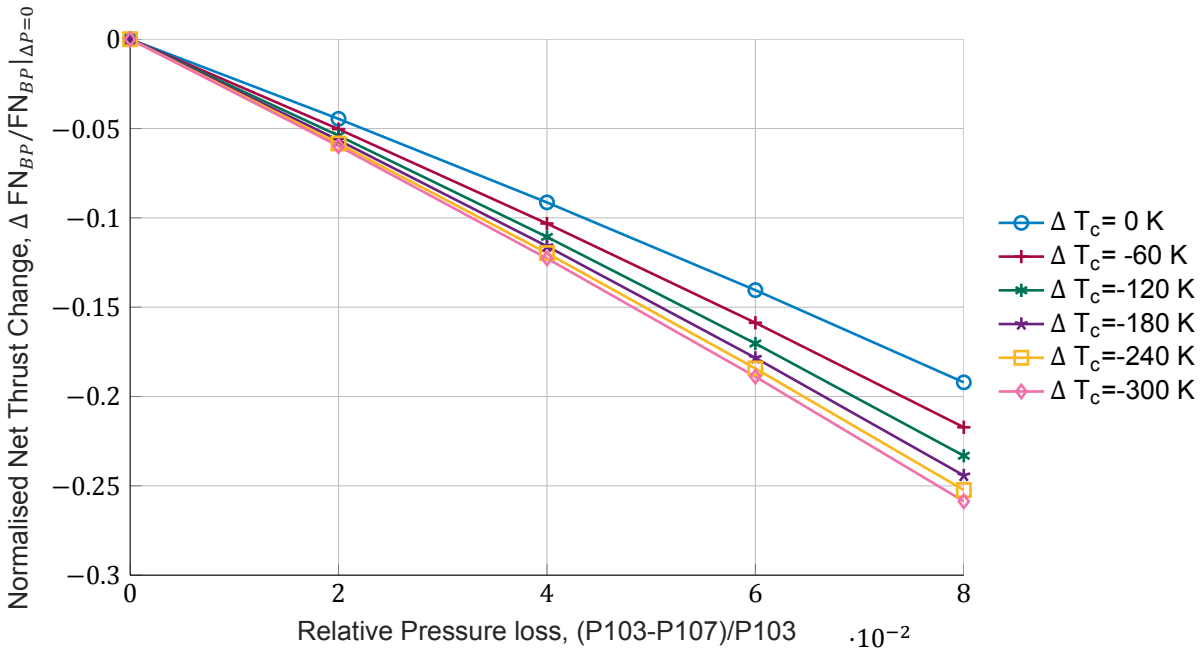

Figure 5.12: Normalised bypass off-take thrust impact of pressure loss across the cooled cooling air heat exchanger for the GTF2050 at Cruise

$$\sqrt{1-\left(\frac{1.013}{1.448(1-0.08)}\right)^{0.286}} = 0.88$$

yields a 12% reduction in exhaust velocity. This translates to the observed net thrust decrease of 13% for the case with no heat transfer to 17% for the case with highest heat transfer. At Cruise, the effect of the pressure drop is higher as the ratio of P103 to the ambient pressure is lower to begin with.

In conclusion, the effect of pressure loss on the bypass off-take thrust is substantial. The penalty to specific fuel consumption and thrust is about 0.2% for 8% pressure loss. This effect is secondary compared to the overall SFC and SFN change from cooled cooling air.

5.3. Scenario Impact Analysis

5.3.1. SIT 1: Evaluating the Impact at Take-Off of Cooling Flow to HPT Efficiency Relationship

In this scenario the impact on engine performance of the improvement in HPT efficiency driven by the reduction in cooling flow is simulated. The results reported in Figure 5.13 show the specific fuel consumption for the nominal case and the case for which the HPT efficiency is kept constant.

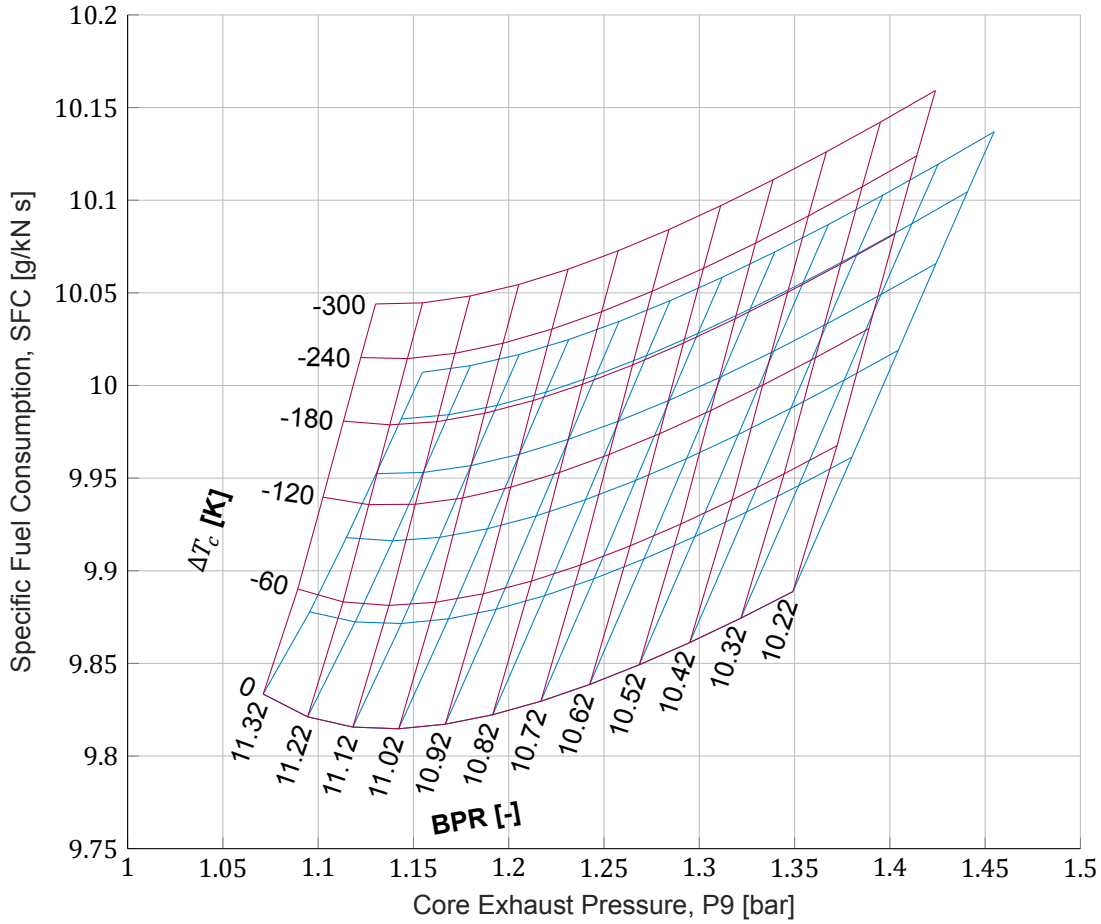

Figure 5.13: Impact of marginal HPT efficiency change driven by cooling flow on Leap-1A Take-Off SFC for various bypass ratio's and coolant temperature change settings. The carpet in blue is the nominal case and red is with constant HPT efficiency.

As expected the specific fuel consumption for the constant HPT efficiency case is worse than the nominal case. Next to the fuel consumption the exit pressure margin drops for the same engine parameters. As the efficiency improvement scales with the reduction in cooling flow, the largest deviation in SFC and P9 are observed at the highest cooling flow temperature drop.

It can be observed that contribution of the change in HPT efficiency is relevant but not dominant compared to the overall change from cooled cooling air. In order to quantify this observation the marginal change in SFC from including the HPT efficiency change is compared to the overall shift in efficiency and plotted in Figure 5.14.

For each bypass ratio the SFC at zero coolant temperature change is taken as the baseline. Subsequently, the change in SFC is determined for the case with and without changing HPT efficiency, designated as $\Delta SFC|_{\eta=\text{variable}}$ and $\Delta SFC|_{\eta=\text{variable}}$. The contribution of the HPT efficiency change is then taken as the difference between these two

$$\Delta SFC|_{\eta=\text{constant}\rightarrow\text{variable}} = \Delta SFC|_{\eta=\text{variable}} - \Delta SFC|_{\eta=\text{constant}} \tag{5.2}$$

Finally, this relative change is normalised with the overall change.

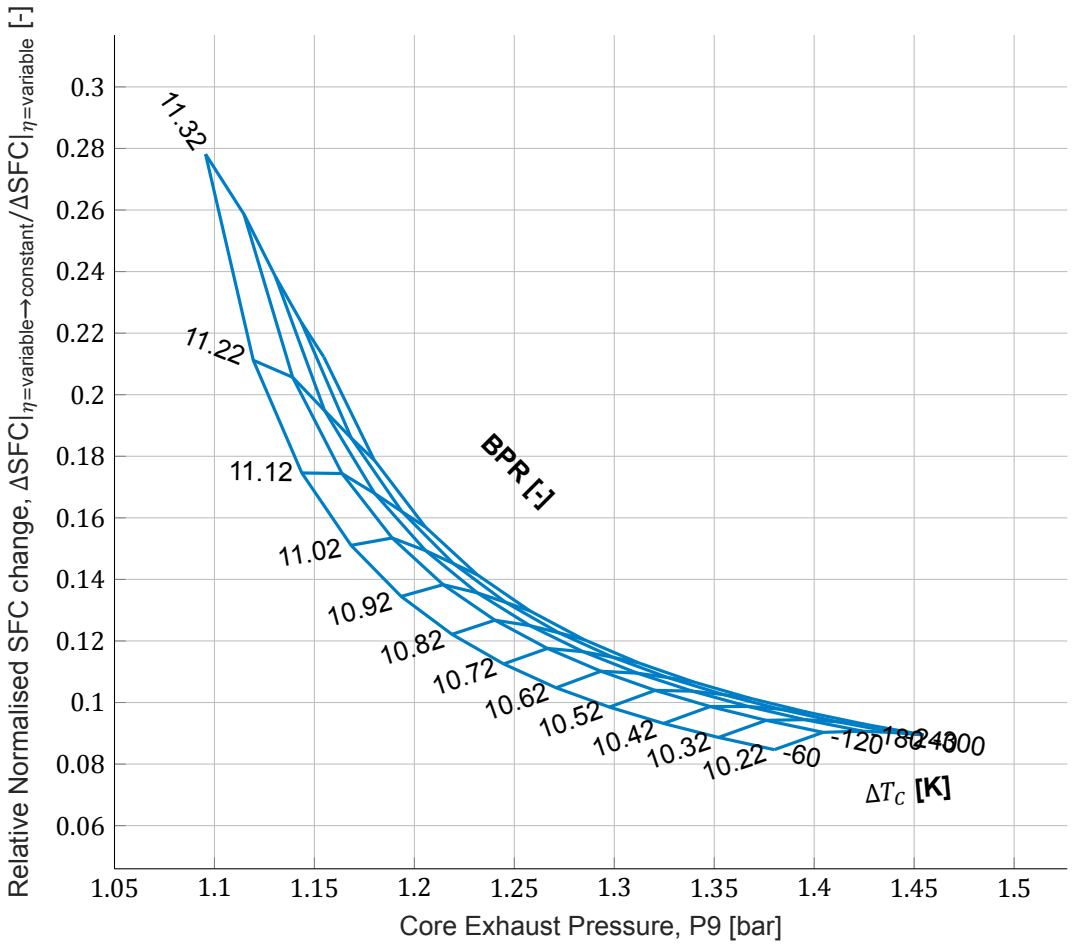

Figure 5.14: Relative size of the shift in specific fuel consumption due to the change in HPT efficiency compared to the overall shift from cooled cooling air.

The scale of the contribution of the HPT efficiency for most of the domain is around 10-14%. When the core exhaust pressure approaches the atmospheric pressure however the relative impact of the efficiency correction grows rapidly. This can be attributed to the relationship between the exhaust pressure and the thrust as shown earlier in equation 5.1. Which implies that a marginal change in exhaust pressure near the ambient pressure has a larger impact on the thrust and in turn on specific fuel consumption. Given the relationship between core exit pressure and BPR, the latter is also a good predictor for the relative impact on SFC from changing HPT efficiency. One might expect a similar relationship with respect to the coolant temperature change, given it's impact on exhaust pressure. However the relative importance of the HPT efficiency change is largely independent from the coolant temperature change.

5.3.2. SIT 2: Evaluating Cruise SFC for Lower CCA HEX Effectiveness Than at Design Condition (TO)

Figure 5.15 shows the impact of changing the Cruise heat exchanger effectiveness with respect to the Take-Off condition on the overall fuel consumption. In the figure the temperature change of the coolant is varied from zero to the temperature chance set at the design condition (TO). The results are normalised with respect to the baseline Cruise SFC.

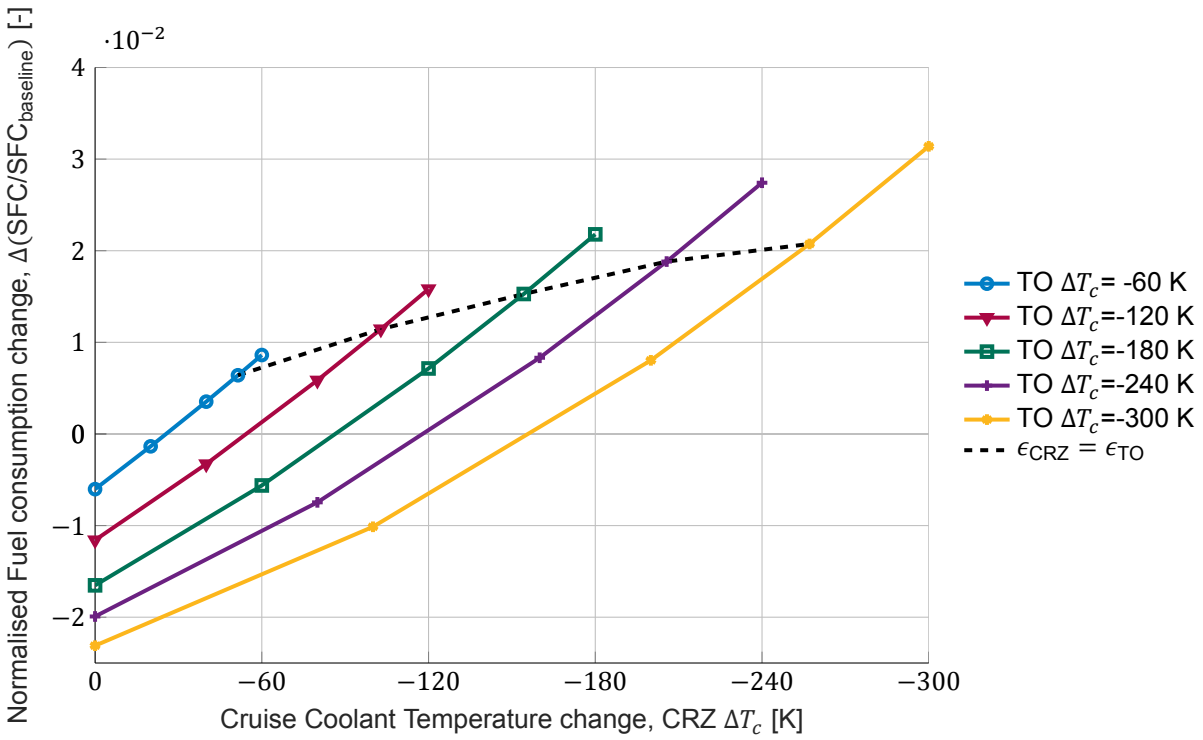

Figure 5.15: Impact of changing Cruise HEX Effectiveness on GTF2050 Cruise SFC for various Take-Off coolant temperature change settings at constant cruise core exhaust pressure

This analysis shows that as the heat exchanger performance goes down at Cruise, the SFC improves. In particular, the drop cooling fraction of 13% at 300K translates to an 2.3% SFC improvement (equivalent to a 0.18% per percentage cooling flow). This represents an extreme case where the heat exchanger does not have any impact at Cruise. Walsh [16] found exchange rates of 0.20% to 0.96% at constant SOT and Kurzke [11] 0.33% at constant T4.

Note: there are some considerations regarding these results. This modelling assumes no pressure loss and no penalty for additional weight of the heat exchanger. Therefore, the reported SFC benefits are not practicably realisable in a built engine. Additionally, in Figure 5.15, the point is indicated where the heat exchanger effectiveness at Cruise and takeoff are equal. At all Cruise coolant temperature changes tested, this remains above 0; this means that if a fixed effectiveness is prescribed the trends as discussed earlier in this chapter will be observed also. In the case that the heat exchanger is designed to have a substantially lower effectiveness at Cruise compared to Take-Off there is an SFC benefit to be had. This result is in line with the examples of the cooled cooling air concept in literature, where a benefit is observed if the heat exchanger is bypassed in Cruise.

5.3.3. SIT 3: Evaluating the Sensitivity of specific fuel consumption on cooling requirement parameters

The sensitivity of the engine performance to the input parameters, s and T_b, of the cooling requirement equation for the GTF2050 engine is given in this section. In Figure 5.16 the impact of the exponent s on the cooling requirement over the considered feed temperature change domain is given. Similarly, the cooling requirement for various values of the maximum allowable material temperature is given in Figure 5.17.

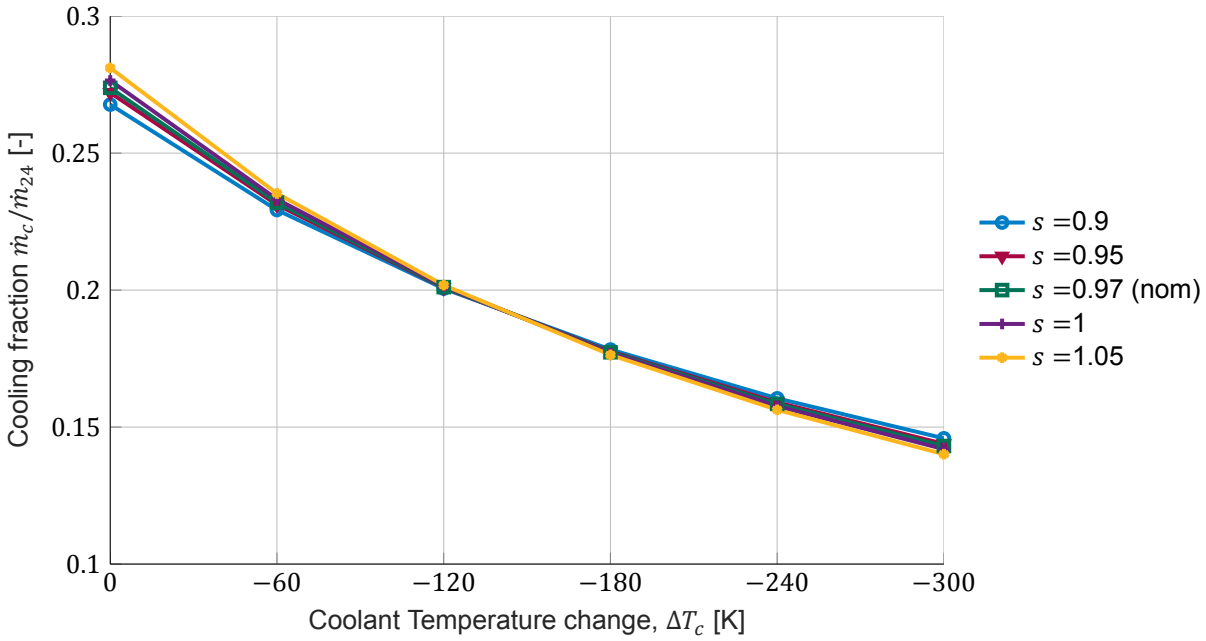

Figure 5.16: Required Cooling fraction as function of the feed coolant temperature change for various values of model exponent s. The nominal value of s is 0.97.

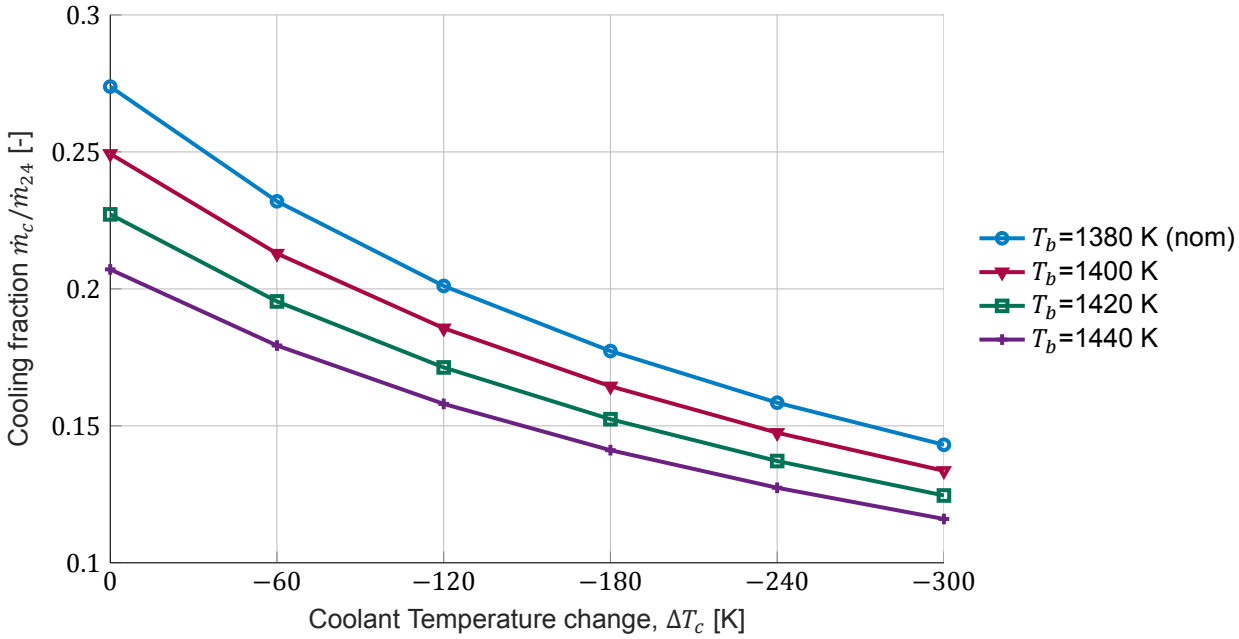

Figure 5.17: Required Cooling fraction as function of the feed coolant temperature change for various values of maximum allowable material temperature. The nominal value of T_b is 1380 K.

It can be observed that the dependency of the cooling requirement as function of the exponent s is low. The impact on the engine performance is therefore also small. It should be noted that in this case, the difference between the gas temperature and the allowable material temperature is comparable to the difference between the coolant temperature and the allowable material temperature. If the ratio between these temperature differences moves away from unity, the dependency of the cooling requirement on the exponent will become larger.

The relationship between the required cooling fraction and the allowable material temperature is significant. Given that the baseline cooling requirement is decreases with increasing T_b, both the take-off and cruise specific fuel consumption improve. In order to see if the fuel consumption trends with respect to the cooling feed temperature change (as reported in the previous sections) is affected, the SFC is normalised with respect to the SFC found in case of no cooled cooling. In Figure 5.18 the SFC change at Take-off is presented and in Figure 5.19 at Cruise.

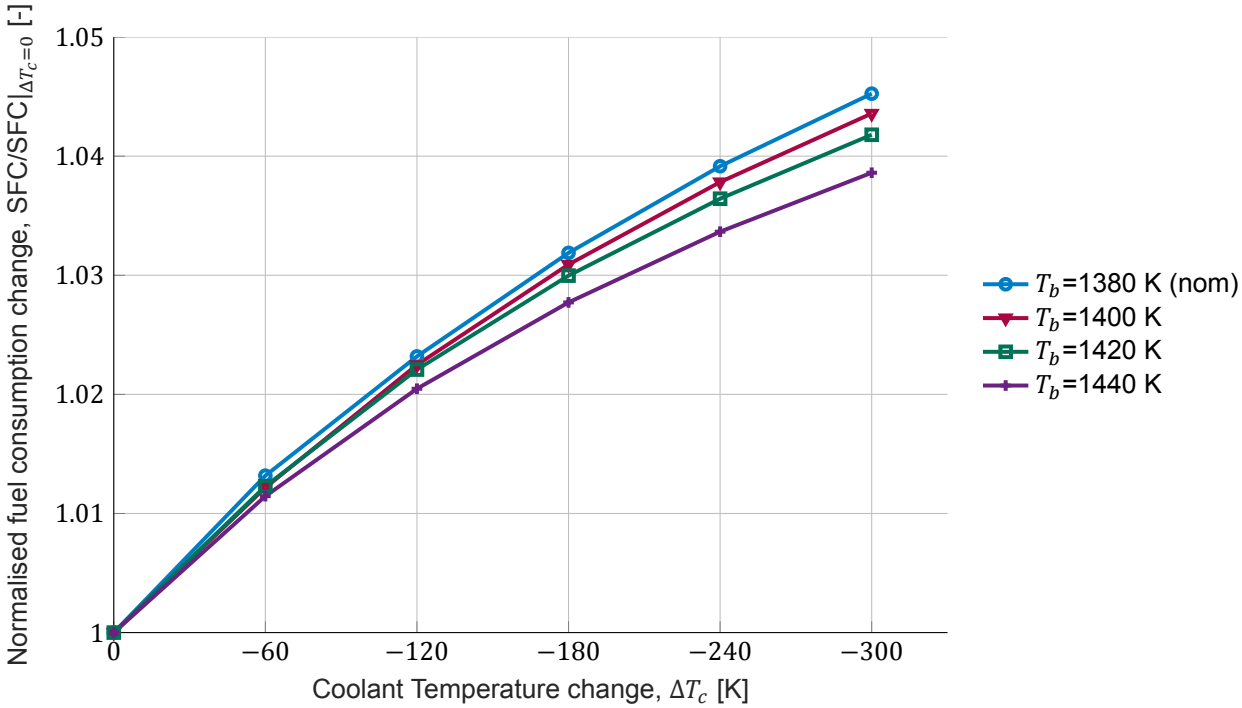

Figure 5.18: Impact of maximum allowable material temperature on relationship between (normalised) specific fuel consumption and the feed coolant temperature change at Take-Off.

.

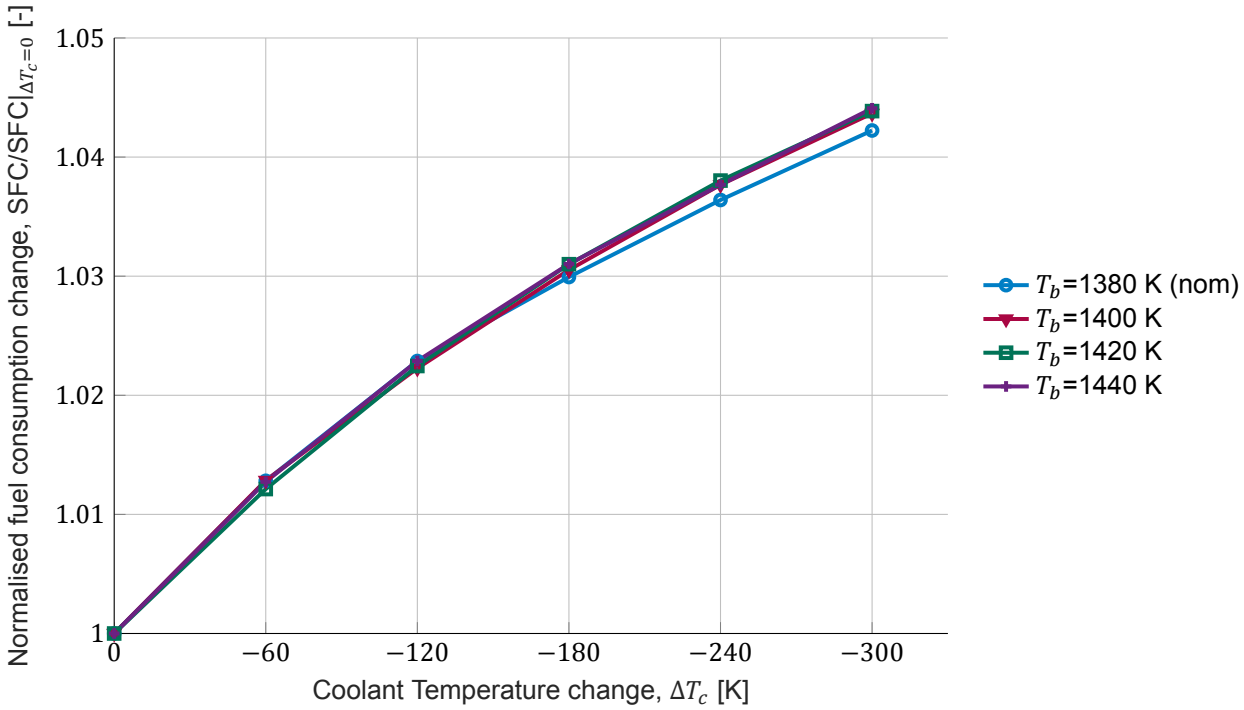

Figure 5.19: Impact of maximum allowable material temperature on relationship between (normalised) specific fuel consumption and the feed coolant temperature change at Cruise.

For both the Take-off and Cruise condition, it can be observed that the overall trend in specific fuel consumption when employing cooled cooling holds for different maximum allowable material temperatures. For the Take-off condition, the relative change in fuel consumption decreases with increasing T_b. This is, however, not the case for the cruise condition, for which the relative change is (mostly) unaffected. It is hypothesised that this difference is down to the relative importance of the coolant-gas mixing loss in the turbine. As, at Cruise, the temperature difference between the gas path and the coolant temperature is significantly smaller than at Take-off.

5.4. Exergy Analysis and Breakdown Contributing Mechanisms

In order to compare different types of losses, an exergy analysis is performed. The results from take-off GTF2050 analysis as presented in the previous section are used for the exergy analysis. With the quantification of the various exergy loss sources, it is also possible to better understand why the adoption of the CCA HEX does not lead to any improvement in the engine SFC.

A top level overview of the exergy analysis is presented in table 5.1. Four different cases are analysed, exploring the extremes of the considered heat exchanger design domain. The feed coolant temperature change is set to 0 and -300 K and the heat exchanger pressure loss is set to 0 and 8%. For the cases with a reduced coolant temperature, the bypass ratio is increased from 16.14 to 17.94 in order to keep the core exhaust pressure equal amongst all cases.

Type	**Exergy [MW]**			
	Baseline	ΔT_c	ΔP_{HEX}	$\Delta T_c \Delta P_{HEX}$
Exergy in Fuel, $\dot{Ex}_{fuel}$	60.94	63.13	60.94	63.13
Total Destruction, $\dot{I}$	23.09	24.29	23.19	24.39
Lost in Exhaust, $\dot{Ex}_{exh,lost}$	25.69	26.62	25.63	26.55
Propulsive Power: $\dot{Ex}_{fuel} - \dot{I} - \dot{Ex}_{exh,lost}$	12.15	12.22	12.12	12.18
Propulsive Power: FN $\cdot V_\infty$	12.14	12.20	12.10	12.16

Table 5.1: Overview of exergy rates in the engine as a result of heat exchanger design parameters at take-off

The fuel is the source of exergy for the system. As the inlet and outlet temperature of the combustor are fixed the exergy from the fuel linearly scales with the fuel massflow. A large part of this exergy is destroyed in the engine or leaves the engine in the exhaust flows. The difference between the exergy in the fuel and the sum of the destruction and exhaust loss is equal to the propulsive power. A comparison is made between the propulsive power as calculated from the exergy analysis and using the net thrust. As the difference between these methods is minor, it is demonstrated that all losses in the engine are accounted for in the exergy analysis.

An overview of just the irreversibilities in the engine is given in figure 5.20. The various loss mechanisms are grouped on the basis of the components they refer to. As the thrust is nearly identical in all the cases, an increase in absolute exergy losses means lower engine efficiency.

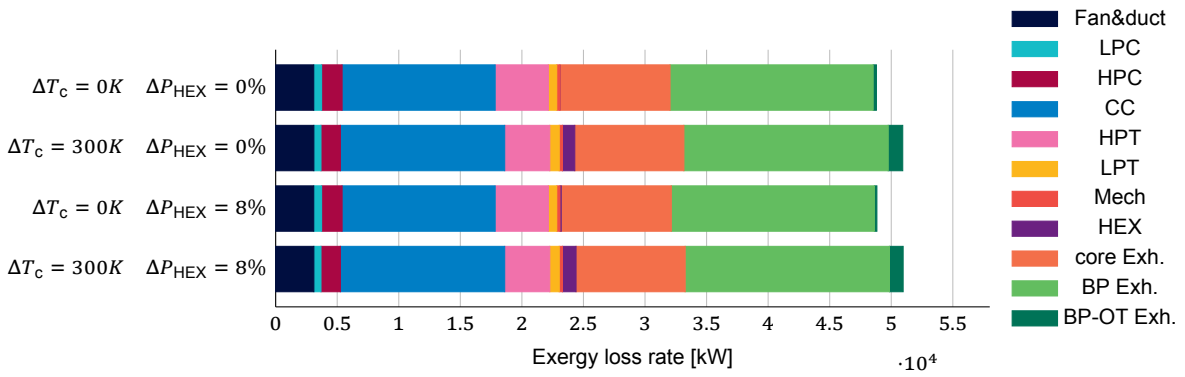

Figure 5.20: Irreversibility breakdown (exergy destruction and unused exergy in exhaust) as a function of the CCA HEX design parameters

The results in figure 5.20 are in line with the results shown in the previous chapter for the intercooled engine used for verification of the exergy analysis implementation. The largest contributors to exergy loss in the baseline engine are associated with the combustion process and the discharge into the environment of the exhausts. The core exhaust loss is significant given the relatively high temperature, and hence enthalpy of the flow that leaves the engine there, while the contribution from the BP exhaust

is small on a per massflow basis. However, because of the high massflow, this is still large in absolute terms. Furthermore, most of the other losses are occurring in the turbomachinery components with the HPT being a significantly large contributor, due partly to the high cooling flow (27% of core massflow) if the cooling air is not cooled.

When comparing the results in figure 5.20, an immediate observation can be made regarding the total exergy loss: it is higher for the case where the cooling air is cooled and only slightly higher in the case of viscous losses in the CCA heat exchanger. This result is in line with the observations with respect to SFC made in the previous sections.

Figure 5.21 presents a more detailed breakdown of exergy losses in components which are most affected as a result of the cooled cooling air heat exchanger design parameters.

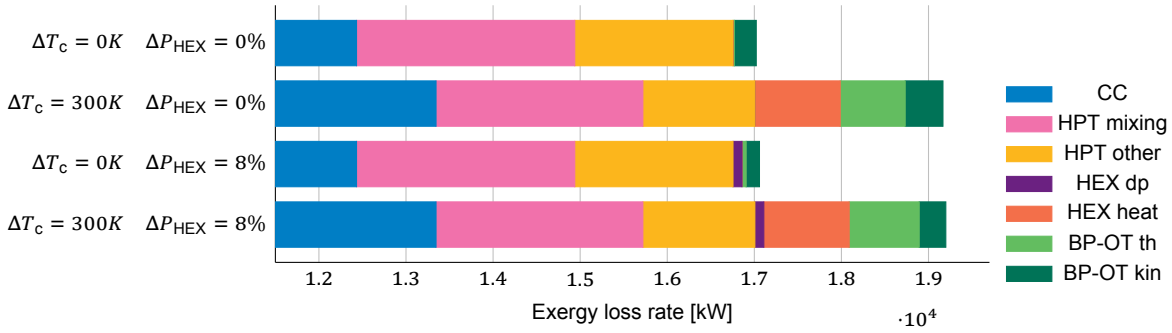

Figure 5.21: Focused irreversibility breakdown (exergy destruction and unused exergy in exhaust) of the greatest dependants of the CCA HEX design parameters

It can be observed that, as expected, there is a large reduction in losses in the HPT when the cooling air is pre-cooled, thus enabling a reduction of its massflow rate. Furthermore, given the reduced cooling flow temperature in combination with the slight increase in turbine efficiency, the exhaust temperature is reduced with respect to the baseline case. In turn, this reduces the loss associated with the core exhaust. However, this reduction is obtained by transferring part of the exergy content of the core exhaust to the bypass air flow, with the result that no efficiency improvements are obtained. The net heat rejection to the environment is indeed larger in the cases of the CCA concept, and the total fuel burn is greater. Furthermore, the loss in HPT (from decreased mixing losses and slight isentropic efficiency increase) is largely compensated by the exergy destruction in the heat exchanger. The causes thereof are explored in more detail below by evaluating the exergy flows and associated losses in the HEX, BP duct and nozzle, the turbines, and the core nozzle.

Looking more closely at exergy losses directly associated with the CCA heat exchanger, there are two relevant mechanisms causing thermodynamic irreversibilities: the heat transfer itself, and the additional pressure loss over the heat exchanger. An overview of the thermodynamic states and the associated exergy losses for the case with $\Delta T_c = -300K$ and a $\Delta P_{HEX} = 8\%$ for the TO operating condition of the engine is presented in figure 5.22.

Due to the high temperature difference in the heat exchanger, the exergy destruction to exergy transfer ratio is substantial, namely 980kW compared to 708kW transferred to the bypass off-take. Considering that the effect of reducing cooling temperature yields diminishing marginal benefit to the required turbine cooling massflow in addition to the induced thermal stresses, it is unlikely that T4c could be reduced much further. With this, the log mean temperature difference will be significant even for very small temperature differences between stations 3c and 107. Therefore, the fundamental exergy destruction from heat transfer will be large even with an optimised HEX design.

Furthermore, the increase in exergy in the bypass off-take flow only yields minimal benefit when it comes to increasing thrust, as the pressure ratio for expansion is low. The total energy in the BP-OT flow is increased by 706kW, which translates to a kinetic energy increase at the outlet of only 242kW;

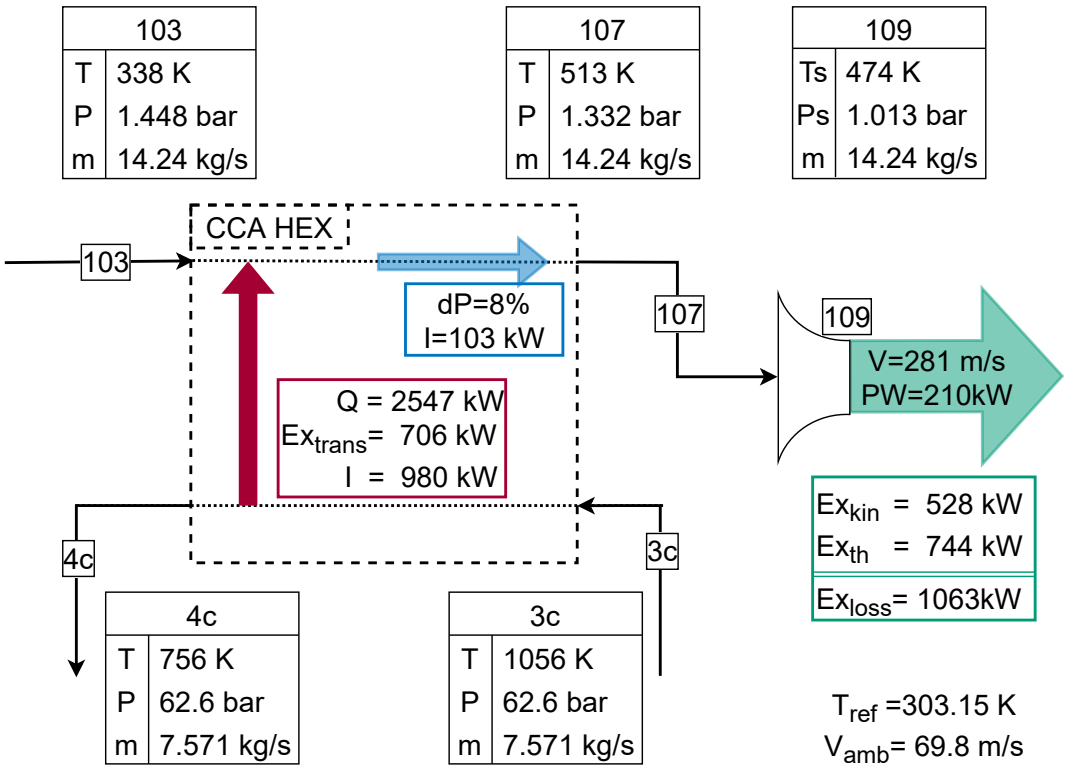

Figure 5.22: Schematic of the CCA heat exchanger and the bypass off-take exhaust, reporting the exergy losses and thermodynamic states at take-off condition

the remaining is vented as thermal energy. Note that even in the case of a higher P103 the benefit would only be effectively increased up until the nozzle is choked. Therefore, most of the transferred energy would still go unused.

The exergy loss from the pressure loss endured over the heat exchanger is relatively small compared to the other exergy losses. The direct exergy destruction is 103kw for 8% pressure drop. Furthermore, a reduction in pressure reduces the nozzle's ability to convert the total exergy into kinetic exergy. This also implies that the impact is compounded with additional thermal exergy from the heat transfer. In the case without heat transfer, this leads to a reduction of kinetic exergy by 124kW. In the case with heat transfer, the reduction is 164kW. Part of the reduction in kinetic exergy translates to a reduction of propulsive power, the remainder is conserved in the exhaust by means of an increase in thermal exergy. Hence, the marginal loss in the exhaust is caused specifically by the reduction in propulsive power (from 246 kW to 210kW). This reduction (17% of nominal power) is consistent with the observed thrust decrease in the bypass off-take observed in figure 5.9. The total exergy loss change from pressure loss is 139 kW. In the nominal case, the propulsive power is 213kW: this means that the net effect on the thrust is about neutral, a conclusion also made by Zhao et al. [100] in a similar scenario, namely the bypass off-take for an intercooler.

To understand the driving mechanisms for the turbines, three steps are considered. These three steps represent the three changing parameters that directly influence the turbine exergy loss: the cooling fraction, the HPT efficiency and the BPR. The effect of the three steps is demonstrated sequentially on a T-s diagram in figure 5.23.

Firstly, a reduction in the cooling ratio from 27% to 14% results in multiple effects on the turbine: there is a higher massflow through the system, a higher T41, and subsequently, a greater T45; polytropic efficiency remains constant.

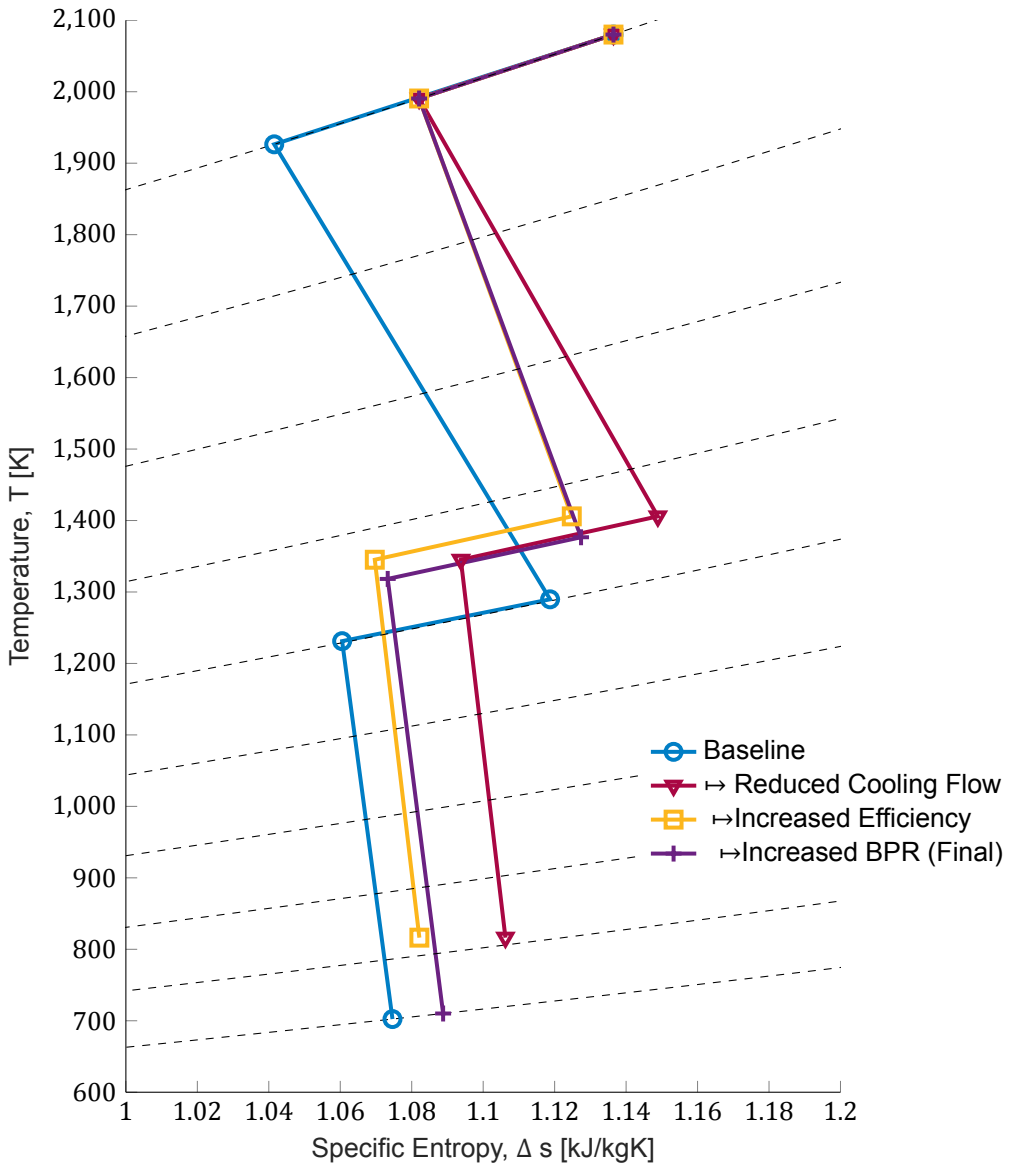

Figure 5.23: T-s diagram of both HP and LP turbines for the $\Delta T_c = -300$K case w.r.t the baseline case demonstrated in steps at Take-off.

As a result of this higher massflow, the pressure ratio becomes smaller. This drop reduces exergy destruction by 167 kW or 20% of the total exergy reduction in the HPT.

The net effect of the above is that per unit of massflow, there is more exergy remaining in the flow at the LPT exit. Note, regarding the T4 to T41 temperature drop, the magnitude of the change is reduced by the lower coolant temperature.

The change in cooling flow also reduces mixing losses, as this is a fundamental source of entropy production from heat transfer: these are lower by 131kW, or 15% of HPT exergy destruction change. As the cooling flow is at a significantly reduced temperature when compared to the baseline case, the entropy production from heat transfer is significantly larger per unit massflow. If the cooling fraction was reduced without the reduction in temperature, the mixing losses would reduce by 1199kW instead.

Secondly, the change in HPT efficiency: there is less exergy destruction in the turbine itself than in the baseline case. For this particular case, the HPT polytropic efficiency increases from 0.825 to 0.860.

Comparing with the previous step, the exergy destruction is decreased by 364kW or 43% of the total exergy reduction in the HPT.

Thirdly, increasing the bypass ratio enables the extraction of the exergy margin created by the two aforementioned mechanisms. With the BPR increasing from 16.14 to 17.94, the massflow at the core exit is reduced by 9.4%. As the massflow in the HPC is reduced, the HPT per unit massflow power output largely stays the same. This can be observed in the T-s diagram by considering the HPT outlet temperature. This temperature and hence the HPT-specifc power is not identical, however, as two factors change.

These are that the HPC-specific power input increases (3.7%) due to the “last blade height” correction, and that the mechanical loss per unit massflow for the high pressure shaft increases (4.2%) as it is defined in absolute terms. Both of these effects are the result of the method of scaling and are not inherent to the application of the CCA concept. Nonetheless, down-scaling an engine core will induce efficiency losses due to non-linearities such as the aforementioned. A scaling study on conventional and intercooled engines by Rolt et al. also shows an increased SFC from scaling down engines [22]. In absolute terms, the exergy destruction decreases by 189kW or 22% of the total exergy reduction in the HPT.

The LPT per unit massflow power output is increased significantly as the fan absolute required power is increased and the total LPT massflow is decreased. The net exergy destruction in the LPT increases from 679kW to 769kW. The exergy in the core exhaust is reduced per unit massflow (compared to the previous step) and in absolute terms is significantly lower. Compared to baseline, the exergy in the exhaust increases but due to the massflow reduction the absolute exergy loss in the exhaust is reduced by 79kW.

A summary of the exergy losses attributable to the discussed effects is presented below in table 5.2.

Comp.	Mechanism	Exergy Loss [kW]			
		Baseline	ΔT_c	ΔP_{HEX}	$\Delta T_c \Delta P_{HEX}$
Fan	Isentropic efficiency	2186	+3	$\pm$0	+3
LPC	Isentropic efficiency	555	-52	$\pm$0	-52
	Pressure Loss duct	84	-8	$\pm$0	-8
HPC	Isentropic efficiency	1663	-158	$\pm$0	-158
CC	Heat transfer	12288	+930	$\pm$0	+930
	Incomplete Combustion	31	+3	$\pm$0	+3
	Pressure Loss	113	+7	$\pm$0	+7
Shafts	Mechanical Loss	261	+1	$\pm$0	+1
HPT	Isentropic efficiency	1817	-720	$\pm$0	-720
	Mixing Loss	2506	-131	$\pm$0	-131
LPT	Isentropic efficiency	679	+90	$\pm$0	+90
HEX	Heat Transfer	0	+980	$\pm$0	+980
	Pressure Loss	0	$\pm$0	+103	+104
Core Exh.	Propulsive Efficiency	376	+1	$\pm$0	+1
	Thermal Exergy	8565	-80	$\pm$0	-80
BP Exh.	Propulsive Efficiency	15548	+92	$\pm$0	+92
	Thermal Exergy	949	+6	$\pm$0	+6
BP-OT Exh.	Propulsive Efficiency	252	+182	-99	+54
	Thermal Exergy	14	+542	+99	+630

Table 5.2: Change in exergy losses as a result of heat exchanger design parameters at take-off

6

Conclusions & Recommendations

6.1. Conclusions

The outcomes of the analysis described in this paper find clear conclusions. All the results covered in the scope of this study definitively show that there is no significant benefit to SFC from the CCA concept at both Cruise (CRZ) and Take-Off (TO). This result is consistent across a range of variables, including ones that are deliberately constructed to be at the extremes of normal conditions. These results persist even under permissive assumptions which, on net, would be expected to be generally favourable to the CCA concept as a mechanism for increasing efficiency.

It can be observed from the results that the core specific power output increases, which if not utilised, increases the specific and absolute thrust. But, when utilised by increasing the bypass ratio, the specific thrust cannot be effectively traded to improve SFC.

One exception to this conclusion is that when the Cruise heat exchanger effectiveness is (significantly) reduced compared to Take-off effectiveness, there is a theoretical specific fuel consumption benefit to be had. This benefit does not include penalties to account for several important installation effects.

Exergy analysis showed the relative scale of the loss and gain mechanisms associated with cooled cooling. One dominant loss source is heat rejection to the bypass off-take. This causes direct exergy destruction in the HEX (980kW) and another 684kW vented out the exhaust. A limited amount of the energy transferred is utilised to increase thrust (the net effect is small, but sufficient to compensate an 8% pressure loss). Another significant loss source is additional combustion losses (940kW) caused by an increased combustor air and subsequent fuel massflow. The main improvement from cooled cooling air is observed in the high pressure turbine where the total exergy destruction is reduced from 4323 to 3472 kW.

Reduction in injection losses (η_{is} improvement) between main gas flow and the cooling flow is the predominant factor, accounting for 43.3%. In Scenario Impact Test 1 the effect of this phenomena on the whole engine performance was shown to be moderate, however. Net losses from mixing are reduced by 131kW accounting for only 15% of the total HPT improvement, as the benefit from a reduced cooling flow (-1199kW destruction) is dampened by the lowered cooling temperature. Finally, re-scaling the engine is necessary to utilise the additional exergy left in the core flow. (For a full analysis of the complex set of exergy loss changes, see chapter 5.4).

6.2. Recommendations

Findings from the exergy analysis reinforce the expected result that losses from HPT cooling are significant, and suggest that further investigation on improving SFC should look at non-CCA methods such as the feasibility of active cooling massflow control; improvements in acceptable material temperatures, and other technologies that may reduce cooling requirements.

The scope of this study did not consider alternative heat sinks, which may be worth investigating. Of particular interest would be those where the heat rejection of a CCA system is not to the environment (e.g. cryogenic fuel). Very high OPR and TIT parameters were excluded from this study because of limitations in current (and projected) HPC and low-NO_x-combustion technology, respectively.
Furthermore, in the investigation, it was assumed that increased cooling flow can always be used to meet cooling requirements. If this were to be limited, i.e. by higher combustor massflow requirements, it may become viable to consider reducing the coolant feed temperature.

In general, the infeasibility of the CCA concept, as determined by this study, warrants validation given that it contradicts expectations from literature. It is therefore recommended that follow-up studies examine the methodology utilised here and whether the conclusions can be replicated under alternative approaches. This will help to refine our understanding of the CCA concept as a whole.

Bibliography

[1] *BLOOM ENGINEERING – Industrial Burner*. [Online]. Available: https://bnbloomeng.com/.

[2] M. Darecki, C. Edelstenne, T. Enders, *et al.*, "Flightpath 2050 Europe's vision for aviation," *Off. Eur*, 2011.

[3] "Waypoint 2050," Air Transport Action group, Tech. Rep., 2020, p. 30.

[4] E. Baharozu, G. Soykan, and M. B. Ozerdem, "Future aircraft concept in terms of energy efficiency and environmental factors," *Energy*, vol. 140, pp. 1368–1377, 2017, Advanced Energy Technologies in Aviation, ISSN: 0360-5442. DOI: https://doi.org/10.1016/j.energy.2017.09.007. [Online]. Available: http://www.sciencedirect.com/science/article/pii/S036054421731513X.

[5] M. Hepperle, "Electric Flight - Potential and Limitations," in *Energy Efficient Technologies and Concepts of Operation*, Lisbon, Portugal, Oct. 2012.

[6] P. Wheeler, "Technology for the more and all electric aircraft of the future," in *2016 IEEE International Conference on Automatica (ICA-ACCA)*, IEEE, 2016, pp. 1–5.

[7] R. Avellán, "On the Design of Energy Efficient Aero Engines Some Recent Innovations," Ph.D. dissertation, Chalmers University of Technology, 2011, ISBN: 9789173855648. [Online]. Available: http://publications.lib.chalmers.se/records/fulltext/144502.pdf.

[8] D. Kellari, E. F. Crawley, and B. G. Cameron, "Influence of Technology Trends on Future Aircraft Architecture," 2017. DOI: 10.2514/1.C034266. [Online]. Available: www.aiaa.org/randp..

[9] J.-C. Han, S. Dutta, and S. Ekkad, *Gas turbine heat transfer and cooling technology*. Taylor & Francis, 2000, p. 646, ISBN: 9781560328414.

[10] M. J. Kroes and T. W. Wild, *Aircraft powerplants.* 9th ed. New York, N.Y;Glencoe: McGraw-Hill Education, 2018, p. 749, ISBN: 9781259835707.

[11] J. Kurzke and I. Halliwell, *Propulsion and Power: An Exploration of Gas Turbine Performance Modeling*. Springer, 2018.

[12] G. B. Bruening and W. S. Chang, "Cooled Cooling Air Systems for Turbine Thermal Mangement," Tech. Rep., 1999. [Online]. Available: http://asmedigitalcollection.asme.org/GT/proceedings-pdf/GT1999/78606/V003T01A002/2412146/v003t01a002-99-gt-014.pdf.

[13] S. Yamawaki, C. Nakamata, R. Imai, *et al.*, "Cooling Performance of an Integrated Impingement and Pin Fin Cooling Configuration," in *Volume 5: Turbo Expo 2003, Parts A and B*, ASME, 2003, pp. 133–142, ISBN: 0-7918-3688-6. DOI: 10.1115/GT2003-38215. [Online]. Available: http://proceedings.asmedigitalcollection.asme.org/proceeding.aspx?articleid=1577563.

[14] Rolls-Royce plc., *The jet engine.* Derby, England, 1996, p. 288, ISBN: 9781119065999.

[15] F. Yin, "Modeling and characteristics of a novel multi-fuel hybrid engine for future aircraft," 2016.

[16] P. P. Walsh and P. Fletcher, *Gas Turbine Performance Second Edition*, second. Blackwell Science Ltd, 2004, ISBN: 063206434X. [Online]. Available: www.blackwellpublishing.com.

[17] A. M. Rolt and K. G. Kyprianidis, "Assesment of New Aeroengine Core Concepts and Technologies in the EU Framework 6 NEWAC Programme," in *international congress of the aeronautical sciences*, Rolls-Royce Plc., Cranfield University, 2010. [Online]. Available: www.newac.org.

[18] I. P. Van Dijk, A. G. Rao, and J. P. Van Buijtenen, "Stator Cooling and Hydrogen Based Cycle Improvements," *Int. Soc. of Air Breathing Engines 2009*, pp. 1165–2009, 2009.

[19] F. Tiemstra, “Design of a semi-empirical tool for the evaluation of turbine cooling requirements in a preliminary design stage,” 2014.

[20] G. Wilfert, J. Sieber Andrew Rolt, N. Baker Armel Touyeras, and S. Colantuoni, “New Environmental Friendly Aero Engine Core Concepts,” Tech. Rep., 2010. [Online]. Available: http://citeseerx.ist.psu.edu/viewdoc/download?doi=10.1.1.619.6911&rep=rep1&type=pdf.

[21] A. M. Rolt, K. G. Kyprianidis, and R. Plc, “Assesment of New Aeroengine Core Concepts and Technologies in the EU Framework 6 NEWAC Programme,” Tech. Rep. [Online]. Available: www.newac.org.

[22] A. Rolt, V. Sethi, F. Jacob, *et al.*, “Scale effects on conventional and intercooled turbofan engine performance,” *The Aeronautical Journal*, vol. 121, no. 1242, pp. 1162–1185, Aug. 2017, ISSN: 0001-9240. DOI: 10.1017/aer.2017.38. [Online]. Available: https://www.cambridge.org/core/product/identifier/S0001924017000380/type/journal_article.

[23] P. Elango and D. Walker, “An investigation of flush off-takes for use in a cooled cooling air system,” Jan. 2016. [Online]. Available: https://repository.lboro.ac.uk/articles/An_investigation_of_flush_off-takes_for_use_in_a_cooled_cooling_air_system/9221225.

[24] A. Spanelis, A. D. Walker, and P. A. Beecroft, “The aerodynamic design of the low pressure air delivery ducts for a cooled cooling air system,” in *Turbo Expo: Power for Land, Sea, and Air*, vol. 50794, American Society of Mechanical Engineers, 2017, V02BT42A007, ISBN: 079185079X.

[25] A. D. Walker, B. Koli, and P. A. Beecroft, “Influence of Purge Flow Swirl at Exit to the High-Pressure Compressor on OGV/Pre-Diffuser and Combustion System Aerodynamics,” *Journal of Turbomachinery*, vol. 141, no. 9, Sep. 2019, ISSN: 0889-504X. DOI: 10.1115/1.4043781. [Online]. Available: https://asmedigitalcollection.asme.org/turbomachinery/article/doi/10.1115/1.4043781/725529/Influence-of-Purge-Flow-Swirl-at-Exit-to-the.

[26] S. Farokhi, *Aircraft propulsion*. John Wiley & Sons, 2014, ISBN: 1118806778.

[27] J. Gauntner, “Algorithm for calculating turbine cooling flow and the resulting decrease in turbine efficiency,” 1980. [Online]. Available: https://ntrs.nasa.gov/search.jsp?R=19800011581.

[28] J. H. Horlock, “LOSSES AND EFFICIENCIES IN AXIAL-FLOW TURBINES,” Tech. Rep., 1960, pp. 48–75. [Online]. Available: https://people.unica.it/tizianoghisu/files/2020/05/Horlock_TurbineLosses.pdf.

[29] J. Kurzke and I. Halliwell, *Propulsion and Power An Exploration of Gas Turbine Performance Modeling*. Springer, Cham, 2018, ISBN: 978-3-319-75977-7. DOI: 10.1007/978-3-319-75979-1. [Online]. Available: https://link-springer-com.tudelft.idm.oclc.org/content/pdf/10.1007%2F978-3-319-75979-1.pdf.

[30] K. C. Kim, S. K. Kim, and S. Y. Yoon, “PIV measurements of the flow and turbulent characteristics of a round jet in crossflow,” *Journal of Visualization 2000 3:2*, vol. 3, no. 2, pp. 157–164, 2000, ISSN: 1875-8975. DOI: 10.1007/BF03182408. [Online]. Available: https://link.springer.com/article/10.1007/BF03182408.

[31] R. J. Margason, “Fifty years of jet in cross flow research,” *In AGARD*, 1993.

[32] J. D. Haldeman, D. S. Liscinskr, and D. B. Bain, “Mixing of Multiple Jets With a Confined Subsonic Crossflow Part II-Opposed Rows of Orifices in Rectangular Ducts,” [Online]. Available: http://asmedigitalcollection.asme.org/GT/proceedings-pdf/GT1997/78699/V002T06A056/2409072/v002t06a056-97-gt-439.pdf.

[33] B. R. Morton and A. Ibbetson, “Jets Deflected in a Crossflow,” *Experimental Thermal and Fluid Science*, vol. 12, pp. 112–133, 1996.

[34] C. Moreno Castan, *Film cooling aerodynamic performance: Flow structures and aerodynamic losses in an airfoil with pressure side injection*, 2018. [Online]. Available: https://repository.tudelft.nl/islandora/object/uuid%3A1769608d-3c1d-413d-95b5-61b08a45ac8b.

[35] R. M. Kelso, T. T. Lim, and A. E. Perry, “An experimental study of round jets in cross-flow,” *Journal of Fluid Mechanics*, vol. 306, pp. 111–144, Jan. 1996, ISSN: 1469-7645. DOI: 10.1017/S0022112096001255. [Online]. Available: https://www-cambridge-org.tudelft.idm.oclc.org/core/journals/journal-of-fluid-mechanics/article/an-experimental-study-of-round-jets-in-crossflow/4301861CE913C315D60B390A77053977.

[36] T. F. Fric and A. Roshko, “Vortical structure in the wake of a transverse jet,” *Journal of Fluid Mechanics*, vol. 279, pp. 1–47, 1994, ISSN: 1469-7645. DOI: 10.1017/S0022112094003800. [Online]. Available: https://www.cambridge.org/core/journals/journal-of-fluid-mechanics/article/vortical-structure-in-the-wake-of-a-transverse-jet/79CFDA2A9200C76E5B16E2B2C4C2B515.

[37] J. D. Denton, “Loss mechanisms in turbomachines,” *Journal of Turbomachinery*, vol. 115, no. 4, pp. 621–656, 1993, ISSN: 15288900. DOI: 10.1115/1.2929299.

[38] E. M. Greitzer, C. S. Tan, and M. B. Graf, *Internal flow: concepts and applications*. Cambridge University Press, 2007, vol. 3, ISBN: 1139451111.

[39] J. L. Kerrebrock, *Aircraft engines and gas turbines.* Cambridge, Mass : MIT Press, 1992, 1 online resource (478 blz.) ISBN: 1615833455.

[40] J. H. Horlock and L. Torbidoni, “Calculations of Cooled Turbine Efficiency,” 2008. DOI: 10.1115/1.2771250. [Online]. Available: http://asmedigitalcollection.asme.org/gasturbinespower/article-pdf/130/1/011703/5706288/011703_1.pdf.

[41] J. B. Esgar, R. S. Colladay, and A. Kaufman, *An analysis of the capabilities and limitations of turbine air cooling methods*. National Aeronautics and Space Administration, 1970.

[42] M. Jonsson, O. Bolland, D. Bücker, and M. Rost, “Gas turbine cooling model for evaluation of novel cycles,” in *ECOS 2005 - Proceedings of the 18th International Conference on Efficiency, Cost, Optimization, Simulation, and Environmental Impact of Energy Systems*, 2005, pp. 641–650, ISBN: 8251920418.

[43] J. Kurzke, “Performance Modeling Methodology: Efficiency Definitions for Cooled Single and Multistage Turbines,” in *Volume 1: Turbo Expo 2002*, ASME, Jan. 2002, pp. 85–92, ISBN: 0-7918-3606-1. DOI: 10.1115/GT2002-30497. [Online]. Available: http://proceedings.asmedigitalcollection.asme.org/proceeding.aspx?articleid=1574617.

[44] F. ; Yin, F. S. Tiemstra, and A. Rao, “Development of a Flexible Turbine Cooling Prediction Tool for Preliminary Design of Gas Turbines,” *Journal of Engineering for Gas Turbines and Power*, vol. 140, no. 9, 2018. DOI: 10.1115/1.4039732. [Online]. Available: https://doi.org/10.1115/1.4039732.

[45] N. E. Holgate, I. Cresci, P. T. Ireland, and A. Rawlinson, “PREDICTION AND AUGMENTATION OF NOZZLE GUIDE VANE FILM COOLING HOLE PRESSURE MARGIN,” [Online]. Available: www.euroturbo.eu.

[46] D. K. Walters and J. H. Leylek, “A Detailed Analysis of Film-Cooling Physics: Part I—Streamwise Injection With Cylindrical Holes,” *Journal of Turbomachinery*, vol. 122, no. 1, pp. 102–112, Jan. 2000, ISSN: 0889-504X. DOI: 10.1115/1.555433. [Online]. Available: https://asmedigitalcollection.asme.org/turbomachinery/article/122/1/102/419794/A-Detailed-Analysis-of-Film-Cooling-Physics-Part-I.

[47] T. Grönstedt, C. Xisto, V. Sethi, *et al.*, “Ultra Low Emission Technology Innovations for Mid-Century Aircraft Turbine Engines,” *Proceedings of the ASME Turbo Expo*, vol. 3, Sep. 2016. DOI: 10.1115/GT2016-56123.

[48] O. Thulin, O. Petit, C. Xisto, X. Zhao, and T. Grönstedt, “First and Second Law Analysis of Radical Intercooling Concepts,” *Journal of Engineering for Gas Turbines and Power*, vol. 140, no. 8, Aug. 2018, ISSN: 0742-4795. DOI: 10.1115/1.4038364. [Online]. Available: https://asmedigitalcollection.asme.org/gasturbinespower/article/doi/10.1115/1.4038364/367723/First-and-Second-Law-Analysis-of-Radical.

[49] F. Watanabe, T. Nakamura, and Y. Mizokami, “Design and Testing for Ceramic Matrix Composite Turbine Vane,” Aug. 2017. DOI: 10.1115/GT2017-63264.

[50] Z. Wang, J. Xu, and L. Nie, “Research Progress of Continuous Fiber Reinforced Ceramic Matrix Composite in Hot Section Components of Aero engine You may also like Effect of Test Voltage and Age on the Resistivity of Carbon Fiber Reinforced Concrete,” DOI: 10.1088/1757-899X/678/1/012043.

[51] A. S. van Heerden, D. M. Judt, S. Jafari, C. P. Lawson, T. Nikolaidis, and D. Bosak, “Aircraft thermal management: Practices, technology, system architectures, future challenges, and opportunities,” *Progress in Aerospace Sciences*, vol. 128, p. 100 767, Jan. 2022, ISSN: 0376-0421. DOI: 10.1016/J.PAEROSCI.2021.100767.

[52] J. P. Van Buijtenen and W. P. J. Visser, “Ideal Cycles,” in *AERO ENGINE TECHNOLOGY, AE4–238*, J. Singh, Ed., fourth, Faculty of Aerospace Engineering, TU Delft, 2018, ch. 2, pp. 17–36.

[53] “Committee on Aviation Environmental Protection Report (Doc 10126),” ICAO, Montreal, Tech. Rep., 2019. [Online]. Available: http://www.icscc.org.cn/upload/file/20200603/20200603140530_45939.pdf.

[54] A. K. Agarwal, A. G. Martínez, A. Kalwar, and H. Valera, “Introduction to Advanced Combustion for Sustainable Transport,” *Energy, Environment, and Sustainability*, pp. 3–6, 2022, ISSN: 25228374. DOI: 10.1007/978-981-16-8418-0{_}1.

[55] N. Seki, N. Morioka, H. Saito, and H. Oyori, “A Study of Air/Fuel Integrated Thermal Management System,” *SAE Technical Papers*, vol. 2015-September, no. September, Sep. 2015, ISSN: 0148-7191. DOI: 10.4271/2015-01-2419. [Online]. Available: https://www.sae.org/publications/technical-papers/content/2015-01-2419/.

[56] A. Muley, K. Kochar, M. Williams, J. Bolla, and H. Strumpf, “Advanced Heat Exchanger Technology for Aerospace Applications OPT IMUM DESIGN OF A COMPACT HEAT EXCHANGER FOR ENVIRONMENTAL CONT ROL OF AN AIRCRA… Advanced Heat Exchanger Technology for Aerospace Applications,”

[57] J. Sousa, L. Villafañe, and G. Paniagua, “Thermal analysis and modeling of surface heat exchangers operating in the transonic regime,” *Energy*, vol. 64, pp. 961–969, Jan. 2014, ISSN: 0360-5442. DOI: 10.1016/J.ENERGY.2013.11.032.

[58] H. Huang, L. J. Spadaccini, and D. R. Sobel, “Fuel-Cooled Thermal Management for Advanced Aeroengines,” *Journal of Engineering for Gas Turbines and Power*, vol. 126, no. 2, p. 284, 2004, ISSN: 07424795. DOI: 10.1115/1.1689361. [Online]. Available: http://GasTurbinesPower.asmedigitalcollection.asme.org/article.aspx?articleid=1421773.

[59] L. D. Gu and J. C. Min, “Airside thermal-hydraulic characteristics for tube bank heat exchangers used to cool compressor bleed air in an aero engine,” *Applied Thermal Engineering*, vol. 141, pp. 939–947, 2018. DOI: 10.1016/j.applthermaleng.2018.06.033. [Online]. Available: www.elsevier.com/locate/apthermeng.

[60] K. G. Kyprianidis and A. M. Rolt, “On the Optimization of a Geared Fan Intercooled Core Engine Design,” *Journal of Engineering for Gas Turbines and Power*, vol. 137, no. 4, Apr. 2015, ISSN: 15288919. DOI: 10.1115/1.4028544/373150. [Online]. Available: https://asmedigitalcollection.asme.org/gasturbinespower/article/137/4/041201/373150/On-the-Optimization-of-a-Geared-Fan-Intercooled.

[61] R. von der Bank, S. Donnerhack, A. Rae, *et al.*, “Compressors for ultra-high-pressure-ratio aeroengines,” *CEAS Aeronautical Journal*, vol. 7, no. 3, pp. 455–470, Sep. 2016, ISSN: 1869-5582. DOI: 10.1007/s13272-016-0200-9. [Online]. Available: http://link.springer.com/10.1007/s13272-016-0200-9.

[62] P. Heinemann, P. Panagiotou, P. C. Vratny, S. Kaiser, M. Hornung, and K. Yakinthos, “Advanced tube and wing aircraft for year 2050 timeframe,” *AIAA SciTech Forum - 55th AIAA Aerospace Sciences Meeting*, 2017. DOI: 10.2514/6.2017-1390.

[63] L. Xu, K. G. Kyprianidis, and T. U. J. Grönstedt, “Optimization Study of an Intercooled Recuperated Aero-Engine,” *Journal of Propulsion and Power*, vol. 29, no. 2, pp. 424–432, Mar. 2013, ISSN: 0748-4658. DOI: 10.2514/1.B34594. [Online]. Available: http://arc.aiaa.org/doi/10.2514/1.B34594.

[64] M. D. Guynn, J. J. Berton, K. L. Fisher, W. J. Haller, M. Tong, and D. R. Thurman, “Engine concept study for an advanced single-aisle transport,” Tech. Rep., 2009.

[65] T. Nagashima, K. Okamoto, T. Shinmyo, and S. Teramoto, “Feasibility Study on Intercooled Turbofan Engines,” en, in *International Symposium; 20th, Air breathing engines; ISABE 2011*, vol. 2, Reston, VA, Gothenburg, Sweden: American Institute of Aeronautics and Astronautics; 2011, pp. 866–874, ISBN: 9781618391803. [Online]. Available: https://www.tib.eu/de/suchen/id/BLCP%3ACN080692468.

[66] F. S. Mastropierro, J. Sebastiampillai, F. Jacob, and A. Rolt, “Modeling Geared Turbofan and Open Rotor Engine Performance for Year-2050 Long-Range and Short-Range Aircraft,” *Journal of Engineering for Gas Turbines and Power*, vol. 142, no. 4, Apr. 2020, ISSN: 15288919. DOI: 10.1115/1.4045077.

[67] L. Xu and T. Grönstedt, “Design and Analysis of an Intercooled Turbofan Engine,” *Journal of Engineering for Gas Turbines and Power*, vol. 132, no. 11, p. 114 503, 2010, ISSN: 07424795. DOI: 10.1115/1.4000857. [Online]. Available: http://GasTurbinesPower.asmedigitalcollection.asme.org/article.aspx?articleid=1475233.

[68] F. Yin and A. Gangoli Rao, “Off-Design Performance of an Interstage Turbine Burner Turbofan Engine,” *Journal of Engineering for Gas Turbines and Power*, vol. 139, Jan. 2017. DOI: 10.1115/1.4035821.

[69] J. Sieber, “European Technology Programs for Eco-Efficient Ducted Turbofans,” *ISABE*, 2015.

[70] *Ultra Low emission Technology Innovations for Mid-century Aircraft Turbine Engines | ULTIMATE Project | Fact Sheet | H2020 | CORDIS | European Commission*. [Online]. Available: https://cordis.europa.eu/project/id/633436.

[71] T. Grönstedt, C. Xisto, V. Sethi, *et al.*, “GT2016-56123 ULTRA LOW EMISSION TECHNOLOGY INNOVATIONS FOR MID-CENTURY AIRCRAFT TURBINE ENGINES,” 2016.

[72] *Ultra-Efficient Engine Technology (UEET) Program - NASA Technical Reports Server (NTRS)*. [Online]. Available: https://ntrs.nasa.gov/citations/20050195882.

[73] N. Pickard, “Efficient and environmentally friendly aero-engine (EEFAE) targeted research action,” *Air & Space Europe*, vol. 3, no. 3-4, pp. 161–162, May 2001, ISSN: 1290-0958. DOI: 10.1016/S1290-0958(01)90082-6.

[74] E. Kors, “SILENCE(R) SIGNIFICANTLY LOWER COMMUNITY EXPOSURE TO AIRCRAFT NOISE Halfway Towards Success,” 2004.

[75] *Significantly lower community exposure to aircraft | SILENCE-R Project | Fact Sheet | FP5 | CORDIS | European Commission*. [Online]. Available: https://cordis.europa.eu/project/id/G4RD-CT-2001-00500.

[76] J.-J. Korsia and S. Guy, “VITAL–European R&D Programme for Greener Aero-Engines,” *18th ISABE*, 2007.

[77] G. Wilfert, J. Sieber, A. Rolt, N. Baker, A. Touyeras, and S. Colantuoni, “New environmental friendly aero engine core concepts,” *ISABE Paper*, no. 2007-1120, 2007.

[78] *NEW Aero Engine Core concepts | NEWAC Project | Fact Sheet | FP6 | CORDIS | European Commission*. [Online]. Available: https://cordis.europa.eu/project/id/30876.

[79] *valiDation of Radical Engine Architecture systeMs | DREAM Project | Fact Sheet | FP7 | CORDIS | European Commission*. [Online]. Available: https://cordis.europa.eu/project/id/211861.

[80] E. Kors, “OPtimisation for low Environmental Noise impact AIRcraft-OPENAIR,” in *INTER-NOISE and NOISE-CON Congress and Conference Proceedings*, vol. 249, Institute of Noise Control Engineering, 2014, pp. 1959–1966, ISBN: 0736-2935.

[81] *OPtimisation for low Environmental Noise impact AIRcraft | OPENAIR Project | Fact Sheet | FP7 | CORDIS | European Commission*. [Online]. Available: https://cordis.europa.eu/project/id/234313.

[82] R. von der Bank, S. Donnerhack, A. Rae, M. Cazalens, A. Lundbladh, and M. Dietz, “LEMCOTEC: Improving the Core-Engine Thermal Efficiency,” in *Volume 1A: Aircraft Engine; Fans and Blowers*, American Society of Mechanical Engineers, Jun. 2014, ISBN: 978-0-7918-4557-8. DOI: 10.1115/GT2014-25040. [Online]. Available: https://asmedigitalcollection.asme.org/GT/proceedings/GT2014/45578/D%C3%BCsseldorf,%20Germany/240070.

[83] *Low Emissions Core-Engine Technologies | LEMCOTEC Project | Fact Sheet | FP7 | CORDIS | European Commission*. [Online]. Available: https://cordis.europa.eu/project/id/283216.

[84] M. Silva, “E-BREAK: engine breakthrough components and subsystems,” *The 7th European Aeronautics Days. London*, pp. 20–23, 2015.

[85] *Engine Breakthrough Components and Subsystems | E-BREAK Project | Fact Sheet | FP7 | CORDIS | European Commission*. [Online]. Available: https://cordis.europa.eu/project/id/314366.

[86] *Final Report Summary - ENOVAL (Engine Module Validators) | FP7 | CORDIS | European Commission*. [Online]. Available: https://cordis.europa.eu/project/id/604999/reporting.

[87] J. Whurr, M. Hepperle, F. Donus, and N. Tantot, “An Overview of the ENOVAL Project: Definition and analysis of advanced low specific thrust propulsion systems and technologies for year 2025-30 civil aircraft,” Tech. Rep., 2019.

[88] S. Boggia and K. Rüd, “Intercooled Recuperated Gas Turbine Engine Concept,” in *41st AIAA/ASME/ SAE/ ASEE Joint Propulsion Conference & Exhibit*, Reston, Virigina: American Institute of Aeronautics and Astronautics, Jul. 2005, ISBN: 978-1-62410-063-5. DOI: 10.2514/6.2005-4192. [Online]. Available: http://arc.aiaa.org/doi/abs/10.2514/6.2005-4192.

[89] W. Visser, “Generic Analysis Methods for Gas Turbine Engine Performance: The development of the gas turbine simulation program GSP,” Ph.D. dissertation, TU Delft, 2015, ISBN: 978-94-6259-492-0. [Online]. Available: https://repository.tudelft.nl/islandora/object/uuid:f95da308-e7ef-47de-abf2-aedbfa30cf63/.

[90] SAE, “Gas Turbine Engine Performance Station Identification and Nomenclature, Aerospace Recommended Practice,” 1974.

[91] T. Edwards, “”Kerosene” fuels for aerospace propulsion - composition and properties,” *38th AIAA/ ASME/ SAE/ ASEE Joint Propulsion Conference and Exhibit*, 2002. DOI: 10.2514/6.2002-3874.

[92] W. C. Reynolds and P. Colonna, *Thermodynamics : fundamentals and engineering applications*. Cambridge, United Kingdom ; Cambridge University Press, 2018, xix, 401 pages : ISBN: 9780521862738.

[93] İ. Dinçer and M. (A. Rosen, *Exergy : energy, environment and sustainable development*. Amsterdam : Elsevier, 2021, 1 online resource, ISBN: 9780128243930.

[94] A. Bejan, G. Tsatsaronis, and M. J. Moran, *Thermal design and optimization*, 7. New York : Wiley, 1996, vol. 19, xv, 542 pages : ISBN: 0471584673. [Online]. Available: https://www.sciencedirect.com/science/article/pii/S0140700797876323.

[95] J. Szargut, D. R. Morris, and F. R. Steward., *Exergy analysis of thermal, chemical, and metallurgical processes*, IA. New York : Hemisphere, 1988, xviii, 332 pages : ISBN: 0891165746. [Online]. Available: http://www.osti.gov/energycitations/product.biblio.jsp?osti_id=5782713.

[96] *Fleet Statistics - CFM International CFM International*. [Online]. Available: https://www.cfmaeroengines.com/engines/fleet-statistics/.

[97] ENOVAL Consortium, “ENOVAL Final Report,” Tech. Rep., 2018.

[98] S. L. Dixon and C. Hall, *Fluid mechanics and thermodynamics of turbomachinery*. Butterworth-Heinemann, 2013, ISBN: 0123914108.

[99] ICAO, “ICAO Engine Exhaust Emissions Databank,” vol. Doc 9646-A, 2021. [Online]. Available: https://www.easa.europa.eu/domains/environment/icao-aircraft-engine-emissions-databank.

[100] X. Zhao, O. Thulin, and T. Grönstedt, “First and second law analysis of intercooled turbofan engine,” *Journal of Engineering for Gas Turbines and Power*, vol. 138, no. 2, Feb. 2016, ISSN: 15288919. DOI: 10.1115/1.4031316.

A

Annotated Process Flow Diagram

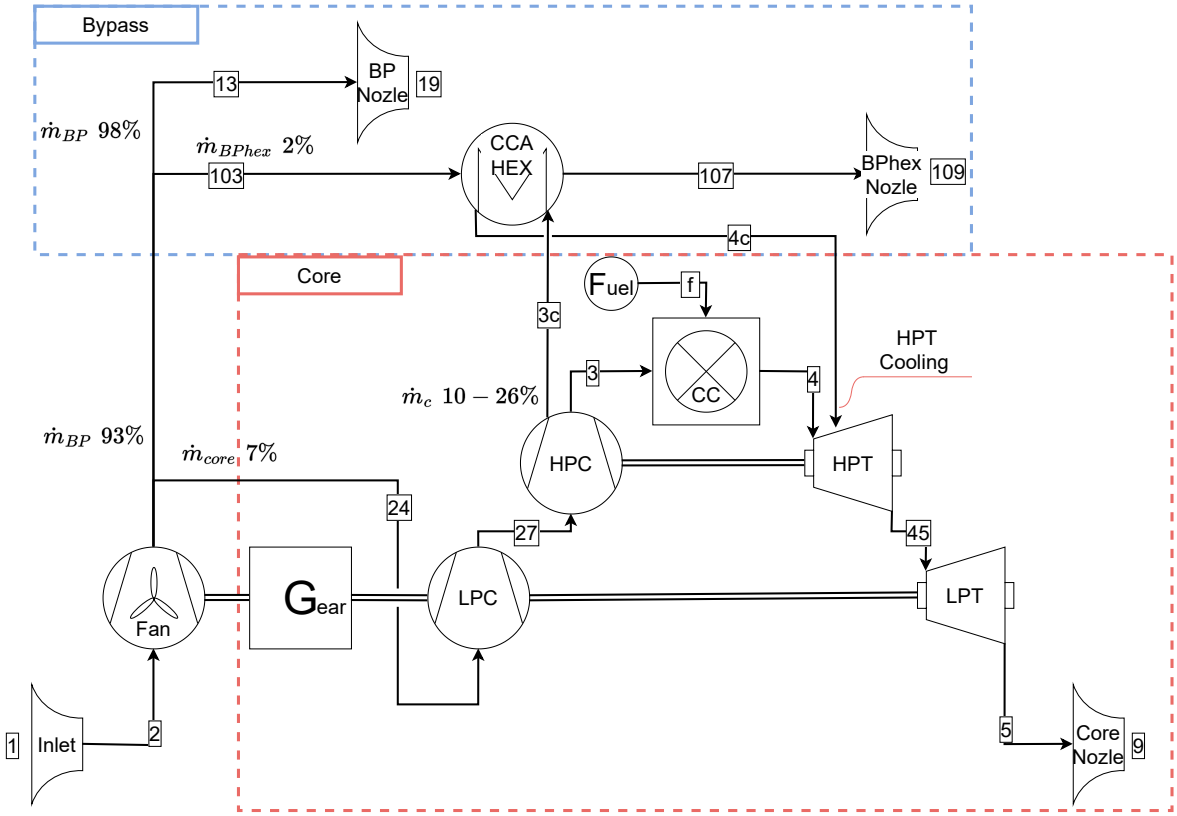

Figure A.1: Annotated process flow diagram of a 2 shaft geared turbofan with a CCA HEX in the bypass